ResearchGate

See discussions, stats, and author profiles for this publication at: https://www.researchgate.net/publication/327014263

Modeling and Control of Underground Coal Gasification

Thesis · July 2016

CITATIONS
4

READS
404

1 author:

Ali Arshad
COMSATS University Islamabad
39 PUBLICATIONS **364** CITATIONS

SEE PROFILE

All content following this page was uploaded by Ali Arshad on 14 August 2018.

The user has requested enhancement of the downloaded file.

Modeling and Control of Underground Coal Gasification

By

Ali Arshad

CIIT/SP12-PEE-005/ISB

PhD Thesis

In

Electrical Engineering

COMSATS Institute of Information Technology
Islamabad-Pakistan

Spring, 2016

COMSATS Institute of Information Technology

Modeling and Control of Underground Coal Gasification

A Thesis Presented to

COMSATS Institute of Information Technology, Islamabad

In partial fulfillment

of the requirement for the degree of

PhD Electrical Engineering

By

Ali Arshad

CIIT/SP12-PEE-005/ISB

Spring, 2016

Modeling and Control of Underground Coal Gasification

A Post Graduate Thesis submitted to the Department of Electrical Engineering as partial fulfillment of the requirement for the award of Degree of PhD in Electrical Engineering

Name	Registration No.
Ali Arshad	CIIT/SP12-PEE-005/ISB

Supervisor

Dr. Shahid Ahmed Khan

Professor, Department of Electrical Engineering

COMSATS Institute of Information Technology, Islamabad

Co supervisor

Dr. Aamer Iqbal Bhatti

Professor, Department of Electrical Engineering

Capital University of Science and Technology, Islamabad

Final Approval

This thesis titled

Modeling and Control of Underground Coal Gasification

By

Ali Arshad

CIIT/SP12-PEE-005/ISB

has been approved

For the COMSATS Institute of Information Technology, Islamabad

External Examiner: _____
Name & Signature
Department, University Name & City

External Examiner: _____
Name & Signature
Department, University Name & City

Supervisor: _____
Prof. Dr. Shahid A. Khan
Department of Electrical Engineering, Islamabad

Head of the Department: _____
Prof. Dr. Shahid A. Khan
Department of Electrical Engineering, Islamabad

Chairperson: _____
Prof. Dr. M. Junaid Mughal
Department of Electrical Engineering, Islamabad

Dean, Faculty of Engineering: _____
Prof. Dr. Shahid A. Khan
Department of Electrical Engineering, Islamabad

Declaration

I Ali Arshad, Reg. # CIIT/SP12-PEE-005/ISB, hereby declare that I have produced the work presented in this thesis, during the scheduled period of study. I also declare that I have not taken any material from any source except referred to wherever due that amount of plagiarism is within acceptable range. If a violation of HEC rules on research has occurred in this thesis, I shall be liable to punishable action under the plagiarism rules of the HEC.

Date: _____ Signature of the student:

_____

Ali Arshad
Reg. # CIIT/SP12-PEE-005/ISB

Certificate

It is certified that Ali Arshad, Reg. # CIIT/SP12-PEE-005/ISB, has carried out all the work related to this thesis under my supervision at the Department of Electrical Engineering, COMSATS Institute of Information Technology, Islamabad and the work fulfills the requirement for award of PhD degree.

Date: _____

Supervisor:

_____
Prof. Dr. Shahid. A. Khan,
Department of Electrical Engineering, Islamabad

Head of the Department:

_____
Prof. Dr. Shahid A. Khan
Department of Electrical Engineering, Islamabad

DEDICATION

To

My homeland

ACKOWLEDGEMENTS

First and foremost, I would like to thank Allah the Almighty, who has blessed me with all the abilities and support required to carry out my research work.

I acknowledge intimate support of my parents throughout my educational career. There prayers, moral and financial support always kept me motivated towards my goal. I also appreciate my spouse for her cooperation, love, support and providing stress free atmosphere during my doctorate's tenure.

I am very grateful to my supervisor Prof. Shahid Ahmed Khan for his support, guidance and encouragement in fulfilling my ambitions. I am also very thankful to my co-supervisor Prof. Aamer Iqbal Bhatti whose keen observance and directives helped me to develop and enhance my skills and complete my research work in time. I also like to express my gratitude to Prof. Vadim Ivanovich Utkin for his kind supervision, which enabled me to develop control system for the underground coal gasification (UCG) process. I also appreciate the efforts of Dr. Erum Shahnzawaz whose expertise in the field of chemical engineering enabled me to develop understanding of the UCG process. I would also like to acknowledge the efforts of my teachers, especially Prof. Saeed ur Rehman, Prof. Aamer Iqbal Bhatti, Prof. Raza Samar, Prof. Vadim Ivanovich Utkin, Dr. Raja Ali Riaz and Dr. Mahmood Pervaiz whose exceptional teaching skills helped me to develop core concepts regardingmy area of research.

I also recognize the constructive comments and suggestions of Control and Signal Processing Research Group (CASPR) members: Dr. Qadeer Ahmed, Dr. Yasir Awais Butt, Dr. Qudrat Khan, Dr. Ijaz Hussain Kazmi, Mr. Ghulam Murtazza, Mr. Imran Khan, Mr. Athar Hanif, Mr. Ahmad Yaar, Mr. Ussama Ali and many others, who contributed a lot in improving this research work.

Last but not least, I acknowledge support provided by CIIT in-house PhD program, UCG project Thar, ICT R&D funds, international research support initiative program (IRSIP), HEC and the Ohio State University, OH, USA

Ali Arshad
Reg. # CIIT/SP12-PEE-005/ISB

ABSTRACT

Modeling and Control of Underground Coal Gasification

Pakistan is going through an acute energy crisis despite being blessed by huge energy potential. Pakistan has approximately 185 billion tonnes of coal, of which 175 billion tonnes of Lignite B is located in Thar. The most suitable technology to harness the potential of the Thar coal reservoirs is the underground coal gasification (UCG), which involves the underground conversion of coal in to synthetic gas that can be used in numerous industrial applications. Therefore, the planning commission of Pakistan allocated the Block V of Thar coal field to UCG project Thar, in order to setup a pilot project. This research work deals with the modeling and control of Thar coal gasifier.

In this research work a computer model is developed for the underground gasification of Block V of the Thar coal field. The numerical solution of the model is carried out by incorporating a pseudo steady state approximation, which replaces gas phase PDEs with ODEs with respect to the length of the reactor. This approximation assumes that the concentration of the gases attain steady steady before any significant change occurs in the densities of coal and char. The PDEs for the densities of coal and char and solid temperature are solved by finite difference method, while the gas phase ODEs are simultaneously solved as a boundary value problem, marching from inlet to outlet. The simulation results show that the solution of the model is capable of providing space and time profiles for different physical quantities, such as, coal and char densities, concentration and molar fractions of different gases, rate of different chemical reactions and solid and gas temperatures. A detailed parametric study is also carried out for the model solution, which shows that the composition of the product gas is sensitive to various coal properties and operating conditions.

The parametrization of a complex process like UCG is a formidable job, which includes a large number of physical and chemical properties of coal, different operating conditions and various in situ phenomena. In order to determine the composition of coal and char, the ultimate analysis of their samples is carried out. The results of the ultimate analysis are prone to uncertainty, because the measurements are obtained from different coal samples, which go through different handling procedures before they are analyzed.

Therefore, in order to cater for the uncertainty in the results of the ultimate analysis two different nonlinear programing problems are formulated, which aim to minimize the square of the relative L_2 norm error between experimental and simulated heating values. The field trial of UCG is carried out by UCG project Thar, which involves the gasification of a single coal seam. The heating value is calculated by the measurements of the molar fraction of different gases provided by the gas analyzer. After optimization, the results of the solved model are compared with the experimental data, which show a good match between experimental and simulated heating values.

In order to increase the efficiency of the UCG process, a SMC is designed which maintains a desired constant heating value over a longer period of time. In order to synthesize the controller analytically, a control oriented model of the process is developed which bears certain assumptions. The SMC is considered for the process as it offers robustness against parametric variations and external disturbances. As the relative degree of the sliding variable is zero, so the trivial solution is to derive an expression for the control input algebraically, but this strategy is not feasible as the right hand side of the control input equation depends upon the unmeasured states. Therefore, the conventional SMC is implemented by adding an exogenous input, which is the derivative of the actual control signal. By doing so the relative degree of the sliding variable becomes one with respect to the exogenous input and then SMC is enforced by selecting a suitable value of the discontinuous gain. The synthesized controller is then implemented on the actual model of the UCG process. The simulation results show that despite the modeling uncertainties and external disturbance the controller keeps the heating value at the desired level.

Table of Contents

List of Figures

List of Tables

List of Acronyms

1D	One dimensional
2D	Two dimensional
3D	Three dimensional
BCFD	Billion cubic feet per day
BTCS	Backward time centered space
CCS	Carbon capture and sequestration
CH_aO_b	Chemical formula for coal
$CH_{\bar{a}}O_{\bar{b}}$	Chemical formula for char
CNG	Compressed natural gas
CO	Carbon monoxide
CO_2	Carbon dioxide
CH_4	Methane
C_nH_m	Higher hydrocarbons
CRIP	Controlled retracting injection point
FD	Finite difference
FTCS	Forward time centered space
H_2	Hydrogen
H_2O (g)	Steam
IGCC	Integrated Gasification Combined Cycle
LVW	Linked vertical Wells
MTOE	Million of tonnes oil equivalent
N_2	Nitrogen
O_2	Oxygen
ODE	Ordinary differential equation
PDE	Partial differential equation
PID	Proportional derivative integral
SMC	Sliding mode control
Syngas	Synthesis gas
UCG	Underground Coal Gasification

List of Publications

1. **Ali Arshad Uppal**, Aamer Iqbal Bhatti, Erum Aamir, Raza Samar and Shahid A. Khan,"Control oriented modeling and optimization of one dimensional packed bed model of underground coal gasification",*Journal of Process Control*, ISSN 0959-1524, Vol. 24, issue 1, pp. 269 - 277, 2014. [Chapter 3,4](impact factor: 2.653).

2. **Ali Arshad Uppal**, Aamer Iqbal Bhatti, Erum Aamir, Raza Samar and Shahid A. Khan,"Optimization and control of one dimensional packed bed model of underground coal gasification",*Journal of Process Control*, ISSN 0959-1524, Vol. 35, issue 11, pp. 11 - 20, 2015. [Chapter 4](impact factor: 2.653).

3. **Ali Arshad Uppal**, Vadim I. Utkin, Yazan Alsmadi, Aamer Iqbal Bhatti and Shahid A. Khan,"Sliding mode control of underground coal gasification",*IEEE transactions on control system technology*, [Chapter 5] (Under review), 2016.

Additional Research Work

4. Imran Khan Yousafzai, Aamer Iqbal Bhatti, Qudrat Khan and **Ali Arshad Uppal**,"Robustness and performance parametrization of smooth second order sliding mode control",*International journal of control automation and systems*, 2015 (Accepted for publication).

5. **A. Arshad**, A.I. Bhatti, R. Samar, Q. Ahmed, and E. Aamir.,"Model development of ucg and calorific value maintenance via sliding mode control",*In 2012 International Conference on Emerging Technologies(ICET)*, pp. 1 - 6, 2012.

6. **A. Arshad**, A.I. Bhatti, R. Samar, Q. Ahmed, and E. Aamir.,"Optimization of 1-D Packed bed Model of Underground Coal Gasification",*In 2013 World engineering Congress*, 2013.

7. Rizwan Azam, A.I. Bhatti, **Ali Arshad Uppal** and M. Zeeshan Babar,"Sensitivity analysis of Wnt Signaling Pathway",*Applied Sciences and Technology (IBCAST), 2013 10th International Bhurban Conference on*, pp. 1 - 6, 2013.

CHAPTER 1

Introduction

The process of underground coal gasification (UCG) involves the conversion of coal in to a useful synthetic gas or syngas, which can be used as a source of energy or a chemical feedstock. The process of UCG occurs under the surface of the earth where the coal seam is located. Due to the advent of clean coal technologies, UCG can be used as a clean source of energy.

This chapter generally builds up the motivation for the undertaken research work and highlights its contributions. The importance of coal in the world's energy mix is explored in Section 1.1, while the fundamentals of UCG process and its importance in the energy crisis of Pakistan are discussed in Sections 1.2 and 1.3 respectively. The contributions of the research work and the structure of the thesis are presented in Sections 1.4 and 1.5 respectively.

1.1 Contribution of coal in the world's energy mix

The World's overall energy consumption in the year 2014 was approximately 12928.4 millions of tonnes oil equivalent (MTOE) [1]. The contribution of various energy resources in the World's energy mix is shown in Table 1.1, of which the share of fossil fuels is approximately 86%. The major advantages of coal over its fossil counter parts are its relative abundance and low and stable cost. Moreover, the deposits of coal are distributed far more evenly over the globe as compared to the reserves of oil and gas [2, 3]. According to [1] the total global reserves of oil, coal and natural gas are $1,688$ billion barrels, 186 trillion m^3 and 892 billion tonnes respectively. By considering the current supply and demand of the fossil fuels it is expected that oil and natural gas will reach extinction in years 2067 and 2069 respectively [1], whereas, the coal reserves will be exhausted in 113 years.

Coal was first mined in Europe as early as $13th$ century, but it has been used as a source of energy for approximately 3 millenniums. During the industrial revolution in the $18th$ century it became an important source of energy. The biggest challenge for the coal industry was the environmental pollution caused by the combustion of coal, which produced oxides of sulfur and

Table 1.1: World's energy consumption by fuel type in 2014

Fuel type		Share (mtoe)	Share (% of total)
Fossil	Oil	4211.1	32.57
	Coal	3881.8	30
	Natural gas	3065.5	23.7
Other	Hydro	879	6.8
	Nuclear	574	4.44
	Renewables	316.9	2.45

nitrogen (N_2), and carbon dioxide (CO_2). The detrimental impact of coal combustion on the air and water quality was addressed by the advent of clean coal technologies which allow the removal of harmful gases before, during and after the burning of coal [2]. Coal has become the leading fuel in the production of electricity [1], due to the introduction of integrated gasification combined cycle (IGCC), a clean coal technology [4–10]. In IGCC coal gasification is integrated with the combined cycle turbine. Gasification is a partial oxidation of coal, which produces gases that preserve there heat of combustion to the maximum extent. Therefore, gases coming out of a gasifier can be burned to produce energy [11, 12]. The high operating pressure of the gasification process makes the separation of the harmful contaminents easier from useful combustible gases, which act as a fuel for the highly efficient combined cycle turbines to generate electric power [8].

Coal can be chemically converted to useful syngas either by gasifying it on surface or by using UCG technology. In surface gasification the coal is initially mined, purified and then gasified in a specially designed chamber at a specific operating pressure to recover low (100 to 200 Btu/ft^3, for air blown gasifiers) to medium (400 to 500 Btu/ft^3, for oxygen blown gasifiers) heating gas [11]. In UCG coal is gasified at its place to yield a low heating value gas. The gas quality from UCG can not match that of the surface gasifier, because in UCG there is a lack of direct control over different operating parameters. Nevertheless, UCG

offers several advantages over the conventional mining, such as increased health and safety for workers, low noise and dust pollution, lower water consumption and lower emission of methane and greenhouse gases to environment [13, 14]. Moreover, UCG becomes the only choice for low rank coal (heating value less than 12 MJ/kg [15]) which is economically infeasible for mining and for the un minable coal deposits. In this way UCG increases the exploitable coal deposits [2]. According to [16] the combination of UCG and carbon capture and sequestration (CCS) can provide a *green* solution for the production of synthetic gas by the storage of CO_2 in the underground cavity formed by the in situ coal gasification.

1.2 Underground coal gasification

The idea of UCG is not new, it dates back to the later half of the nineteenth century. In 1868 Sir William Siemens of Great Britain proposed to gasify coal in the bowels of earth in order to avoid environmental pollution caused by the burning of coal, and the Russian scientist Mendeleev is also credited for his early contributions regarding UCG in 1888 [17, 18]. No further work was carried out in the context of UCG until 1930, when an experimental set up was started in Donetsk Russia, which led to the commercial installation in 1940 [19]. The Russians successfully conducted the in-situ gasiifcation of coal at diferent locations until the 1970*s*. During this era of UCG industrialization 6.6 million tonnes of coal was gasified to produce 25 billion Nm^3 of sythetic gas [2]. Some of the successful industrial UCG operations are carried out at Angren (Uzbekistan), Queensland (Australia), Alberta (Canada), Walanchabi (China) and Majuba (South Africa) [2].

1.2.1 Overview of the process

Fig. 1.1 demonstrates typical steps involved in the in situ gasification of coal.

1. The process of UCG starts by drilling a pair of wells from surface to the coal seam, followed by the establishment of a permeable link between the wells (Fig. 1.1(a)).

2. Prior to the process of gasification the coal seam is ignited to set the initial distribution for the reactor's temperature, which is very critical in the success of the process. The oxidants are admitted to flow through the injection well, which include air and steam (H_2O (g)) or Oxygen (O_2) and H2O (g) or only air, which chemically react with already ignited coal to produce syngas. Apart from the injected gases, H_2O (g) produced by the water influx from the surrounding underground aquifers also participates in the process. The syngas is usually a mixture of carbon monoxide (CO), hydrogen (H_2), methane (CH_4) and traces of higher hydrocarbons (C_nH_m). The recovered gas can be used for power generation, industrial heating or as a chemical feedstock. A number of chemical reactions take place inside the UCG cavity, which include oxidation, gasification and coal pyrolysis. These chemical reactions have different activation energies and they require a certain temperature for there occurrence. The reaction zones shown in Fig. 1.1(b) are in the order of decreasing temperature. Coal is dried and then pyrolyzed in Zone 3 to produce char (a solid produced after the partial combustion of coal) and gases by the heat coming from Zone 1. The char produced in Zone 3 participates in the oxidation and gasification reactions in Zones 1 and 2. The gasification and pyrolysis reactions are responsible for the production of syngas, while the oxidation reactions maintain a desirable temperature in the reactor.

3. When the coal is gasified, the cavity is flushed with water and/or H_2O to remove the pollutants from the cavity (Fig. 1.1(c)). This step is necessary to avoid the contamination of the aquifers. With the passage of time, the water which participates in the process of gasification from the surrounding aquifers is replenished.

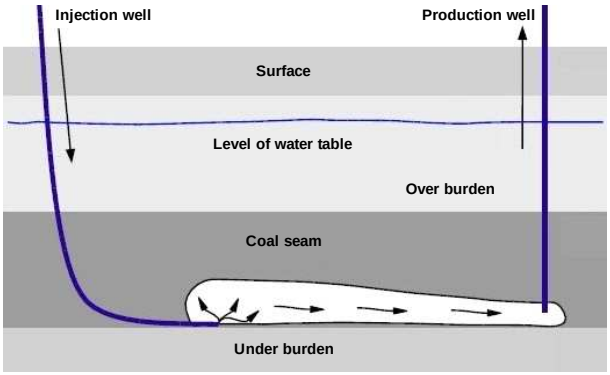

(a) Step 1: Well drilling and link establishment.

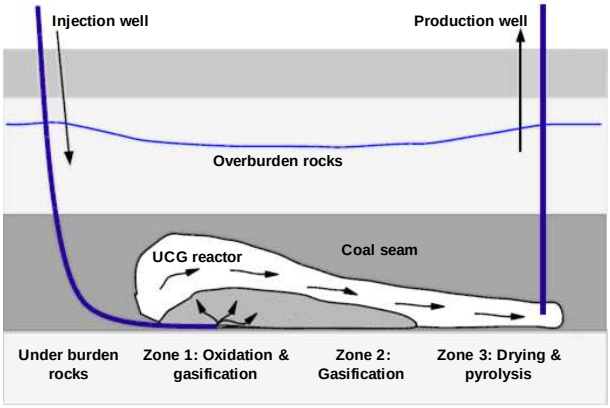

(b) Step 2: Gasification of coal seam.

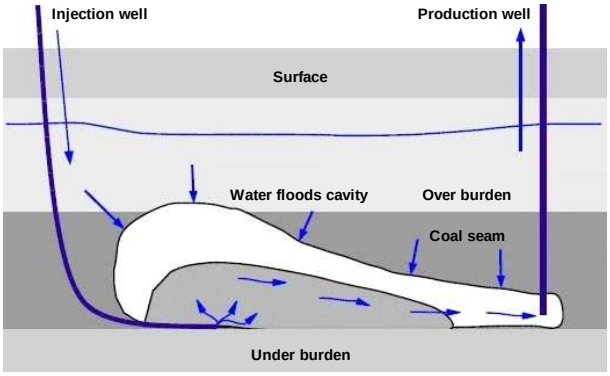

(c) Step 3: Flushing cavity with steam and water

Figure 1.1: Steps involved in a typical UCG process [3]

1.2.2 Design challenges and concepts in UCG

The design of a UCG process is a formidable job, especially when it needs to compete with sophisticated surface gasifiers for the quality of gas production and resource utilization. As UCG involves the in situ gasification of the coal,

therefore, there is a lack of direct control over a number of process parameters. A successful design of a UCG process needs to address following challenges: interaction of injected gases with the coal seam to produce desired gas, regulating the influx of water from the underground aquifers, prevention of excessive heat and gas loss, ensuring a relatively constant gas quality, avoiding the failure of the injection and production wells from possible subsidence of the over burden rocks and minimization of the environmental impacts of the process [3].

The important design concepts which are widely used for UCG process are: linked vertical well (LVW) [17, 20–22], control retraction of the injection point (CRIP) [23–27] and steeply dipping coal seams [28, 29]. These concepts mainly differ in the drilling and placements of the wells and in well linking techniques. However, in some cases the geology of the coal seam requires a particular design.

1.2.3 Performance indicators of UCG

The key indicators for measuring the success of a UCG process are calorific/heating value of the syngas and the resource recovery of the coal seam for a given injection and production well configuration [3].

The heating value of the syngas depends on its composition, which is further dependent on a number factors: composition and flow rate of the injected gas mixture, type of coal, behavior of over and under burden strata containing the coal seam and the hydrological conditions. The site selection for UCG is very important, as most of the parameters are fixed for a particular coal type and its surrounding strata. Therefore, for a site specific UCG process the only tuning knobs for yielding a desired heating value are the composition and the flow rate of the oxidants.

1.2.4 UCG as a technology of future

The first ever commercial UCG setup was established by Russia in 1940, but, the technology has not yet been undertaken by the coal industry, especially in

the western world. The commercialization of UCG has been hampered due to the availability of mature alternate technologies, which produce a consistence high quality syngas for various industrial applications. The stake holders of coal industry are also reluctant to adopt UCG, because of various difficulties associated with the process:

- There is a lack of sufficient knowledge of the variation in the UCG performance with changes in various physical and chemical processes occurring underground.
- In UCG the number of adjustable parameters are a lot fewer than the surface gasification, therefore, it is a big challenge to produce the same quality of the syngas.
- As the process occurs in situ so it is either very difficult or impossible to measure certain important parameters of the process.
- There is also a lack of computer modeling tools which can evaluate the performance estimates of the process.

As the energy statisticians claim that the deposits of oil, gas and mineable coal will reach extinction in approximately next hundred years. Therefore, UCG can play a pivotal role in fulfilling the World's energy needs of the future by harnessing the energy of unmineable coal deposits. In order to make UCG a preferred choice of syngas production, there is a need to carry out a multidisciplinary research and development to address the most significant issues regarding the process. This can be achieved by the combination of laboratory experiments, actual field trials and theoretical investigations. In this scenario a comprehensive computer model can be of a paramount importance to validate the theoretical findings against the results from the large scale field trials. The development of a robust UCG control system can also increase the efficiency of the process by addressing the uncertainties in process parameters and modeling inaccuracies.

1.3 Importance of UCG in Pakistan's energy crisis

Pakistan is going through an acute energy crisis despite being blessed by huge energy potential. The severity of the ongoing crisis can be witnessed by the worst electricity blackouts of the history and long queues of vehicles in front of Compressed Natural Gas (CNG) stations.

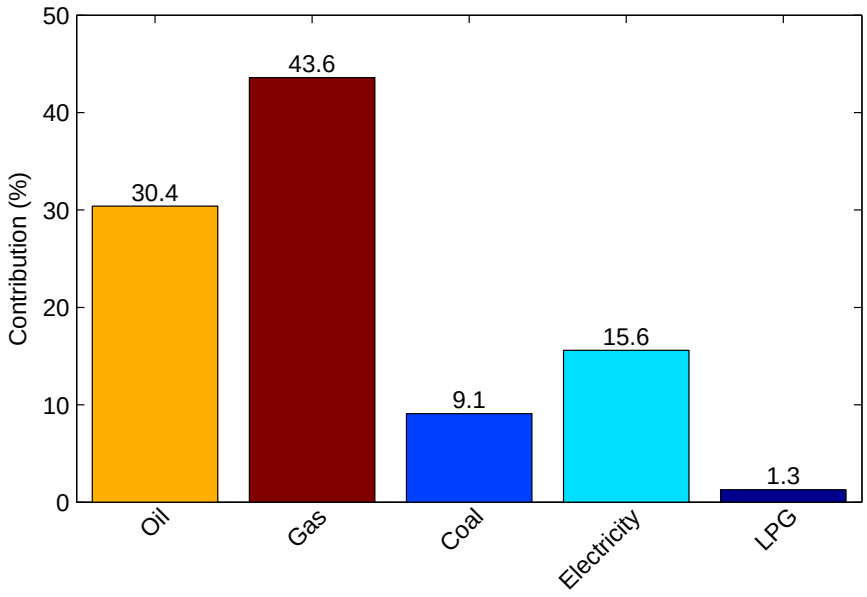

Figure 1.2: Pakistan's energy consumption by fuel type in 2013 [30]

Fig. 1.2 shows the contribution of different sources in the energy mix of Pakistan, of which the share of fossil fuels is 83%. Among the fossil fuels, oil and natural gas are the main contributors. The natural gas is a local product which is being produced at 4 billion cubic feet per day (BCFD), whereas its demand is approximately 6 BCFD. The scenario with crude oil is more alarming as Pakistan spends billions of USD to import most of the crude oil for the energy sector. The import of the crude oil will increase in the future as the gap between its consumption and local production is widening. If the supply and demand of the natural gas and oil remains the same then there reserves will be consumed in next 16 and 13 years respectively [32].

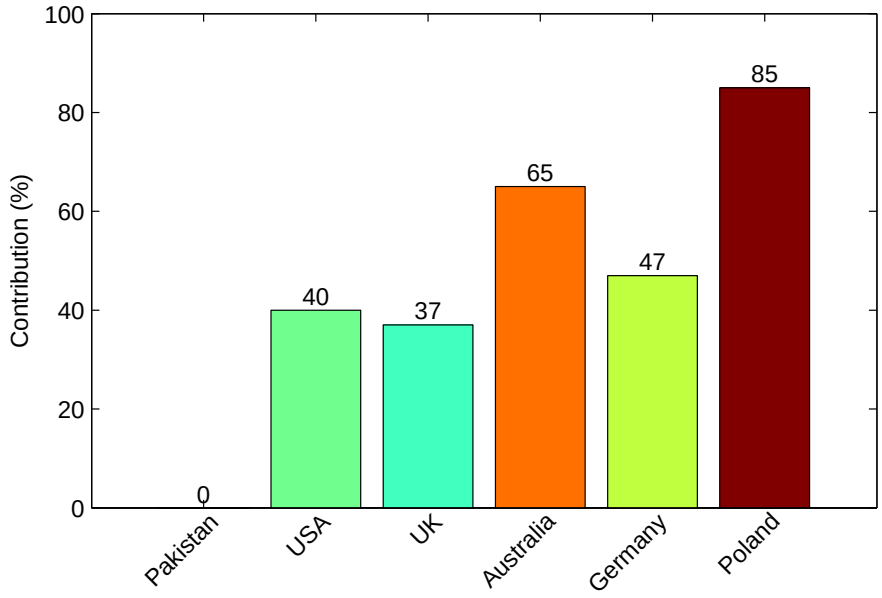

Figure 1.3: Contribution of coal in electricity production for different countries in 2013 [31]

Pakistan has approximately 185 billion tonnes of coal [33], of which 175 billion tonnes of Lignite B is located in Thar [34]. Lignite is a young coal which is brownish balck in colour and is also known as brown coal. According to [35, 36], Lignite coal can be further categorized in two types: Lignite A and Lignite B. Lignite A has gross calorific value less than 19.3 MJ/kg and Lignite B has a gross calorific value less than 14.7 MJ/kg. Thar coal field has a potential to generate $20,000$ MW of electricity for the next 40 years [2]. Despite the huge coal deposits, Pakistan has not produced any electricity from them since 1990 (Fig. 1.3). By considering type of coal, depth and thickness of coal seam and location of water aquifers under the surface of the earth, the preferred technology for gasifying the Lignite B coal of Thar is UCG. Gasifying the coal in situ is also favorable because the coal has calorific value less than 12 MJ/kg and it contains volatile matter greater than 20% [15]. Therefore, the planning commission of Pakistan allocated the Block V of Thar coal field to the UCG

project Thar, in order to setup an R&D based UCG project [37]. The project aims to establish a UCG based power plant capable of generating 100 MW of electricity. First test burn was successfully conducted on 11th Dec, 2011 [37, 38]. The success of this project will be a huge breakthrough in addressing the energy crisis of Pakistan, especially in the power sector.

1.4 Thesis contributions

The main contribution of the thesis is the development of the computer model for analysis and control of the large scale UCG set up in Block V of Thar coal fields. The following individual contributions lead to this objective:

1. **Development of a computer model for the Thar UCG setup**: The process parameters are incorporated in the equations of [39] to develop a mathematical model of the process. The parametrization of the UCG process includes all the operating conditions, physical and chemical properties of the subjected coal seam and effect of the various geological and hydrological conditions affecting the process. The model is then numerically solved in MATLAB to yield the composition and the heating value of the product gas mixture. The computer model also gives a comprehensive insight of some important process variables whose measurement is not available at the UCG site. The solution of the model is also used to study the effect of various operating conditions on the performance of the process.

2. **Optimization and validation of the model**: The inconsistency in the measurements of coal and char composition parameters and uncertainty in the H_2O (g) to O_2 ratio within the UCG reactor are addressed by formulating a nonlinear optimization problem. The optimized value of the parameters is obtained by minimizing the objective function, which is the sum of the squares of the relative error of the experimental and simulated heating values of the process. After the optimization, the effectiveness of

the model is assessed by making a comparison between the experimental and simulated results. The measured variables at the UCG site are compared with the results of the solved model. The comparison of different data sets validate the computer model of the process.

3. **Development of the control oriented model of the UCG process**: The control oriented model of the process is developed by incorporating the output equation with the already developed computer model. The model includes the UCG reactor and the gas analyzer. The input of the model is the flow rate of the injected gases at the inlet well and heating value calculated by the gas analyzer is the output.

4. **Sliding mode control design for the process**: The control of UCG is a formidable job due to two reasons: the measurement of only few model parameters is available, and the fact that the mathematical model is comprised of nonlinear partial differential equations (PDEs). The model based sliding mode control (SMC) is designed for the process, and the stability of the overall closed system is also derived. The simulation results show that the controller successfully maintains the desired heating value of the product gases. The robustness of the closed loop system against the in situ disturbance and modeling inaccuracies is also shown.

1.5 Thesis structure

Chapter 2 gives an account of the the literature related to the modeling and control of the UCG process. A number of mathematical models of the process have been reviewed in order to select a suitable model feasible for assisting field trials conducted at Block V of Thar coal field and designing the control system of the process. It has been observed that there exists a tradeoff between model accuracy and its computational complexity. In literature there are only a few evidences for the control of UCG process. As SMC is designed for the UCG process, therefore some literature related to the fundamentals of SMC is also

reviewed in the Chapter.

Chapter 3 explains the development of the computer model in detail. The mathematical equations for conservation of energy, mass and momentum of solids and gases, parametrization of the model and its numerical solution are the topics of discussion in this Chapter. The effect of changing various operating conditions on the solution variables is also presented through the simulation results.

Chapter 4 validates the effectiveness of the model for the large scale UCG set up. This Chapter begins with the description of the experimental setup for the UCG Thar site. Two different optimization problems have been formulated to address the uncertainty in some model parameters. The objective function in both the cases is the sum of the squares of the relative error of the experimental and simulated heating values of the process. In the end, comparison is made between the results of the solved model and the experimental measurements for both the optimization cases.

Chapter 5 describes the development of the control oriented model of the process and its subsequent control design. All the steps involved in the design of SMC are discussed in detail. After the SM is enforced, the stability of the internal dynamics is also proved, which confirms the boundedness of the overall closed loop system, and hence the success of the control design. The performance and the robustness of the SMC design is also shown by the simulation results.

Chapter 6 concludes the thesis and provides a list of future recommendations.

CHAPTER 2

Literature Survey

This chapter gives an account of the literature relevant to the modeling and control of UCG process. In Section 2.1 a brief review of different types of mathematical models of UCG process is presented. The literature regarding the UCG process control is discussed in Section 2.2 and the chapter ends with the conclusions in Section 2.3.

2.1 Mathematical models of UCG

Modeling has been an important tool to study the effect of various physical and chemical properties of coal seam, and operating conditions on the performance of UCG process. Because, conducting field trials and acquiring process data are very expensive and difficult. For the quantitative description of the complex UCG process, a number of specific models are required. A model is required to predict the chemical composition of product gas against composition and flow rate of injected gas, coal type, thickness of coal seam, and water intrusion. A multidimensional model is required for the optimization of resource recovery for a particular well pattern, this model needs to be coupled with chemical composition model. Numerous other models are required for the linking process, environmental effects, such as subsidence and aquifer contamination and many other additional details associated with the final system design. All of these physical and chemical models need to be coupled with economics to evaluate a candidate UCG site. It is evident that the development of such a comprehensive model of UCG which includes all the above characteristics is not a trivial job. Therefore, most of the models in the literature belong to a particular class of aforementioned sub models. These mathematical models can be categorized in the following four types [3, 40, 41].

- **Coal block models:** In this type of models coal seam is considered as a wet slab of coal, which is initially dried and then gasified. The coal slab is divided in to three zones: wet zone, dry zone and ash layer. The wet zone contains wet coal which is initially evaporated and then pyrolyzed to form volatiles (char and product gases), the dry zone contains char (highly

reactive coal), which is gasified by the inlet gases to produce more product gases and the ash layer finally contains the exhausted char, which is accumulated on the char surface. The products of pyrolysis and gasification, along with the inlet gases are accumulated in a gas film adjacent to the coal block. The net heat flux is from the gas film to the coal block to facilitate the pyrolysis and gasification reactions, and the net mass flux (product gases) is from coal block to the gas film.

Tsang [42] proposed a model for mass and heat transfer in a cylindrical sub bituminous coal ([43]) block. The locations of pyrolysis and drying fronts, and the temperature and the concentration of various volatiles in different zones of the coal block were witnessed.

Massaquoi and Riggs [44, 45] modeled the laboratory gasification of Texas Lignites by drying and combustion of a wet coal slab. The numerical simulation of the model shows the flame position, rate of combustion and temperature on the surface of coal.

Park and Edgar [46] developed a one dimensional (1-D) unsteady-state model of the coal block gasification, which predicts the movement of the cavity and the drying front. The model predictions were compared with experimental results of the combustion of Texas lignites.

In [47], Perkins and Sahajwalla developed a generalized 1D model of UCG, which is capable of simulating the gasification process in particles, cylindrical blocks and semi-infinite blocks of coal. The foundations of the model are multi component diffusion and a random pore model which changes coal reactivity with conversion. The model is used to simulate cavity growth and the typical results highlight many important aspects of the UCG process. This model was also used to study the effect of operating conditions and coal properties on cavity growth in UCG [48].

Most of the above mentioned models ignore thermomechanical properties of overburden and hydrology of coal aquifers. It is also assumed that the gasification process occurs in an oxidizing environment and at at-

mospheric pressure, these approximations contradict conditions in actual UCG process.

- **Packed bed models:** In packed bed modeling technique a link is established between the injection and production wells by permeation method, also known as percolation or filtration method. This technique is used for low and medium rank coals, e.g, lignite and sub-bituminous, these coal types have relatively higher permeability than anthracite. In this technique the coal seam is initially fractured with chemical explosives and the resultant high permeability zone is ignited and then gasified by suitable inlet gases. The permeation method resembles the packed bed chemical reactor, in which the stationary coal bed is consumed by the inlet gases with the passage of time, so the mathematical models which consider this method are known as packed bed models. This method is more efficient than channel model, because the porous medium provides an intimate contact between gas and solid, and also provides a large surface area for the gasification reaction. Thus the bypassing of oxidants does not occur, which avoids a serious decrease in the calorific value of the product gas.

  Gunn and Whitman [49] developed a linear 1D model for forward combustion (gasification) in UCG process. The work devises a method for determining optimum operating conditions: injection flow rate, air to steam ratio, and preheating of the injection air. The results of the solved model were also compared with a field test conducted near Hanna, Wyoming.

  Thorsness and Rosza [50, 51] developed a 1D packed bed model of UCG. The detail description of the model can be found in [39]. The solid phase PDEs were solved using finite difference method, while two different strategies were adopted for the solution of gas phase ordinary differential equations (ODEs). The region along the length of the reactor where the system of equations becomes stiff, the gas phase ODEs were solved by simple non-iterative modified Euler method and for the coarse zone an

iterative upstream differencing method was used. The results of the model were compared with a 1.6 m long experimental UCG reactor developed in Lawrence Livermore Laboratories. The main objective of the research work was to predict the reaction front propagation rate and product gas composition against coal bed properties and process operating conditions.

Winslow [52] developed a computer program which simulated a modified model of [50]. The gas phase equations were PDEs in time and one space dimension, because he ignored the steady state assumption of [50]. In order to improve the accuracy of the model predictions the computational cost of the computer model was also increased. The main contribution of the author is the development of a 1D prototype of UCG process which can be extended to two or three space dimensions.

Thorsness and Kang [53] formulated a set of time dependent 2D PDEs, which represented combustion and multi component chemical reactions in UCG. The model equations are comprised of conservation laws for mass, energy and momentum for gasses and solids. The model was solved by the method of lines (MOL) approach [54], which is useful for modeling the transient 2D packed bed flows related to UCG conditions. The authors used Livermore solver for ordinary differential equations (LSODE) [55], which implements the algorithm of [56].

Abdel Hadi and Hsu [57] developed a 2D packed bed model, incorporating a moving boundary method. The analysis was performed using finite element method and the results of numerical solution were compared with the laboratory measurements of [39].

Khadse et al. [58] also used the model of [50] with some modifications. The model considers coal and char as the only solids in the UCG reactor and the reactions involving fixed and mobile water are also excluded from the set of chemical reactions. The finite difference method was used for the solution of solid PDEs, while the simultaneous gas phase ODEs were solved using a stiff Matlab solver: ODE15s [59]. The effect of chang-

ing operating conditions on solid temperature and gas composition was studied for two different coal types.

Like the coal block models, these models also ignore the dynamics of water influx from surrounding aquifers and the effect of coal and rock spalling from the overburden. The packed bed models also disregard the phenomenon of cavity growth with time.

- **Channel models:** Channel model is used for the UCG process in which injection and production wells are physically linked by a horizontal borehole, to allow the flow of gas through the coal seam. Ignition occurs at the gas inlet and proceeds in the direction of gas flow. The coal is gasified at the perimeter of the channel. The channel grows continuously with time, and a large portion of inlet gases pass through the channel without reacting with coal, which decreases the calorific value of the product gas with the passage of time. This type of method is used for the high rank coal which has very poor permeability, e.g, anthracite [43]. These models can give estimates for composition of the produced gas and the cavity growth rate through heterogeneous reactions.

  Magnani and Farouq Ali [60] developed a linear, 1D steady state channel model of UCG process. A set of five coupled ODEs was solved by incorporating the respective boundary conditions. The equations were solved analytically to yield closed form solutions of important parameters of the gasification process, the details of the solution are given in [61]. The model was used to predict results of the field test, evaluate performance of the process and to study over all process sensitivity to input variables. This model also served as a foundation for more accurate 2D models [62, 63]. However, the model of Pasha and Ali [63] assumes an unsteady state flow of gases. Along with the composition of the produced gas, the model also shows the increase in the diameter of the gasification channel with time.

  Dinsmoor et al. [64] studied the feasibility of UCG field tests using a

mathematical model of a gaisification channel . On the basis of simulation results it was concluded that UCG in a channel configuration was not feasible. The phenomena of cavity growth and its ultimate size were also analyzed through model solution.

Batenburg et al. [65, 66] developed a 1D channel model for calculating gas composition and coal conversion rate for a UCG process. The model considers heat transfer through radiation between channel walls and mass transfer through natural convection within a section of the channel. The model demonstrates the effect of various operating conditions, such as pressure and rates of air and water injection on product gas composition. The performance of Pricetown I gasifier was also predicted.

Kuyper et al. [67–69] used a simplified model of gasification process to study the influence of the channel geometry on the natural convection flow and mass transfer rates. The study of gasification process in a rectangular channel was also carried out. The predictions of the gas composition were also compared with the Pricetown I field trial.

Perkins and Sahajwalla [70] developed a 1D channel model to estimate rate and composition of the syngas. A zero dimensional steady state model of cavity growth was also incorporated in the model. It was assumed that the process of UCG occurs in an open channel. The model includes equations for mass transfer through convection, characteristics of fluid flow, heat transfer, reaction rates and physical properties. The results of the model were compared with small scale field trials conducted at Centralia USA.

Seifi et al. [71] also developed a 1D steady state channel model for UCG. The structure of the model is quite similar to [60]. The ODEs of the model were analytically solved to study effect of various operating conditions on the composition of the syngas.

- **Process models:** There is not even a single model in the literature which

can alone describe the complete process of UCG. The main factors which influence the lack of a comprehensive model are complexity and poor understanding of the physical phenomena. The subject of UCG process modeling is comprised of, but not limited to various traditional disciplines such as rock mechanics, hydrology, geology, geophysics, mining and chemical engineering. In the context of reviewed literature, it is obvious that most of the research is scattered, mostly focused on a local objective. It can also be concluded that the reported laboratory scale experiments are insufficient for understanding the actual process. One possible way to develop new insights in the process is through field scale testing, but it is expensive and consumes a lot of time. However, some efforts in the development of a process model of the UCG are discussed in the following.

Britten and Thorsness [72] developed CAVSIM; a comprehensive 3D computer model of UCG. All the major research contributions of Lawrence Livermore National Laboratory during 1970's and 1980's in the field of UCG [73–79] are incorporated as sub models in CAVSIM. The main objective of the model is to estimate cavity growth and resource recovery during underground gasification of coal. The influence of overburden on growth of the cavity and phenomena like water influx from coal aquifer, rock/coal spalling in the reactor and laws of heat and mass transfer are considered in the model.

Biezen et al. [80, 81] developed a process model which gives a 3D picture of the development of an underground coal gasifier cavity. The effects of heat and mass transfer through chemical reactions and thermo mechanical failure properties of overburden rocks are combined in the model.

Nitao et al. [82] demonstrated the progress and initial application of an integrated 3D simulator developed at Lawrence Livermore National Laboratory [83]. Sub models for cavity wall, rock spalling, cavity boundary tracking, 1D cavity gas reactive transport, rudimentary rubble heat, mass

and reaction model were incorporated with the existing hydrology simulator. The phenomena of cavity collapse and overburden subsidence were also included in the geomechanical simulator. With the aforementioned advancements it was claimed that the model can predict rate and composition of injected and product gases, cavity growth, process interaction with host environment, and simulator can also support the site selection. The simulation results were compared with Hoe Creek III field test [84]. It was also mentioned that an enhanced rubble zone model will be developed, along with the integration of computational fluid dynamics (CFD) cavity gas and geomechanical models.

Samdani et al. [85, 86] developed two process models for the cavity growth of UCG. In [85] an unsteady state model is developed for the vertical growth of cavity from injection well to overburden. The experimental data from Indian lignite coal is used to solve the model equations. In [86] horizontal growth of UCG cavity towards the production well is modeled. Both models were solved simultaneously to predict the performance of UCG field test at Vastan, India.

- **Miscellaneous UCG models:** Yang et al. [87–92] performed various computer simulations to study heat and mass transfer phenomena, coupled thermohydromechanical process of coal seam, gasification of underground coal with H_2O (g) and O_2, convection diffusion for gasification agents and the effect of using temperature control blasting seepage combustion technique in UCG, respectively.

The summary of the models reviewed in this section is given in Table 2.1, which shows that how much detail of the UCG process is incorporated in a particular model. In general, a comprehensive model of a UCG process is comprised of a sub model for cavity growth, heat and mass transport model and models describing the interaction of the process with the environment [3].

Table 2.1: Summary of the reported UCG models

Author/s	Year	Model structure		Cavity growth			Heat transfer			Fluid flow[1]	Interaction with environment		
		Geometry	Dependence on time	Chemical reactions	Thermomechanical failure	Bulk collapse	Conduction	Convection	Radiation		Water influx	Heat loss	Mass loss
Packed bed models													
Gunn & Whitman [49]	1976	1D	✓	✓			✓	✓		D			
Winslow [52]	1977	1D	✓	✓			✓	✓		D			
Thorsness et al. [39, 51]	1978	1D	✓	✓			✓	✓		D			
Thorsness & Kang [53]	1984	2D	✓	✓	✓		✓	✓		D			
Abdel Hadi & Hsu [57]	1987	1D	✓	✓			✓	✓					
Channel models													
Magnani & Ali [60]	1975	1D		✓			✓	✓					
Pasha et al. [63]	1978	2D	✓	✓			✓	✓					
Dinsmoor et al. [64]	1978	1D	✓	✓			✓	✓	✓	P	✓	✓	
Batenburg [66]	1994	1D		✓			✓	✓	✓	D		✓	
Kuyper & Van [68]	1994	2D	✓	✓			✓	✓	✓	NS		✓	
Perkins & Sahajwalla [70]	2008	1D		✓	✓		✓	✓		P			
Coal block models													
Tsang [42]	1980	1D	✓	✓			✓	✓	✓				
Massaquoi & Riggs [44, 45]	1983	1D	✓	✓			✓					✓	
Park & Edgar [46]	1987	1D	✓	✓			✓	✓		D			
Perkins & Sahajwalla[47]	2005	1D	✓	✓			✓	✓	✓				
Process models													
Britten & Thorsness [72]	1989	2D	✓	✓	✓		✓	✓	✓	M	✓	✓	✓
Biezen et al. [80]	1995	3D	✓	✓	✓					D			
Nitao et al. [82, 83]	2011	3D	✓	✓	✓	✓	✓	✓	✓		✓	✓	✓
Samdani et al. [85, 86]	2015	2D	✓	✓	✓		✓	✓	✓	D			

D=Darcy, P=Plug, NS=Navier Stokes and M=Mixed

The main objectives of the models reviewed in this section are: quantitative description of the process, evaluating a potential site for UCG and the study of various phenomena occurring within the UCG reactor. These models do not lend themselves to control applications easily, mainly due to their complex geometry and computational complexity of the solution strategy. Most models of UCG are comprised of highly nonlinear PDEs with at least two independent variables one each for time and length. The analysis and control of such systems is not

a trivial task [93, 94]. The following section discusses the problem of UCG control in detail.

2.2 Control of UCG process

As discussed in Section 1.2.3, heating value is one of the key factors in determining the success of a UCG process. A closed loop control system can be of paramount importance in increasing the performance of a UCG system by providing a constant desired heating value over a longer period of time.

The control of UCG is an emerging area of research. In [95, 96] a lab scale UCG setup is controlled by some versions of the conventional PID controller [97]. The idea of UCG control system can not be mapped directly from lab scale set up to an actual field test, because it is not possible to create an actual UCG environment in lab experiments. One way to approach the problem of UCG control system design is to select an appropriate mathematical model, then a model based control strategy can be adopted for achieving the desired objective and finally the idea can be implemented on the actual UCG site. Apart from the model complexities discussed in the end of Section 2.1, some other factors further increase the challenges in UCG control system design, such as the interaction of in situ environment with the process and unavailability of the measurement of important model parameters. As the process of UCG takes place in situ, and it is either impossible or very expensive and difficult to install sensors at different locations in the reactor, so normally the available measurement is for the molar fraction of gases at the production well.

Two factors are needed to be considered while selecting an appropriate model for UCG control: accuracy of model predictions and ease of control design. The accuracy of the model increases its complexity and makes control design more difficult. Therefore, for UCG system with nonlinearities, in situ disturbances and parametric uncertainties a control technique is required which can keep a constant desired heating value of syngas, in spite of fact that design procedure is performed based on approximate model. One such technique is the sliding

mode control (SMC) [98–100]. In our earlier work [101], a simplified time domain model of UCG was developed by incorporating various assumptions in unsteady state model of [52]. A first order SMC, based on equivalent control method [102] was designed to keep a constant heating value in the presence of input disturbance. The model does not include the effect of change in length of the reactor on the system's states, and assumes that the input, output and all the chemical reactions take place at the same location. Despite some fundamental flaws in modeling, the idea of heating value control through flow rate of injected gases is demonstrated.

The rest of the section gives an account on the fundamental theory of SMC.

2.2.1 Sliding mode control

The SMC has been evolved as a preferred choice for the robust control design of complex higher order nonlinear systems operating under uncertainty conditions. The major advantage of this technique is insensitivity to parametric variations and external disturbances. SMC reduces the complexity of control design by decoupling the overall system motion into independent partial components of lower dimension. The control action in sliding mode can be implemented by discontinuous elements, such as relays or pulse width modulation (PWM) switching. These attractive properties motivated high level research in both academia and industry, and SMC has been proven to be applicable to a wide range of problems in electric drives and generators, robotics, process control, vehicle and motion control.

The idea of SMC was first proposed by Emelyanov and co-researchers in early 1950's in the former Soviet Union [99]. Ryan and Coreless [103] proposed a general SMC for linear systems with bounded disturbance. In order to avoid chattering, Burton and Zinober [104] presented continuous approximation of SMC. Woodham and Zinober [105] incorporated pole placement technique with SMC to achieve desired closed loop dynamics. The practical implementation of SMC requires estimation of unmeasured states. Bondarev et al. [106]

proposed an asymptotic state observer based on sliding mode. A complete sliding mode observer controller design can be found in [107, 108]. The aforementioned literature is related to linear control systems. The survey papers of Ramirez [109] and Pisano and Usai [110] give a detail account on some notable literature related to SMC of nonlinear systems, where as design methodology of such systems can be found in the text books of Utkin et al. [111, 112] and in [113].

2.2.2 Design concept of sliding mode control

Consider a nonlinear system, affine in control

$$\dot{x} = f(x,t) + B(x,t)\,u \tag{2.1}$$

where $x \in \Re^n$ is the system state vector, $f \in \Re^n$ is the nonlinear function of states, $B(x) \in \Re^{n\times m}$ is the input matrix and $u \in \Re^m$ is the input vector.

A set of m switching surfaces is given as:

$$S = \left\{ x \in \Re^n : s(x) = [s_1(x), \ldots, s_m(x)]^T \right\} \tag{2.2}$$

Then overall problem of SMC design can be partitioned into two sub problems of lower dimension, which can be decoupled for a large class of systems.

2.2.2.1 Switching surface design

The switching surface is designed in order to achieve the desired dynamics of the closed loop system. The design of switching surface represents the dynamics of the system during sliding mode, which is defined as, ”motion with state trajectories in some manifold of the state space with finite time needed for the state to reach this manifold” [114]. The sliding mode equation is:

$$s(x) = Gx = 0 \tag{2.3}$$

where $G = (\partial s/\partial x)$ is an $m \times n$ matrix with gradients of functions: $s_i(x)$.

Since the dynamics of sliding mode lie in the null space of G, they are called null space dynamics. For linear systems, switching surface design can solve the problem of eigenvalue placement.

2.2.2.2 Enforcing sliding mode

The objective of this step is to ensure finite time convergence of system states on the switching surface. Despite the modeling inaccuracies, parametric variations and external disturbances, the controller should confine the system states to the sliding manifold. When the system is not in the sliding mode, $s \in range(G)$. Hence the dynamics in the reachability phase ($s \neq 0$) is called range space dynamics. In this phase the controller is designed to make the the switching surface attractive. Consider the following Lyapunov function [112]:

$$V(x) = \frac{1}{2} s^T(x)\, s(x) \tag{2.4}$$

then finding its time derivative:

$$\dot{V}(x) = \dot{s}^T(x)\, s(x)$$

The controller is designed to ensure:

$$\dot{s}^T(x)\, s(x) < 0 \tag{2.5}$$

which is formally known as reachability condition, and confirms the asymptotic convergence of system states to the sliding manifold. However, for finite time convergence, the modified reachability condition is [115]:

$$\dot{s}^T(x)\,s(x) \leq -\eta\left|s(x)\right| \tag{2.6}$$

The equivalent control is one of the methods for SMC design, in which the control input is:

$$u = u_e + u_d \tag{2.7}$$

where,

$$u_e(x) = -\left[G(x)\,B(x)\right]^{-1} G(x)\,f(x)$$

$$u_d = -M\,\mathrm{sign}(s)$$

where u_e is the continuous function of states and is found by solving $\dot{s} = Gf + GBu_e = 0$, and it cancels out all the known terms in the right hand side of $\dot{s}$. The other part u_d is discontinuous and ensures finite time convergence to the chosen surface in the presence of uncertainties and disturbances.

2.2.3 The chattering problem

In an ideal sliding mode the control commutes with infinite frequency, and the system states are confined to $s = 0$ in finite time. Whereas, in real sliding mode the state trajectories can only reach in the vicinity of $s = 0$, and exhibit sustained oscillations with finite frequency and amplitude, known as *chattering phenomenon*. There are two reasons which cause imperfection in an ideal sliding mode, and result in the chattering: the discontinuous implementation of the continuous control and the presence of unmodeled dynamics. The fast switching of sliding mode controllers excite the unmodeled dynamics resulting in the high frequency oscillations.

The chattering problem results in low control accuracy, high heating losses in electrical power circuits and can cause wear and tear of moving mechanical parts. Fortunately, control engineers and researchers have developed some

methods to avoid the phenomenon of chattering. Some of these methods are given in [112].

2.2.4 Design example: Position control of underwater vehicle

Fig. 2.1 shows the free body diagram for a simple underwater vehicle system. It is assumed that the vehicle only moves in the *x* direction.

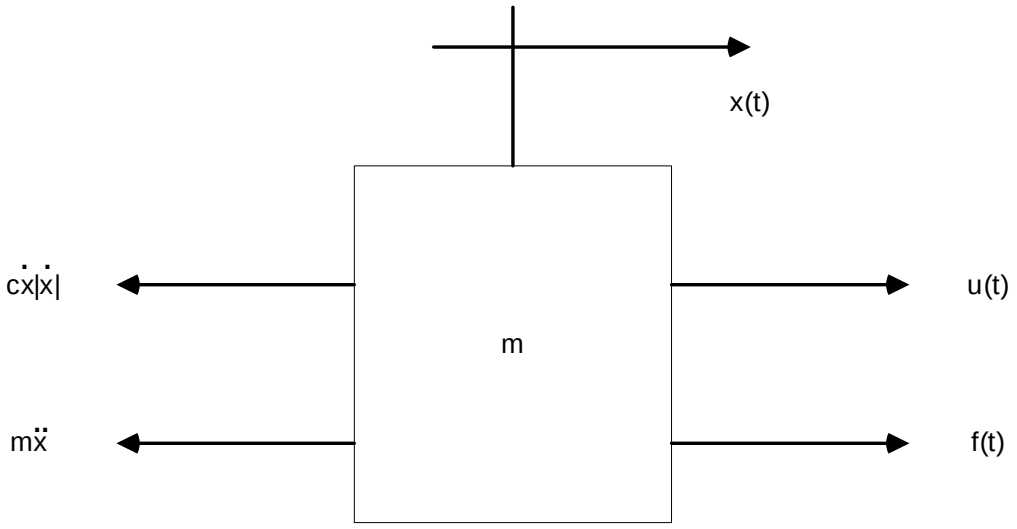

Figure 2.1: Free body diagram for underwater vehicle, showing all the forces.

By using Newton's law of motion the nonlinear dynamical model of the system is obtained [116].

$$m\ddot{x} + c\dot{x}\left|\dot{x}\right| = u(t) + f(t) \tag{2.8}$$

where x is the position of vehicle (m), u is the force provided by propellers (N), $f(t)$ is the force generated from ocean current and waves, which is considered as the disturbance for the system: $\left\| f(t) \right\| \leq f_0$, and m and c are model parameters representing mass (kg) and drag coefficient (kg/m) of underwater vehicle, respectively.

The system in Eq. (2.8) can be written in generalized controller canonical form (GCCF) [117] as:

$$\dot{x_1} = x_2$$
$$\dot{x_2} = \frac{1}{m}\left[u + f - cx_2\left|x_2\right|\right] \tag{2.9}$$

where the state variables x_1 and x_2 are the position and velocity of the underwater vehicle respectively.

Here it is desired to design a SMC for the underwater vehicle system, which can control the position x in the presence of disturbing force generated by ocean current and waves.

Two different controllers are designed for the system in order to achieve following control objectives:

2.2.4.1 State regulation ($x_1 = x_2 = 0$)

1. Let s be a linear combination of the system states:

$$s = kx_1 + x_2 \tag{2.10}$$

2. By applying the equivalent control method, $u_e = x_2\left(c\left|x_2\right| - mk\right)$ is found by solving

$$\dot{s} = kx_2 + \frac{1}{m}\left[u_e - cx_2\left|x_2\right|\right] = 0$$

It is important to note that $f(t)$ is excluded from u_e, because it is unknown. The discontinuous part of the control input is $u_d = -M\,\mathrm{sign}\,s$. The reachability condition for the system is:

$$s\dot{s} \leq -\left|s\right|\left[M - f_0\right] \tag{2.11}$$

As both $f(t)$ and $u(t)$ lie on the plane ($x_1 = 0$), therefore, the disturbance can be rejected by SMC. If $M > f_0$ then sliding mode is established.

The dynamics of the system under sliding are governed by:

$$\dot{x_1} = -kx_1 \tag{2.12}$$

The solution of Eq. (2.12): $x_1(t) = x_1(0)\exp(-kt)$ shows that x_1 will exponentially decay to 0, with the rate k. As $x_2 = \dot{x_1}$, therefore, $x_2 = 0$ when $x_1 = 0$ and the control problem is solved. Eq. (2.12) also shows the inherent properties of the sliding mode:

- **Order reduction**: The order of sliding motion is one, as compared to the second order system.
- **Invariance**: The sliding mode dynamics are independent of model parameters, therefore any uncertainty in m and c will not effect the control objective.

The numerical solution of the closed loop system is performed with the step size of $dt = 0.01$s, and for the following parameter values: $m = 100$, $c = 20$, $k = 1$, $M = 10$ and $f(t) = 9\sin(t)$.

Fig. 2.2 shows the success of control design, and the state vector converges from its initial value $x_0 = [0.05 \quad 0]^T$ to the origin. Therefore, the underwater vehicle stays at rest even in the presence of the input disturbance shown in Fig. 2.4.

The phase portrait of the vehicle position and velocity is shown in Fig. 2.3. The region where $s \neq 0$ is called reaching phase, while the sliding phase starts when $s = 0$. During the reaching phase the controller forces the states towards the surface. The sliding phase shows the motion of system under sliding, which only depends on the design variable k. The phenomenon of chattering is also visible in the vicinity of $s = 0$, which is due to the finite sampling frequency $f_s = 1/dt = 100hz$ and modeling uncertainty caused by the unknown disturbance.

Fig. 2.4 shows that the controller exhibits robustness against the variations in the input disturbance, and confines the system states to $s = 0$, once the sliding mode is established.

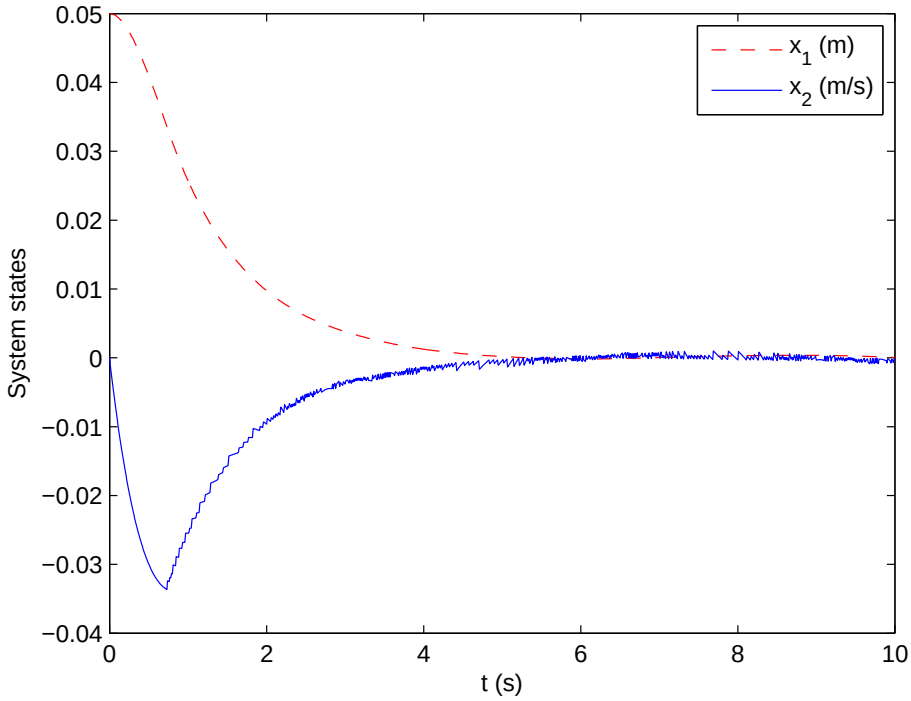

Figure 2.2: Evolution of system states with time

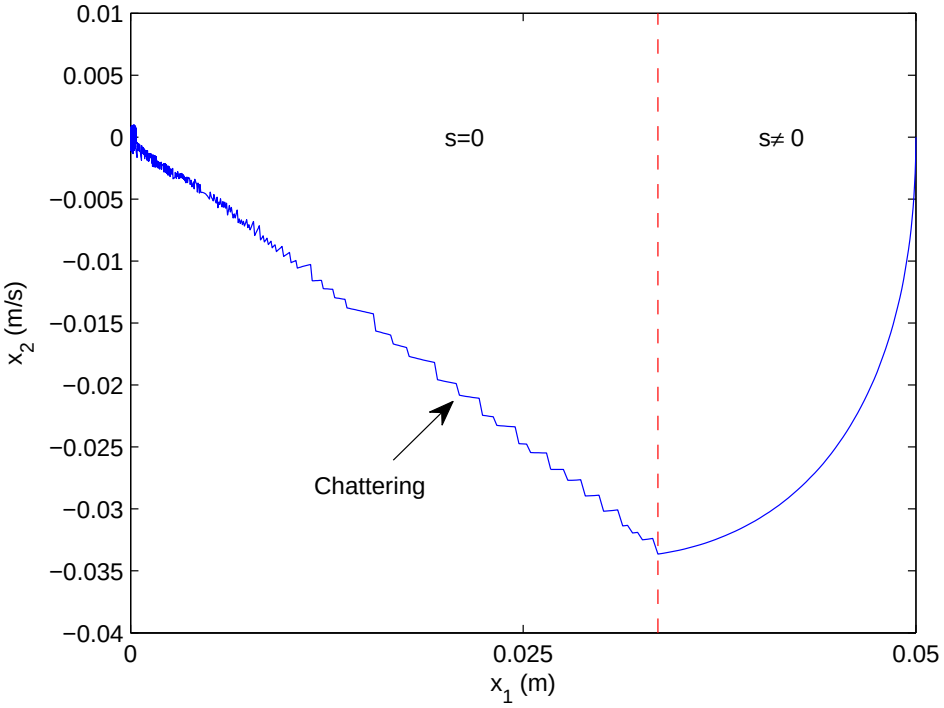

Figure 2.3: Phase portrait of system states

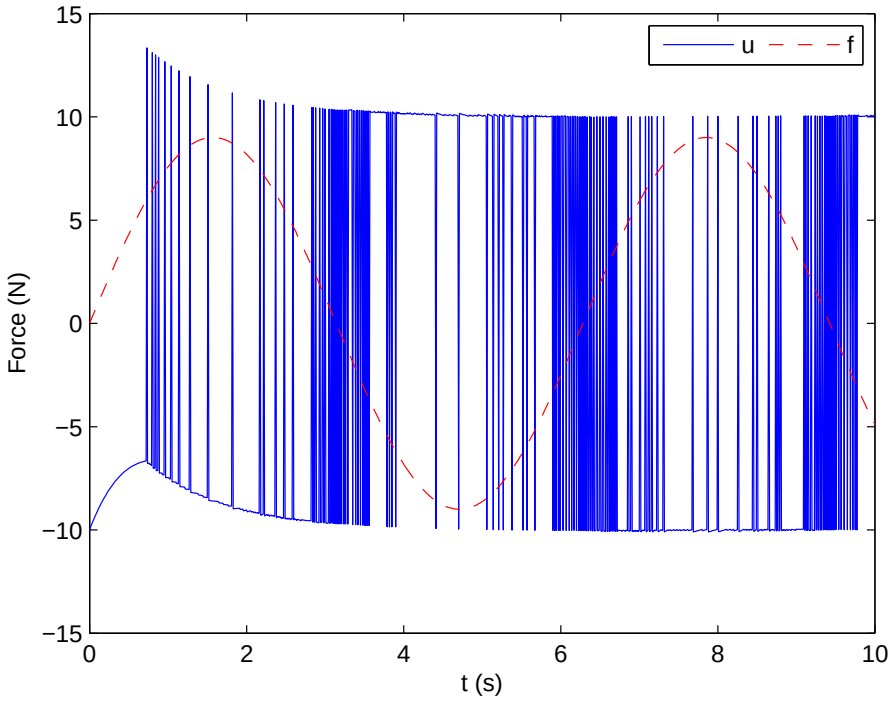

Figure 2.4: Control input and disturbance with time

2.2.4.2 Reference tracking ($x_1 = x_{1_d}, x_2 = x_{2_d}$)

Now it is desired to keep the velocity of the underwater vehicle at 1m/s in the presence of $f(t)$.

1. The switching surface is the linear combination of error states.

$$s = ke_1 + e_2 \tag{2.13}$$

where,

$$e_1 = x_1 - x_{1_d}$$

$$e_2 = x_2 - x_{2_d}$$

x_{1_d} and x_{2_d} are the desired values for position and velocity of the vehicle, respectively.

2. The application of equivalent control method yields $u_e = x_2\left(c\left|x_2\right| - mk\right) + mkx_{2_d}$. The reachability condition will take the form $s\dot{s} \leq -\left|s\right|[M - f_0]$, and the sliding mode exists for $M > f_0$

The sliding motion is governed by the first order differential equation:

$$\dot{e_1} = -ke_1 \tag{2.14}$$

The solution of Eq. (2.14): $e_1(t) = e_1(0)\exp(-kt)$ shows that e_1 will exponentially decay to 0, with the rate k, which also makes $e_2 = 0$ and the control problem is solved.

For simulations $dt = 0.01$s, $m = 100$, $c = 20$, $k = 1$, $M = 20$, $f(t) = 15\sin(t)$ and $x_0 = [0.05 \quad 0]^T$.

The results in Fig. 2.5 show that the vehicle moves with a uniform velocity of $1m/s$ after finite time. The phase portrait of the state errors is shown in Fig. 2.6. The region enclosed in the dotted circle corresponds to the sliding phase. While, the error trajectory outside $s = 0$ circle correspond to the reaching phase. Once they enter in the sliding manifold, the controller confines the error states to the switching surface, even in the presence of the disturbance (Fig. 2.7).

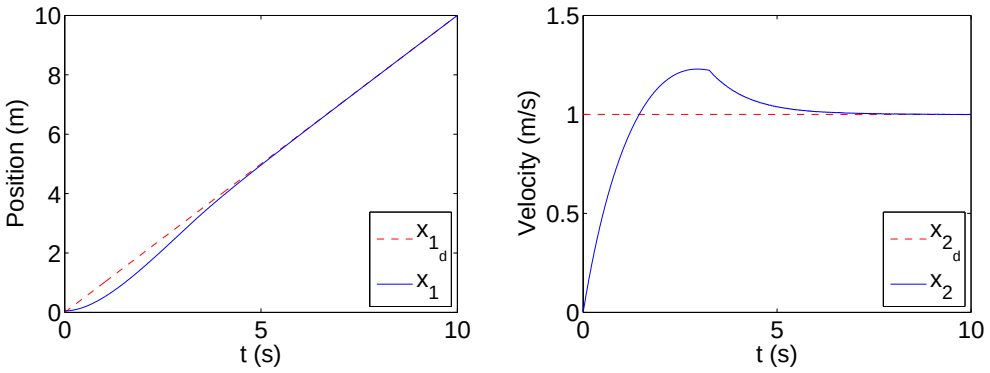

(a) Position of underwater vehicle (b) Velocity of underwater vehicle

Figure 2.5: Evolution of system states with time

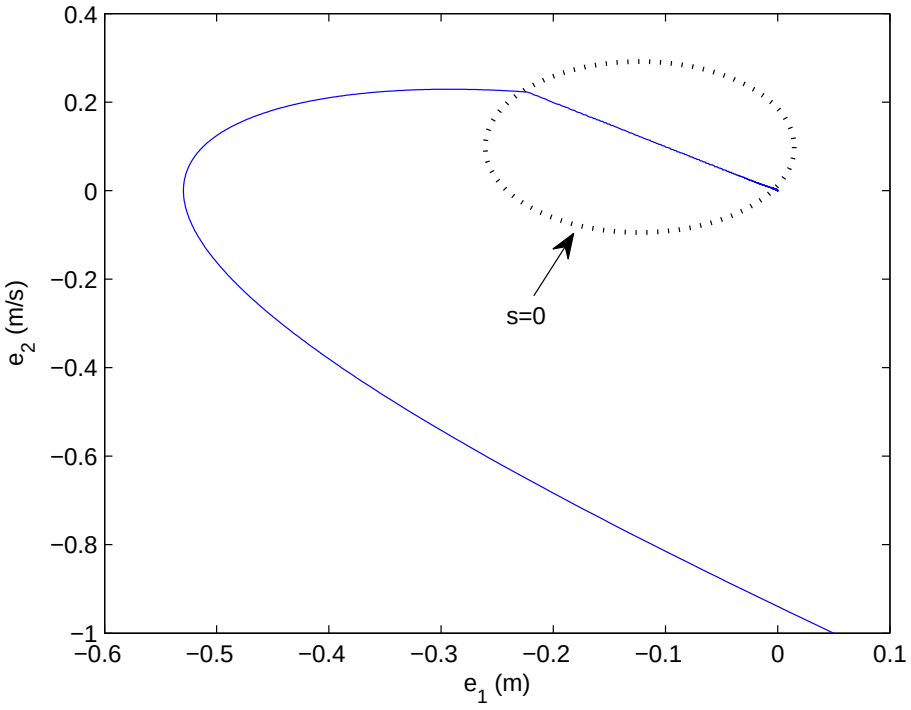

Figure 2.6: Phase portrait of error states

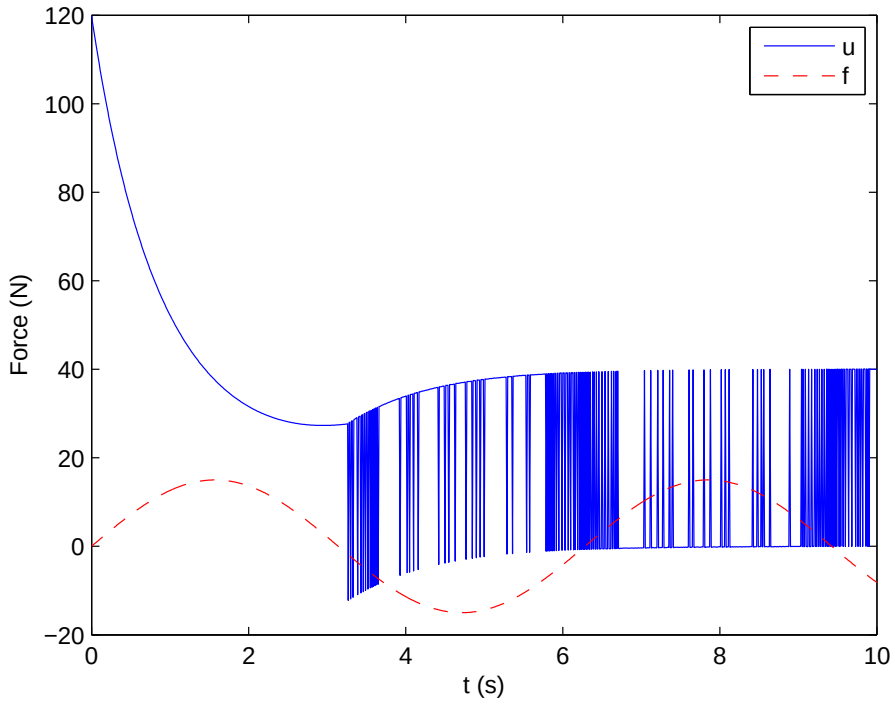

Figure 2.7: Control input and disturbance with time

2.3 Conclusion

Most of the models reviewed in Section 2.1 are used to study a set of phenomena occurring in the UCG reactor, and the outcome of the theoretical investigations is at the best validated against laboratory experiments. Only in few cases the results of the solved model are compared with a UCG field test. It is also detailed in Section 2.2 that these models can not be used for the control of UCG process, unless they are modified.

The objective of this research work is two fold:

1. Development of a computer model for UCG, which can predict the composition of the product gas in response to various operating conditions for field scale tests, conducted by UCG project Thar.

2. Development of a model based control of UCG process, which can increase its performance by providing a constant desired heating value of the product gas over a longer period of time.

The first objective demands an accurate model of the process, which results in complexity of its mathematical equations. While for control design a relatively simpler model is required. Therefore, a compromise is made between both requirements, and the 1D packed bed model of [39] is selected to fulfill both research aims. The complexity of the model is moderate, as it ignores multidimensional phenomena occurring in the UCG reactor and its surroundings. Importantly the model is capable of predicting product gas composition as a function of operating conditions and coal properties. The model is solved for the underground gasifiction of Lignite B coal of Thar in Chapter 3, which yields time and length profiles of solution variables. The accuracy of the model is increased by optimizing some uncertain input parameters in Chapter 4 and the robust SMC is designed for the process in Chapter 5.

CHAPTER 3

Computer Model of UCG Process

This chapter gives a detail description of the computer model developed for the in-situ gasification of the Block V of Thar coal field. This model can assist the actual field trials conducted by UCG project Thar and in the subsequent control of the process. The model is capable of predicting time and space profiles of some important parameters, such as, solid and gas temperatures, densities of coal and char, concentrations of different gases and rates of important chemical reactions in response to various operating conditions and coal properties. Most of these parameters are either impossible or very expensive to measure. The model also gives information about the movement of pyrolysis and reaction fronts, which can be further used to predict the life of the UCG reactor.

The UCG reactor model which incorporates the 1D packed bed model of [39] and parametrization of the Thar UCG setup is given in Section 3.1, the strategy adopted for numerical solution of the reactor model is detailed in Section 3.2. The capabilities of the solved model are presented in Section 3.3, the effect of varying different operating conditions on the UCG process is discussed in Section 3.4 and the chapter is concluded in Section 3.5.

3.1 UCG reactor model

A typical schematic of UCG process is shown in Fig. 3.1. The coal seam is located between the overburden and underburden rocks. The UCG reactor is contained in a cavity within the coal seam, which evolves with time as the process of gasification proceeds. The underground water reaches the reactor through the cracks in the strata above the coal seam, and participates in the gasification process.

The salient features and assumptions considered in the model are listed below. These assumptions help to reduce the computational complexity associated with the numerical solution of the reactor model.

- UCG reactor model is comprised of eight gases: CO, CO_2, H_2, H_2O, CH_4, N_2, O_2 and tar, and two solids: coal and char. The pseudo specie tar

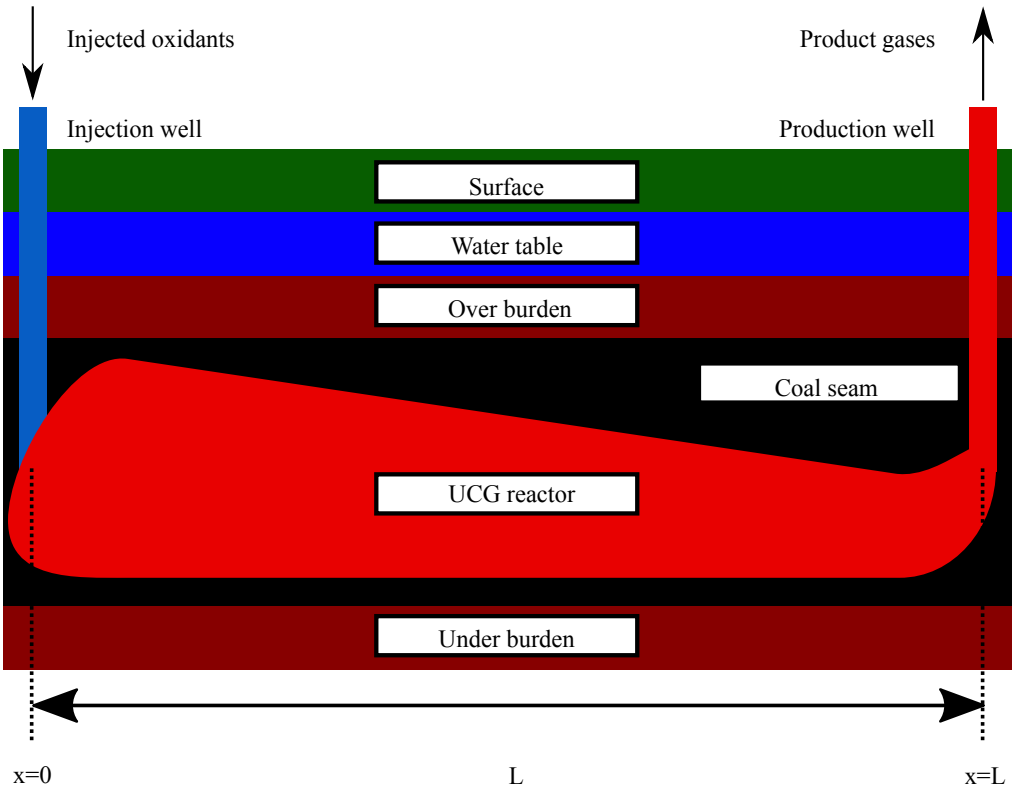

Figure 3.1: Schematic of UCG reactor with surrounding environment

is used to maintain the stoichiometric balance of coal pyrolysis reaction. Moreover, the small amount of higher hydrocarbons produced during the gasification of coal is also included in tar.

- The flow rate of the injected air is the input, while the heating value of the product gas is the output of the model.
- There are separate equations for energy and mass balances of gases and solids. These equations are derived from the fundamental conservation laws of energy and mass
- 1D geometry is assumed for the model, which ignores some important in-situ phenomena, such as, growth of the UCG cavity, thermomechanical properties of overburden and heat loss through adjacent coal seam. But these assumptions are important for model simplifications.
- A set of six important chemical reactions is used to describe the chemical kinetics of the process, which include coal pyrolysis, four heterogeneous

(char-gas) reactions and one homogeneous (gas-gas) reaction.

- Heat source generated from chemical reactions is written separately for solids and gases, which neglects detailed interaction at the point of reaction between the two phases.

- There is a large difference in characteristic times of solids and gases, e.g., the gas velocity ranges from $36 \rightarrow 360$ m/hr, while the rate of coal burning is only $0.1 \rightarrow 0.2$ m/hr. Therefore, it can be assumed that the gas phase reaches steady state before any significant change occurs in solids. This assumption is formally known as pseudo/quasi steady state approximation. Due to this approximation the gas phase equations are only ODEs in length domain, because all the conductive transport is lumped in solid phase and accumulation terms are neglected in the gas equations.

- Coal seam is assumed to be a porous medium, and Darcy's law is used as momentum balance for gas phase.

3.1.1 Model equations

3.1.1.1 Mass balance of solids

The effect of different chemical reactions on the rate of change of solid density distribution is described by Eq. (3.1).

$$\frac{\partial \rho_i}{\partial t} = M_i \sum_{j=1}^{6} a_{s_{ij}} R_j \tag{3.1}$$
$$\rho_i(0,x) = \rho_{i_0}(x), \quad 0 \leq x \leq L$$

where ρ_i is the density of ith solid (kg/cm^3) in point (t,x), a_{sij} is the stoichiometric coefficient of solid i in reaction j, R_j is the rate of reaction j (mol/cm^3/s), M_i is the molecular weight of solid component i (kg/mol) and t and x are variables for time (s) and length (cm) respectively, $\rho_{i_0}(x)$ is the initial density distribution of solid i and L is the length of the reactor (cm).

3.1.1.2 Solid phase energy balance

The parabolic heat Eq. (3.2) shows that how does solid temperature distribution change with time due to heat transfer through conduction (between adjacent coal layers) and convection (inter phase heat transfer caused by the movement of gases), and heat of chemical reactions.

$$\begin{aligned}
&\frac{\partial T_s}{\partial t} = \frac{\frac{\partial}{\partial x}\left[(1-\phi)k\frac{\partial T_s}{\partial x}\right] + h(T-T_s) - H_s}{C_s} \\
&T_s(0,x) = T_{s_0}(x), \quad 0 \le x \le L \\
&\frac{\partial T_s}{\partial x}(t,0) = \frac{\partial T_s}{\partial x}(t,L) = 0, \quad t \ge 0 \\
&C_s = \sum_{i=1}^{2} \rho_i c_{s_i} \\
&H_s = \sum_{j=1}^{5} \Delta H_j R_j
\end{aligned} \tag{3.2}$$

where T_s is the solid temperature (K) in point (t,x), T is the gas temperature (K), ϕ is the coal bed porosity, k is the effective thermal conductivity of solids (cal/cm/s/K), h is the heat transfer coefficient (cal/s/K/cm^3), $T_{s_0}(x)$ is the initial distribution of solid temperature, C_s is the total solid phase heat capacity (cal/K/cm^3), H_s is the solid phase heat source (cal/s/cm^3), c_{s_i} is the specific heat capacity of component i (cal/g/K) and ΔH_j is the heat of the reaction for heterogeneous (solid-gas) reactions (cal/mol).

The values of spatial derivatives at $x = 0$ and $x = L$ in Eq. (3.2) constitute the Neumann type boundary conditions. The homogeneous boundary conditions mean that the ends of the reactor $x = 0$ and $x = L$ are isolated and no heat flux can enter or leave the reactor.

3.1.1.3 Gas phase mass balance

The concentration of a gas is changed when it moves from inlet $x = 0$ to outlet $x = L$. The change is brought by the chemical reactions and superficial gas phase

velocity. In porous media, the superficial velocity is a hypothetical velocity of gas phase considered over whole cross sectional area by ignoring the solid phase [118]. Gas phase diffusion is neglected in Eq. (3.3).

$$\frac{dC_i}{dx} = \frac{1}{v_g}\left(-C_i\frac{dv_g}{dx} + \sum_{j=1}^{6} a_{ij}R_j\right) \tag{3.3}$$

where C_i is the concentration of ith gas (mol/cm^3), v_g is superficial gas velocity (cm/s) and a_{ij} is the stoichiometric coefficient of gas i in reaction j (a_{ij} is positive for product gases and negative for reactants).

3.1.1.4 Gas phase energy balance

The gas temperature in Eq. (3.4) is only affected by convective heat transfer effect and heat of water gas shift reaction. The accumulation terms are neglected due to quasi-steady state assumption.

$$\begin{aligned}
\frac{dT}{dx} &= -\frac{1}{v_g C_g}\left[h_T(T-T_s) + H_g\right] \\
C_g &= \sum_{i=1}^{8} C_i c_{p_i} \\
H_g &= \Delta H_6 R_6
\end{aligned} \tag{3.4}$$

where c_{p_i} is the molar heat capacity of gas i (cal/mol/K)

3.1.1.5 Momentum balance equation

The solid species in the model are immovable, so momentum balance given by Eq. (3.5) is only written for gas phase, using Darcy's law.

$$\frac{dP}{dx} = -\frac{v_g \mu}{2K} \tag{3.5}$$

where P is the gas pressure (atm), K is the gas permeability coefficient (cm^2), and μ is the viscosity (Pa.s).

3.1.1.6 Equation of state

Ideal gas law is used to relate the gas phase pressure, temperature and concentration in Eq. (3.6).

$$C_T = \frac{P}{RT} \qquad (3.6)$$
$$C_T = \sum_{i=1}^{8} C_i$$

where R is the universal gas constant (cm^3.atm/mol/K) and C_T is the sum of concentration of all the gases

3.1.1.7 Superficial gas phase velocity

The concentrations of all the gases are obtained from Eq. (3.3), which are substituted in Eq. (3.6) to yield Eq. (3.7).

$$\frac{d}{dx}v_g = -\frac{v_g}{P}\frac{dP}{dx} + \frac{v_g}{T}\frac{dT}{dx} + \frac{RT}{P}\sum_{i=1}^{8}\sum_{j=1}^{6} a_{ij}R_j \qquad (3.7)$$

3.1.2 Model parametrization

3.1.2.1 Thermal conductivity of solids

The effective thermal conductivity of solids is given by Eq. (3.8) [39], which takes into account conduction in solids and radiant transfer and conduction through fluid adjacent to solids.

$$k = \frac{1-\phi}{\left(\frac{1}{\lambda_s}\right) + \left(\frac{1}{25\lambda_g + dL_s}\right)} + \phi dL_v \qquad (3.8)$$
$$L_s = 3.16 \times 10^{-12} {T_s}^3$$
$$L_v = \frac{5.4 \times 10^{-12} {T_s}^3}{1 - 0.125\left(\frac{\phi}{1-\phi}\right)}$$

where λ_s and λ_g are thermal conductivities of char and H_2 (cal/s/K/cm), respectively.

3.1.2.2 Interphase transport coefficients

The inter-phase heat transfer coefficient h determines how quickly the heat transfers from one phase to another by the process of convection. The heat transfer coefficient is given by Eq. (3.9) [39].

$$h = 3C_g u_g^{0.49} T^{1.5} \left[\frac{6(1-\phi)}{d}\right]^{0.51} \times 10^{-5} \tag{3.9}$$

where d is particle diameter (cm).

The inter-phase mass transfer coefficient used in the reaction rates is given by Eq. (3.10) [39].

$$k_y = 0.1 h_T \tag{3.10}$$

3.1.2.3 Chemical reactions and their kinetics

A large number of chemical reactions take place in an actual UCG process. But, in order to simplify the reaction kinetics, only six important chemical reactions are considered, which are listed in Table 3.1.

It is assumed that coal and char have molecular formulas CH_aO_b and $CH_{\bar{a}}O_{\bar{b}}$ respectively. The values of a, b, $\bar{a}$, and $\bar{b}$ are determined by coal and char ultimate analysis for the Lignite B coal of Thar coal field. The molecular formula for tar is C_9H_c, where the hydrogen content c is chosen to balance the coal pyrolysis reaction. It is arbitrarily assumed that tar has nine carbon atoms.

The coal pyrolysis is an irreversible reaction, which involves the decomposition of coal into numerous gases and char. Reactions $2-5$ are heterogeneous reactions representing char oxidation and various gasification reactions. The water gas shift reaction is homogeneous as both the reactants are gases.

Table 3.1: Chemical reactions considered in the model

Sr	Chemical equations
1.	**Coal pyrolysis**
	$CH_aO_b \rightarrow \lvert a_{s_{2,1}}\rvert CH_{\bar{a}}O_{\bar{b}} + \lvert a_{1,1}\rvert CO + \lvert a_{2,1}\rvert CO_2 + \lvert a_{3,1}\rvert H_2 + \lvert a_{4,1}\rvert H_2O + \lvert a_{5,1}\rvert CH_4 + \lvert a_{8,1}\rvert C_9H_c$
2.	**Char oxidation**
	$CH_{\bar{a}}O_{\bar{b}} + \lvert a_{7,2}\rvert O_2 \rightarrow \lvert a_{2,2}\rvert CO_2 + \lvert a_{4,2}\rvert H_2O$
3.	**Steam gasification**
	$CH_{\bar{a}}O_{\bar{b}} + \lvert a_{4,3}\rvert H_2O \rightleftharpoons \lvert a_{1,3}\rvert CO + \lvert a_{3,3}\rvert H_2$
4.	**CO_2 gasification**
	$CH_{\bar{a}}O_{\bar{b}} + \lvert a_{2,4}\rvert CO_2 \rightleftharpoons \lvert a_{1,4}\rvert CO + \lvert a_{4,4}\rvert H_2O$
5.	**Methanation**
	$CH_{\bar{a}}O_{\bar{b}} + \lvert a_{3,5}\rvert H_2 \rightleftharpoons \lvert a_{1,5}\rvert CO + \lvert a_{5,5}\rvert CH_4$
6.	**Water gas shift reaction**
	$\lvert a_{1,6}\rvert CO + \lvert a_{4,6}\rvert H_2O \rightleftharpoons \lvert a_{2,6}\rvert CO_2 + \lvert a_{3,6}\rvert H_2$

3.1.2.3.1 Calculation of stoichiometric coefficients

Table 3.2: Input parameters for formulating stoichiometric coefficients

Sr	Parameter	Description
1.	a, b	Coal composition parameters
2.	$\bar{a}$, $\bar{b}$	Char composition parameters
3.	$a_{s_{2,1}}$	Moles of char per mole of coal
4.	$a_{3,1}$	Moles of H_2 per mole of coal
5.	$a_{5,1}$	Moles of CH_4 per mole of coal
6.	s	Atoms of C in coal which become atoms of C in TAR
7.	r	H to C ratio of TAR

The stoichiometric coefficients $a_{i,j}$ in Table 3.1 are calculated using Eq. (3.11) by using coal, char and tar composition parameters in Table 3.2.

$$
\begin{aligned}
\left|a_{4,1}\right| &= \frac{1}{2}\left(a-\bar{a}a_{s_{2,1}}-2a_{3,1}-4a_{5,1}-rs\right) \\
\left|a_{2,1}\right| &= b-1+a_{s_{2,1}}\left(1-\bar{b}\right)-a_{4,1}+a_{5,1}+s \\
\left|a_{1,1}\right| &= 1-a_{s_{2,1}}-a_{2,1}-a_{5,1}-s \\
\left|a_{8,1}\right| &= \frac{s}{9} \\
\left|a_{4,2}\right| &= \frac{\bar{a}}{2} \quad = \quad \left|a_{4,4}\right| \\
\left|a_{7,2}\right| &= 1+\frac{\bar{a}}{4}-\frac{\bar{b}}{2} \\
\left|a_{3,3}\right| &= 1+\frac{\bar{a}}{2}-\bar{b} \quad = \quad \left|a_{2,4}\right| \\
\left|a_{4,3}\right| &= 1-\bar{b} \quad = \quad \left|a_{5,5}\right| \\
\left|a_{1,4}\right| &= 2+\frac{\bar{a}}{2}-\bar{b} \\
\left|a_{3,5}\right| &= 2-\frac{\bar{a}}{2}-2\bar{b} \\
\left|a_{1,5}\right| &= \bar{b}
\end{aligned}
\tag{3.11}
$$

All the other coefficients in Table 3.1 have a unity magnitude.

The rates of chemical reactions in Table 3.1 are given below, which are taken from [39]

3.1.2.3.2 Coal pyrolysis reaction rate

$$
R_1 = 5\frac{\rho_1}{M_1}\exp\left(\frac{-6039}{T_s}\right) \tag{3.12}
$$

where M_1 is the molecular weight of coal.

3.1.2.3.3 Char oxidation reaction rate

$$
\begin{aligned}
R_2 &= \frac{1}{\frac{1}{R_{c_2}}+\frac{1}{k_y y_7}} \\
R_{c_2} &= \frac{9.55\times 10^8 \rho_2 y_7 P \exp\left(\frac{-22142}{\tilde{T}}\right)\tilde{T}^{-0.5}}{M_2}
\end{aligned}
\tag{3.13}
$$

$$\tilde{T} = \beta T_s + (1-\beta)\, T$$

where M_2 is the molecular weight of char and $y_7 = C_7/C_T$ is the molar fraction of O_2. For simulations $\beta = 1$.

3.1.2.3.4 Steam Gasification Reaction Rate

$$\begin{aligned}
R_3 &= \begin{cases} \frac{1}{\frac{1}{R_{c_3}} + \frac{1}{k_y y_4}}, & \text{if } y_4 - \left(\frac{y_1 y_3}{K_{E_3}}\right) > 0 \\ \frac{1}{\frac{1}{R_{c_3}} - \frac{1}{k_y y_1}}, & \text{if } y_4 - \left(\frac{y_1 y_3}{K_{E_3}}\right) < 0 \end{cases} \\
R_{c_3} &= \frac{{R_{c_3}}^+}{y_4}\left(y_4 - \frac{y_1 y_3}{K_{E_3}}\right) \\
{R_{c_3}}^+ &= \frac{\rho_2 y_4^2 P^2 \exp\left(5.052 - \frac{12908}{\tilde{T}}\right)}{M_2\left[y_4 P + \exp\left(-22.216 + \frac{24880}{\tilde{T}}\right)\right]^2}
\end{aligned} \tag{3.14}$$

where $y_1 = C_1/C_T$, $y_3 = C_3/C_T$ and $y_4 = C_4/C_T$ are molar fractions of CO, H_2 and H_2O respectively, and K_{E_3} is equilibrium constant for steam gasification reaction.

3.1.2.3.5 CO_2 gasification reaction rate

$$\begin{aligned}
R_4 &= \begin{cases} \frac{1}{\frac{1}{R_{c_4}} + \frac{1}{k_y y_2}}, & \text{if } y_2 - \left(\frac{y_1^2}{K_{E_4}}\right) < 0 \\ \frac{1}{\frac{1}{R_{c_4}} - \frac{2}{k_y y_1}}, & \text{if } y_2 - \left(\frac{y_1^2}{K_{E_4}}\right) > 0 \end{cases} \\
R_{c_4} &= \frac{{R_{c_4}}^+}{y_2}\left(y_2 - \frac{y_1^2}{K_{E_4}}\right) \\
{R_{c_4}}^+ &= \frac{1.15 \times 10^4 \rho_2 y_2 P \exp\left(\frac{-23956}{\tilde{T}}\right)}{M_2 D} \\
D &= 1 + 0.014 y_1 P \exp\left(\frac{7549}{\tilde{T}}\right) + 0.21 y_2 P \exp\left(\frac{3171}{\tilde{T}}\right)
\end{aligned} \tag{3.15}$$

where $y_2 = C_2/C_T$ is the molar fraction of CO_2, and K_{E_4} is equilibrium constant for CO_2 gasification reaction.

3.1.2.3.6 Methanation reaction rate

$$R_5 = \begin{cases} \frac{1}{\frac{1}{R_{c_5}} + \frac{2}{k_{yy_3}}}, & \text{if } y_3^2 - \left(\frac{y_5}{K_{E_5}}\right) > 0 \\ \frac{1}{\frac{1}{R_{c_5}} - \frac{1}{k_{yy_5}}}, & \text{if } y_3^2 - \left(\frac{y_5}{K_{E_5}}\right) < 0 \end{cases} \tag{3.16}$$

$$R_{c_5} = \frac{{R_{c_5}}^+}{y_3^2}\left(y_3^2 - \frac{y_5}{K_{E_5}}\right)$$

$${R_{c_5}}^+ = \frac{\rho_2 y_3^2 P^2 \exp\left(2.803 - \frac{13673}{\tilde{T}}\right)}{M_2\left[1 + y_3 P \exp\left(-10.452 + \frac{11698}{\tilde{T}}\right)\right]}$$

where $y_5 = C_5/C_T$ is molar fraction of CH_4, and K_{E_5} is equilibrium constant for methanation reaction.

3.1.2.3.7 Water Gas Shift Reaction Rate

$$R_6 = \begin{cases} \frac{1}{\frac{1}{R_{c_6}} + \frac{2}{k_{yy_1}}}, & \text{if } C_1 C_4 - \left(\frac{C_2 C_3}{K_{E_6}}\right) > 0 \\ \frac{1}{\frac{1}{R_{c_6}} - \frac{1}{k_{yy_2}}}, & \text{if } C_1 C_4 - \left(\frac{C_2 C_3}{K_{E_6}}\right) < 0 \end{cases} \tag{3.17}$$

$$R_{c_6} = \frac{{R_{c_6}}^+}{C_1 C_4}\left(C_1 C_4 - \frac{C_2 C_3}{K_{E_6}}\right)$$

$${R_{c_6}}^+ = 3 \times 10^7 \phi C_1 C_4 \exp\left(\frac{-7250}{\tilde{T}}\right)$$

where C_1, C_2, C_3 and C_4 are concentrations of CO, CO_2, H_2 and H_2O respectively, and K_{E_6} is equilibrium constant for water gas shift reaction.

3.1.2.4 Thermodynamic properties of solids and gases

Constant values are assigned to the heat of the reactions ΔH_j and equilibrium constants of the reaction rates K_{E_i}. The specific heat capacity of coal is also constant, while that of char is given by Eq. (3.18) [39].

$$c_{s_2} = M_2\left(\bar{c_{s_g}} + 0.88\bar{a} + 5.8\bar{b}\right) \tag{3.18}$$

where $\bar{c_{s_g}}$ is molar heat capacity of graphite (cal/g/mol/K).

The specific heat capacities of gases are functions of only gas temperature [119], there polynomials are given by:

$$
\begin{aligned}
&CO : cp_1 = 0.0015T + 6.39 \\
&CO_2 : cp_2 = -0.0000038T^2 + 0.010T + 6.30 \\
&H_2 : cp_3 = 0.00000069T^2 - 0.00057T + 7.10 \\
&H_2O\,(g) : cp_4 = 0.0028T + 6.97 \\
&CH_4 : cp_5 = -0.0000048T^2 + 0.019T + 2.65 \\
&N_2 : cp_6 = 0.0014T + 6.38 \\
&O_2 : cp_7 = -0.0000012T^2 + 0.0037T + 5.90 \\
&tar : cp_8 = c_{s_1} - c_{s_2}
\end{aligned}
$$

3.2 Method of solution

The UCG reactor model yields two sets of equations, a set of eleven first order gas phase ODEs in length domain: Eq. (3.3) for all gases, and Eqs. (3.4), (3.5) and (3.7), and a set of three solid phase PDEs in time and space: Eq. (3.1) for each solid and Eq. (3.2). These equations can not be solved analytically, because they are highly nonlinear and strongly coupled. The coupling and nolinearity is introduced by the model parameters given in Section (3.1). Therefore, both sets of equations are numerically solved to yield 2D solution for every dependent variable as a function of simulation time and length of the reactor. The solid phase equations are discretized before they are solved numerically.

3.2.1 Discrete equations for solids

The finite difference method is used for the numerical solution of the solid Eqs. (3.1) and (3.2), which yields an approximate solution for $\rho_i\,(t,x)$ and $T_s\,(t,x)$, at a finite set of t and x. It is assumed that the discrete points in t and x are uni-

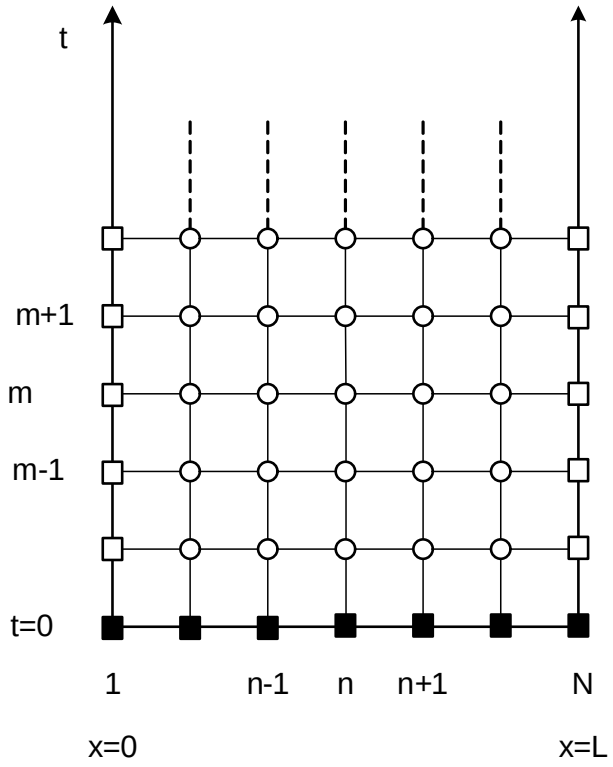

Figure 3.2: Mesh on a semi infinite strip used for the solution of solid equations: $z(t,x) = [\rho_i \quad T_s]^T$. The black squares along $t = 0$ represent the initial distribution: $z(t = 0,x)$, while the white squares along $x = 0$ lines represent the boundary values: $z(t,x = 0)$. The finite difference approximation is computed on the white circles.

formly spaced over the intervals $0 \leq t \leq t_{max}$ and $0 \leq x \leq L$ respectively, where t_{max} (s) is the maximum time for the simulation. The solution domain for discrete solid equations is shown in Fig. 3.2.

The discrete points $x_n \in x$ and $t_m \in t$ are given by Eqs. (3.19) and (3.20) respectively.

$$x_n = (n-1)\Delta x, \quad n = 1,2,\ldots N \tag{3.19}$$

$$\Delta x = \frac{L}{N-1}$$

$$t_m = (m-1)\Delta t, \quad m = 1,2,\ldots M \tag{3.20}$$

$$\Delta t = \frac{t_{max}}{M-1}$$

where N and M are total number of spatial and temporal nodes respectively, Δx is the step size for length and Δt is the step size for time.

3.2.1.1 Finite difference approximations for partial derivatives

The general form for the discrete equivalents of the continuous partial derivatives used in the numerical solution of the solid equations are given by Eqs. (3.21), (3.22) and (3.23). The first order partial derivatives are approximated with forward difference method, while the second order central difference is used for the second order partial derivative.

$$\left.\frac{\partial f}{\partial t}\right|_{t_m} \approx \frac{f_n^{m+1} - f_n^m}{\Delta t} \tag{3.21}$$

$$\left.\frac{\partial f}{\partial x}\right|_{x_n} \approx \frac{f_{n+1}^m - f_n^m}{\Delta x} \tag{3.22}$$

$$\left.\frac{\partial^2 f}{\partial x^2}\right|_{x_n} \approx \frac{f_{n-1}^m - 2f_n^m + f_{n+1}^m}{\Delta x^2} \tag{3.23}$$

where $f(t,x)$ is an arbitrary function

3.2.1.2 Discrete mass balance

The mass balance in Eq. (3.1) is a simple PDE, which involves only one partial time derivative. The forward difference (FD) method is used to discretize the Eq. (3.24).

$$\begin{aligned} \frac{\rho_{i_n}^{m+1} - \rho_{i_n}^m}{\Delta t} &= M_i \sum_{j=1}^{6} a_{s_{ij}} R_{j_n}^m \\ \rho_{i_n}^{m+1} &= \underbrace{\Delta t M_i \sum_{j=1}^{6} a_{s_{ij}} R_{j_n}^m + \rho_{i_n}^m}_{S} \\ \rho_{i_n}^1 &= \rho_{i_0}(n) \end{aligned} \tag{3.24}$$

where $\rho_{i_n}^1$ corresponds to the initial value ($m = 1$ corresponds to $t = 0$, see Fig. 3.2) of solid density at n.

3.2.1.3 Discrete solid temperature

The forward time centered space (FTCS), a finite difference technique [120] is used to solve Eq. (3.2). This technique is not unconditionally stable like its companion finite difference techniques: backward time centered space (BTCS) and Crank Nicolson [120]. However, FTCS method has two advantages over its finite difference counterparts, it is easier to implement and it offers reduced computational time. The computational cost matters a lot for the numerical solution of the complex UCG reactor model over a longer period of time. Therefore, solid temperature is discretized using FTCS scheme, and the selection of Δt and Δx enures the convergence of the solution.

By using the discrete derivatives in Eqs. (3.21), (3.22) and (3.23), the updated value of solid temperature: $T_{s_n}^{m+1}$ is given by Eq. (3.25).

$$\begin{aligned}
\frac{T_{s_n}^{m+1}-T_{s_n}^{m}}{\Delta t} &= \frac{(1-\phi)}{\Delta x^2 C_{s_n^m}}\left[k_n^m\left(T_{s_{n-1}}^m-2T_{s_n}^m+T_{s_{n+1}}^m\right)+\left(T_{s_{n+1}}^m-T_{s_n}^m\right)\left(k_{n+1}^m-k_n^m\right)\right] \\
&\quad+\frac{h_n^m\left(T_n^m-T_{s_n}^m\right)}{C_{s_n^m}}-\frac{H_{s_n}^m}{C_{s_n^m}} \\
T_{s_n}^{m+1} &= \frac{\Delta t\,(1-\phi)}{\Delta x^2 C_{s_n^m}}\left[k_n^m\left(T_{s_{n-1}}^m-T_{s_n}^m\right)+k_{n+1}^m\left(T_{s_{n+1}}^m-T_{s_n}^m\right)\right]+\frac{\Delta t h_n^m\left(T_n^m-T_{s_n}^m\right)}{C_{s_n^m}} \\
&\quad-\frac{\Delta t H_{s_n}^m}{C_{s_n^m}}+T_{s_n}^m
\end{aligned} \tag{3.25}$$

where porosity of the coal bed ϕ is constant, $C_{s_n^m}$ and h_n^m are functions of $\rho_{i_n^m}$ and T_n^m respectively, and k_n^m and $H_{s_n}^m$ depend on $T_{s_n}^m$. The value T_n^m is obtained from the solution of Eq. (3.4).

In order to obtain the values $T_{s_1}^{m+1}$ and $T_{s_n}^{m+1}$, the homogeneous Neumann type boundary conditions in Eq. (3.2) are discretized by forward difference method to yield Eq. (3.26).

$$\begin{aligned}
&\frac{T^m_{s_{n+1}} - T^m_{s_n}}{\Delta x} = 0 \\
&T^m_{s_{n+1}} = T^m_{s_n} \\
&T^m_{s_1} = T^m_{s_2}, \qquad\qquad n = 1 \implies x = 0 \\
&T^m_{s_n} = T^m_{s_{n-1}}, \qquad\qquad n = N-1 \implies x = L
\end{aligned} \tag{3.26}$$

Now the boundary values at advanced time can be computed by substituting $n = 1$ and $n = L$ in Eq. (3.25).

$$\begin{aligned}
T^{m+1}_{s_1} &= \frac{\Delta t\,(1-\phi)}{\Delta x^2 C_{s^m_1}} \left[k^m_1 \left(T^m_{s_0} - T^m_{s_1}\right) + k^m_2 \left(T^m_{s_2} - T^m_{s_1}\right)\right] + \frac{\Delta t h^m_1 \left(T^m_1 - T^m_{s_1}\right)}{C_{s^m_1}} \\
&\quad - \frac{\Delta t H^m_{s_1}}{C_{s^m_1}} + T^m_{s_1} \\
T^{m+1}_{s_n} &= \frac{\Delta t\,(1-\phi)}{\Delta x^2 C_{s^m_n}} \left[k^m_n \left(T^m_{s_{n-1}} - T^m_{s_n}\right) + k^m_{n+1} \left(T^m_{s_{n+1}} - T^m_{s_n}\right)\right] + \frac{\Delta t h^m_n \left(T^m_n - T^m_{s_n}\right)}{C_{s^m_n}} \\
&\quad - \frac{\Delta t H^m_{s_n}}{C_{s^m_n}} + T^m_{s_n}
\end{aligned}$$

where the fictitious values $T^m_{s_0}$ and $T^m_{s_{n+1}}$ can be found by substituting $n = 0$ and $n = N$ in Eq. (3.26) respectively.

3.2.1.4 Computation of solid solutions on the mesh grid

In order to show the progression of the solid solutions on the mesh grid in Fig. 3.2, a single molecule is shown for the computation of both $\rho^{m+1}_{i_n}$ and $T^{m+1}_{s_n}$ in Fig. 3.3.

The FD scheme for obtaining updated solid density is presented in Fig. 3.3(a). In order to compute $\rho^{m+1}_{i_n}$, it is required to evaluate S in Eq. (3.24) at only one point (m,n). For the FTCS method in Fig. 3.3(b), the updated solution $T^{m+1}_{s_n}$ requires the information for current time m at three adjacent locations $(m,n-1)$, (m,n) and $(m,n+1)$.

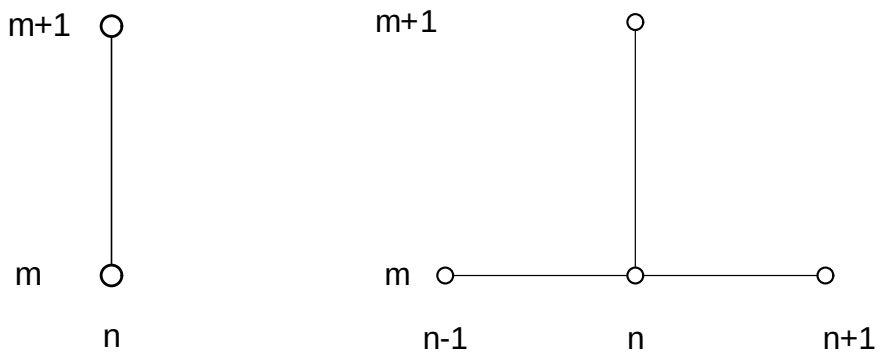

(a) Forward difference (b) Forward time centered space

Figure 3.3: Computational molecules for finite difference approximations of solid phase equations.

3.2.2 System of gas equations

The first order gas phase ODEs with boundary conditions are given below:

$$\frac{dC_i}{dx} = \frac{1}{v_g}\left(-C_i\frac{dv_g}{dx} + \sum_{j=1}^{6} a_{ij}R_j\right)$$

$$C_i^T\,(x=0) = \begin{bmatrix} 0 & 0 & 0 & C_{4_0} & 0 & C_{6_0} & C_{7_0} & 0 \end{bmatrix}$$

$$C_{4_0} = \begin{cases} 0, & \text{ignition} \\ \lambda C_{7_0}, & \text{gasification} \end{cases}$$

$$\frac{dT}{dx} = -\frac{1}{u_g C_g}\left[h_T(T-T_s) + H_g\right]$$

$$T\,(x=0) = T_0$$

$$\frac{dP}{dx} = -\frac{u_g\mu}{2K}$$

$$P\,(x=0) = P_0$$

$$\frac{d}{dx}u_g = -\frac{u_g}{P}\frac{dP}{dx} + \frac{u_g}{T}\frac{dT}{dx} + \frac{RT}{P}\sum_{i=1}^{8}\sum_{j=1}^{6} a_{ij}R_j$$

$$v_g\,(x=0) = \frac{u}{\sum_{i=1}^{8} C_i\,(x=0)}$$

where the elements of $C_i\,(x=0)$ represent initial concentration of CO, CO_2, H_2, H_2O (g), CH_4, N_2, O_2 and tar respectively, λ is the steam to oxygen ratio at

$x = 0$ and u is the flow rate of the injected air (mol/cm^2/s). The gas phase equations are solved simultaneously as a boundary value problem, marching from inlet $x = 0$ to outlet $x = L$. The dynamics of the UCG reactor change abruptly around a location, along the length of the reactor, where incoming O_2 reacts with char. This location is formally known as the *reaction front*. Therefore, the system of equations become stiff around the reaction front, which generally requires a solver with very small step size, otherwise the solution does not converge. Apart from the reaction front, the dynamics of the gas phase change rather slowly, and a solver with relatively bigger step size can be used. In this scenario a fixed step solver increases the computational complexity, because it keeps a smaller step size even for the coarse zone (region along reactor length where dynamics are slow). Therefore, the gas phase equations are solved using *TR-BDF2,* an implicit Runge-Kutta algorithm [121], which is a variable step solver. The step size for this solver is adaptive, smaller for the refined zone (region around the reaction front) and bigger for the coarse zone.

3.2.3 Overall solution strategy

The UCG reactor model is solved in MATLAB, according to the flow chart in Fig. 3.4 [122]. The solution starts by initializing coal parameters and solid phase equations and then solving gas phase system for generating its initial distributions. The initialization of solid temperature mimics ignition of coal bed, which is very critical for solution of the system. When solution progresses in time the solid phase system is updated first and then the gas phase system is advanced in time using the updated solution of solid phase system. Solid phase system uses reaction rates at current time $R(t,x)$, whereas the gas phase system uses the updated reaction rates $R(t+dt,x)$. The solution of the UCG reactor model evolves in both time and space. The change with time is brought by the solid phase PDEs, whereas the change in length domain is caused by the gas ODEs.

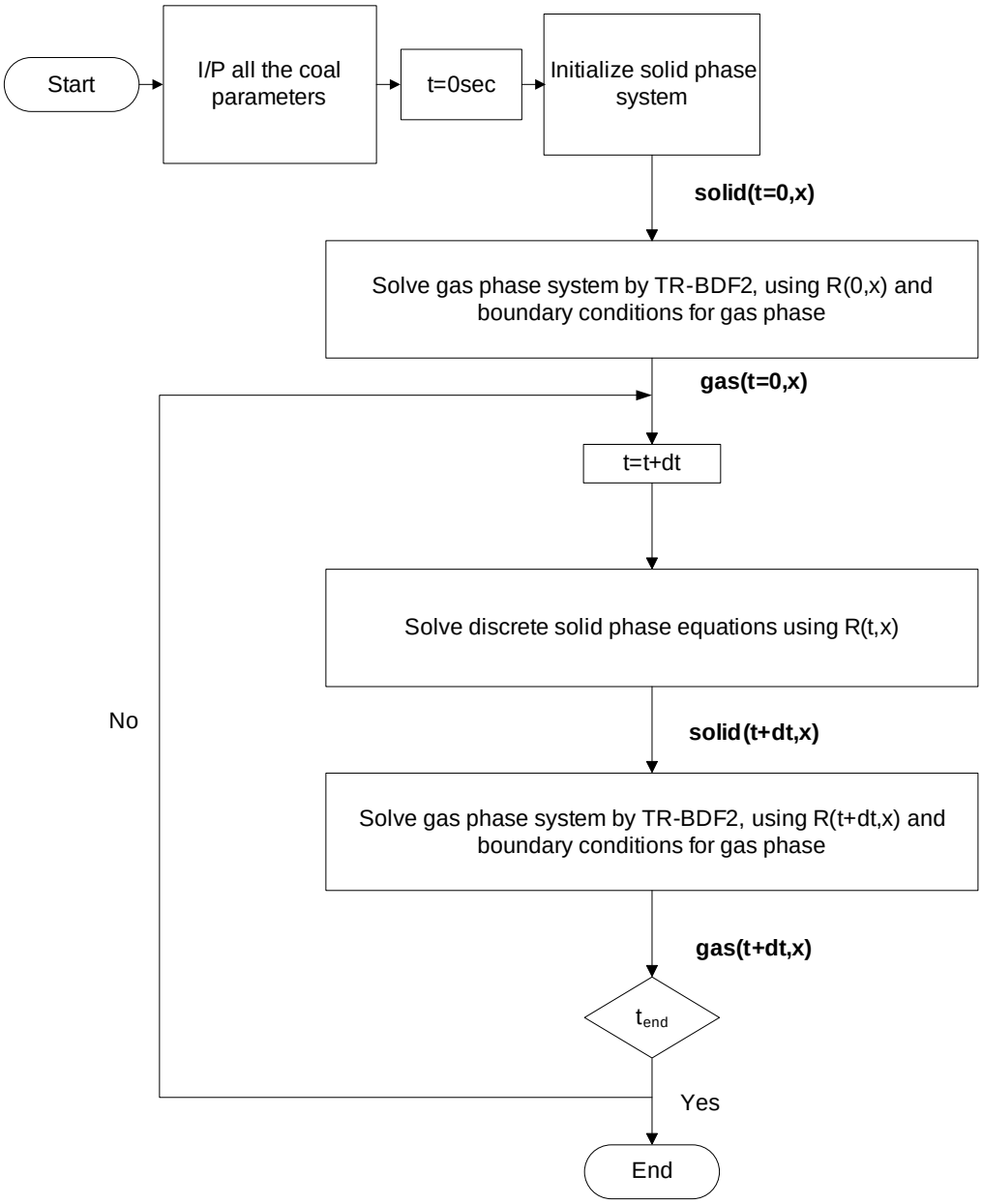

Figure 3.4: Solution strategy for the UCG reactor model

The model is simulated in the ignition phase for first 1000 s and afterwards in the gasification mode. The ignition phase acts as the initial condition for the gasification phase. During ignition, coal bed is heated to pyrolyze the coal into char, and to achieve a sufficient temperature for subsequent gasification reactions. Due to the absence of steam in the UCG reactor, the gasification reactions do not occur in the ignition phase. In gasification mode, an optimum amount of steam is required to facilitate the production of syngas. During the field trials,

the inlet gas does not contain any steam. This means water which intrudes into the UCG reactor from surrounding aquifers, and moisture contained in the coal converts into steam and assists the gasification reactions. The amount of water influx in to the UCG reactor can be controlled by varying the pressure in the reactor [123].

3.3 Model capabilities

The input parameters for the base case simulation are given in Table 3.3.

The simulations are performed for 24 hrs, and during this time the coal bed is only consumed up to 650 cm. Therefore, in order to better analyze the results, only the selected portion of the reactor is shown in the subsequent figures. The selected region highlights the fine details of the solution variables. Some important results of the model are discussed in subsequent paragraphs, which show that the solved model is capable of predicting some important parameters of the UCG process.

Fig. 3.5 shows the movement of length profiles of solid and gas temperatures with time. For all the given cases, gas temperature follows the solid temperature, the gas temperature increases if it is less than the solid temperature and it decreases if it is greater than solid temperature. The solid temperature profiles contain a lot of information, e.g. at 5 hrs the region where $T_s, T > 430$ K, is called the reaction zone, which is shown in Fig. 3.6. The left boundary of the reaction zone where T_s rises to its maximum value is known as the *reaction front* (shown in the zoomed portion of Fig. 3.6). It is the location where the system of equations become stiff. The sudden increase in T_s is due to the highly exothermic char oxidation reaction. The hump towards the right boundary of the reaction zone points to another important location, called as *pyrolysis front*. It is the location along the length of the reactor around which coal is pyrolyzed from the heat coming from the oxidation zone. The region before the reaction front is called rubble zone, while beyond pyrolysis front is the unreacted coal.

Table 3.3: Input data for the base case simulation

Parameter	**Value**
Coal type	Lignite B, Thar coal
Reactor length L	2500 cm
Permeability of coal K	150 D
Particle diameter d	1 cm
Coal bed porosity ϕ	0.2
Maximum simulation time t_{max}	24 hrs
Step size for time Δt	20 s
Step size for length Δx	1 cm (only for discrete solid equations)
Initial values for gas phase	
Flow rate of injected air u	$2 \times 10^{-4} mol/cm^2$/s
Mole fraction of O_2	0.21
Mole fraction of N_2	0.79
Steam to oxygen ratio λ	2.5
Concentration of steam C_{4_0}	$\begin{cases} 0, & \text{for ignition} \\ \lambda C_{7_0}, & \text{for gasification} \end{cases}$
Gas pressure P_0	6.1 atm
Gas temperature T_0	430 K
Initial solid distributions	
$\rho_{1_0}(x)$	$1.25, \quad 0 \leq x \leq L$
$\rho_{2_0}(x)$	$0, \quad 0 \leq x \leq L$
$T_{s_0}(x)$	$\begin{cases} 970x + 430, & \text{for } 0 \leq x \leq 1 \\ -107.7x + 1507.7, & \text{for } 1 < x \leq 10 \\ 430, & \text{for } 10 < x \leq L \end{cases}$

The reaction zone is shown in Fig. 3.6. For avoiding complexity in solution of the system, all the reversible reactions are considered to proceed in the forward direction only. All the reactions have different activation energies, so

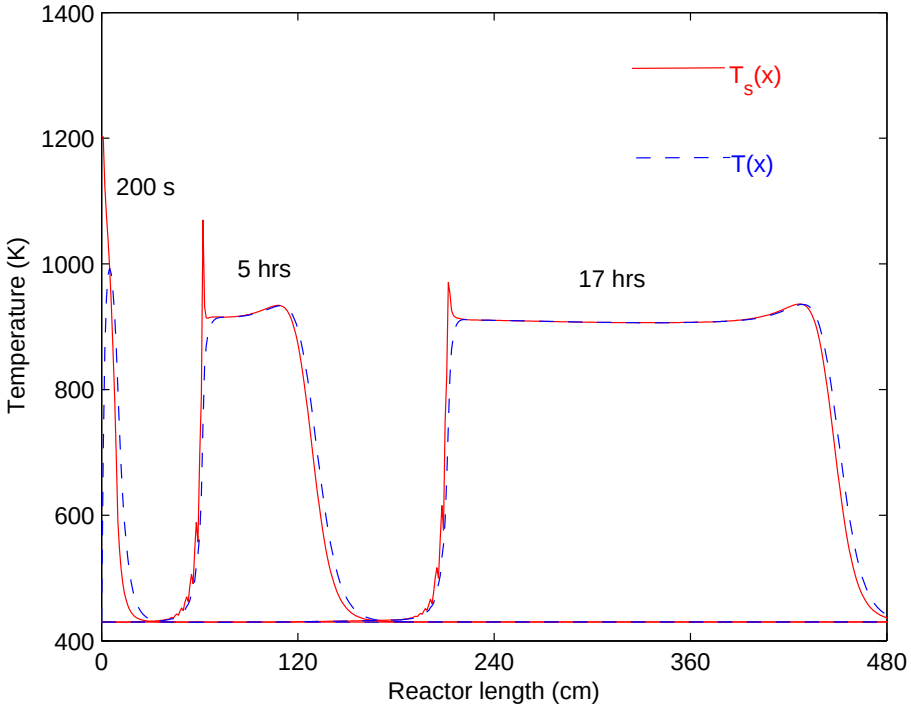

Figure 3.5: Profiles of solid and gas temperatures along the length of the reactor at different simulation times.

they are activated at different temperatures. Along with the dependence on T_s, the heterogeneous chemical reactions also depend on the availability of reactant gases, e.g., R_2 has a significant value around the reaction front where O_2 is available. Similarly, the magnitudes of R_3, R_4 and R_5 also depend on the amount of H_2O (g), CO_2 and H_2 present in the reactor, respectively. R_1 is maximum near the pyrolysis front, where the coal is in excess. It can be seen from Fig. 3.6 that the process of UCG is dominated by three reactions: coal pyrolysis, char oxidation and steam gasification.

Fig. 3.7 shows dry gas molar fractions along length. O_2 coming from the inlet well remains unreacted until the reaction front, where it is entirely consumed by char oxidation reaction giving rise to CO_2 in the reactor. Mole fraction of CO_2 remains constant until the pyrolysis front, where it slightly decreases due to less increase in the concentration of CO_2 in pyrolysis reaction as compared to the other volatiles. CO is generated at the reaction front by steam gasification

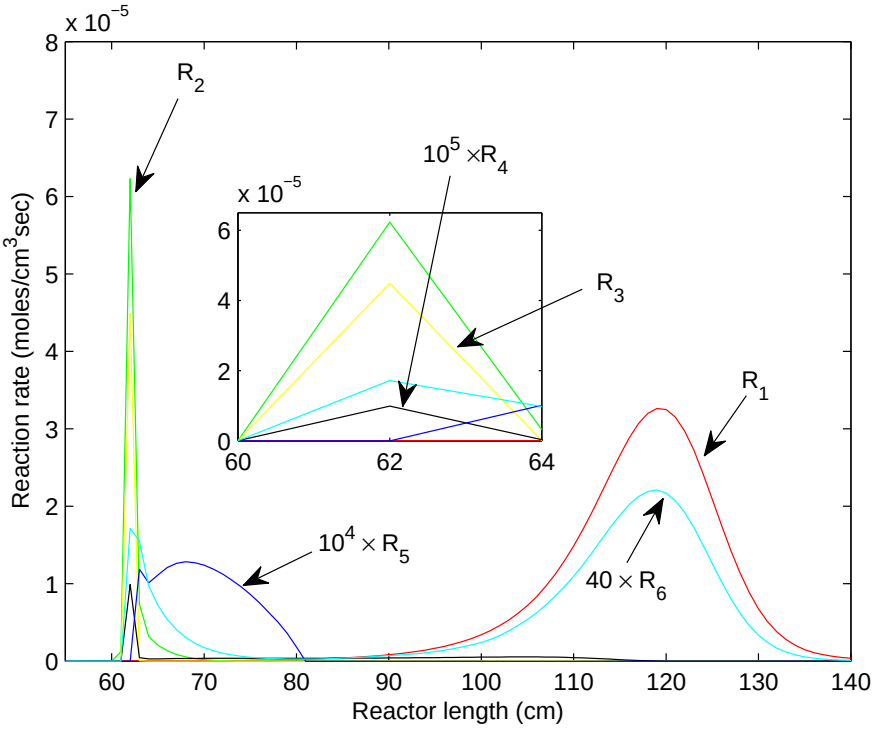

Figure 3.6: Reaction zone at 5 hrs, showing the rates of all the chemical reactions. The zoomed portion of the figure shows the reaction front.

reaction, when CO moves towards the outlet well it is completely consumed by water gas shift reaction before its regeneration by R_1. Like CO, H_2 is also produced by the steam gasification reaction, on its way towards $x = L$ its concentration is first increased by water gas shift reaction (a small increase) and then by pyrolysis reaction (a large increase). CH_4 and tar are the products of pyrolysis reaction, which are produced by R_1 near the pyrolysis front.

The densities of coal and char are shown in Fig. 3.8. Coal is initially dried and then pyrolysed (heating in the absence of O_2) by heat generated in the reaction zone mainly due to the char oxidation reaction, the products of pyrolysis are char and gases which reside in the reaction zone to assist other reactions. Char is produced at the pyrolysis front and consumed at the reaction front, between the boundaries of reaction zone it remains constant. The density distributions of coal and char are pushed towards $x = L$ with time, as the process of UCG proceeds.

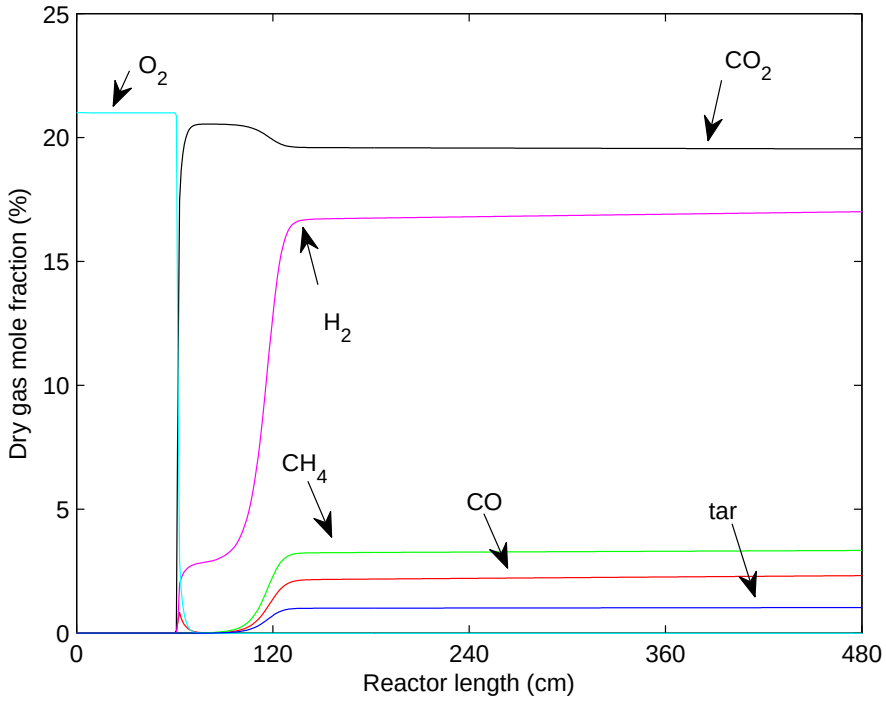

Figure 3.7: Mole fraction of gases without steam along the length of reactor at 5 hrs.

Fig. 3.9 shows the movement of pyrolysis and reaction fronts towards the production well, with time. The results in Fig. 3.9 give a rough approximation of the expected life of UCG reactor. The instantaneous difference between the locations of the fronts gives width of the reaction zone. Fig. 3.9 shows that reaction zone is widening with time, this information is also implicitly provided by Figs. 3.5 and 3.8. The fuel for the reactor is coal and char. When pyrolysis front reaches $x = L$ the coal bed is almost exhausted. The process ends when all the char is consumed in the reactor, which is indicated by reaction front approaching $x = L$. Actually all the chemical reactions take place between reaction and pyrolysis fronts (see Fig. 3.6), therefore when reaction front approaches the outlet well all the reactions stop and the process ends.

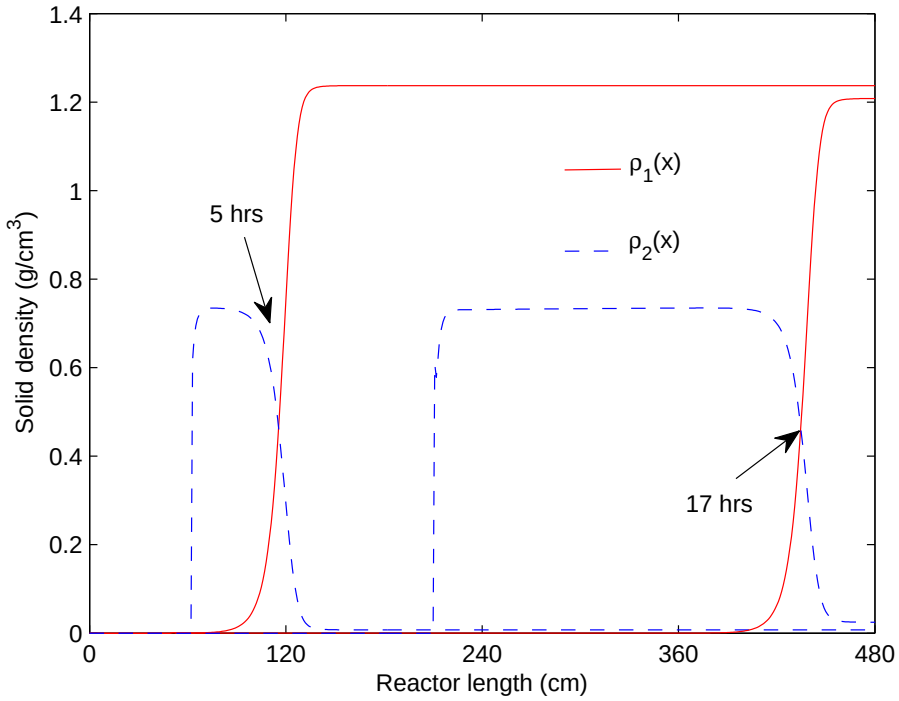

Figure 3.8: Solid phase densities as a function of length for different simulation times.

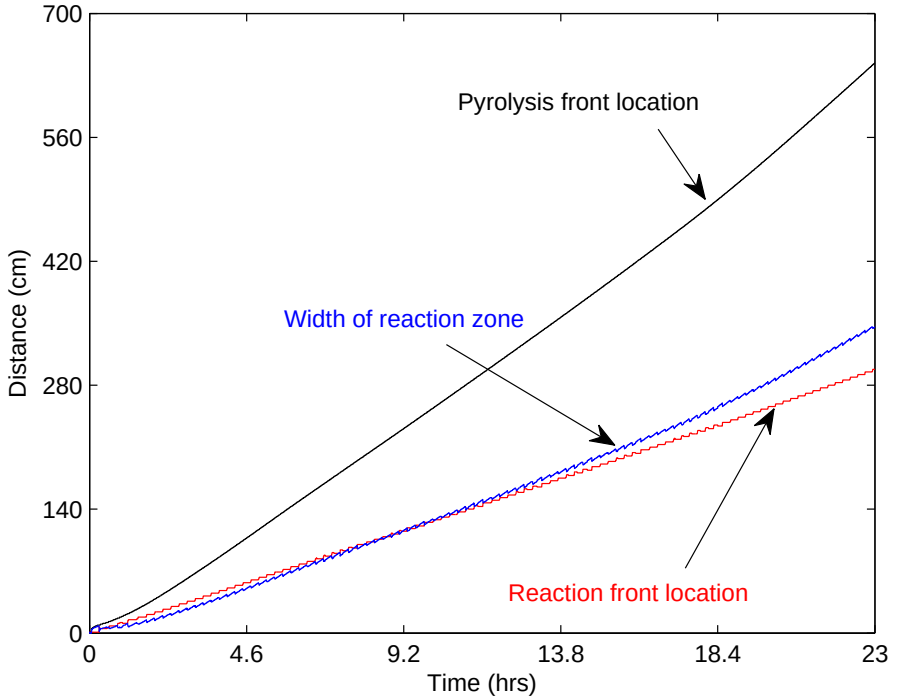

Figure 3.9: Movement of pyrolysis and reaction fronts with time.

The information provided by the above results can not be obtained from UCG field trials. Because, it is not possible to install devices for measuring these parameters at every critical location. Therefore, the role of such a computer model is very important in understanding the hidden dynamics of the process.

3.4 Study of parametric variations on the process

This section shows the effect of varying some important operating conditions on the dynamics of the UCG process. The simulation results are shown for the distribution of solid temperature and the heating value of the product gases. The solid temperature also gives an implicit information about the chemical kinetics and conversion rates of coal and char, while the heating value contains information of the product gas composition. Therefore, these two variables can depict the whole picture of the UCG process.

The heating value is calculated as mentioned in [124] given by Eq. (3.27).

$$y = m_{CO}(L)\,H_{CO} + m_{H_2}(L)\,H_{H_2} + m_{CH_4}(L)\,H_{CH_4} + m_{tar}(L)\,H_{tar} \tag{3.27}$$
$$m_{C_i}(L) = 100 \times \frac{C_i}{\tilde{C_T}}\bigg|_{x=L}$$
$$\tilde{C_T} = \sum_{i=1, i\neq 4}^{8} C_i$$

where y is the heating value (KJ/m^3) of the solved model at $x = L$, $m_{C_i}(L)$ is the percentage molar fraction of gas i at $x = L$, H_i is the heat of combustion of ith gas (KJ/m^3) gas and $\tilde{C_T}$ (mol/cm^3) is total concentration of gases without steam.

3.4.1 Effect of varying the inlet feed of O_2

Here the effect of changing the inlet feed of O_2 on the UCG process is studied. Three different cases are considered in which the percentage molar fraction of injected gases is: $N_2 = 85\%\&O_2 = 15\%$, $N_2 = 79\%\&O_2 = 21\%$ (air, which is

the base case) and $N_2 = 70\%\&O_2 = 30\%$ respectively. The remaining input parameters are same as in Table 3.3.

Fig. 3.10(a) shows the spatial distributions of T_s for the three cases at 4.5 hrs. It is observed that the temperature at the reaction front increases with the increase in the inlet O_2 feed, which is due to the increase in the exothermic char oxidation reaction. It can also be observed that by increasing the O_2 concentration, the velocities of reaction and pyrolysis fronts and the width of the reaction zone also increase. This means that rate of conversion of coal is even greater than that of char.

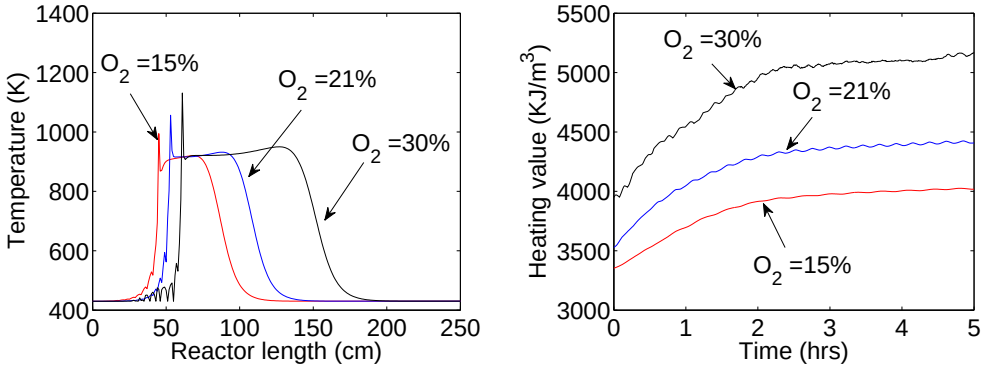

(a) $T_s(x)$ at $t = 4.5$ hrs

(b) y with time in gasification phase

Figure 3.10: Effect of varying inlet concentration of O_2 on spatial distributions of solid temperature T_s and the heating value y of the product gas

With the increase in O_2 concentration, the concentration of H_2O (g) increases and that of N_2 decreases. Due to the increased concentration of the reactant gases, the heating value of the product gas in Fig. 3.10(b) is highest for $O_2 = 30\%$, because the coal consumption is the largest for this case.

3.4.2 Effect of varying H_2O (g) to O_2 ratio: λ

It is very important to note that H_2O (g) is not the part of inlet gases. In order to simulate the effect of water influx it is assumed that a specific amount of H_2O (g): λC_{O_2} is available at $x = 0$ for the gasificaion reactions. Therefore, varying the value of λ only changes the concentration of H_2O (g), while the

concentration of the injected N_2 remains unchanged.

As discussed previously that O_2 is important for providing heat through oxidation of char, which is useful for the endothermic gasification reactions. On the other hand it is also responsible for the production of CO_2, which decreases the heating value of the product gas. H_2O (g) is also a very important reactant for the UCG process, as it increases the heating value by assisting the production of H_2 and CO by H_2O (g) gasification reaction. But, the endothermicity of the H_2O (g) gasification reaction decreases the temperature of the reactor, which in the extreme case can extinguish the process. In short, optimized values of both O_2 and H_2O (g) can yield a higher heating value over a longer period of time.

Here the results are shown for three different cases: $\lambda = 1.5$, $\lambda = 2.5$ (base case) and $\lambda = 3$. The injected gas composition and remaining parameters are similar to the base case simulation.

Fig. 3.11(a) shows that as the amount of λ increases, the maximum value of T_s at the reaction front decreases. This is due to the increase in the concentration of H_2O (g), which increases the rate of endothermic H_2O (g) gasification reaction. It can also be seen that the width of the reaction zone is quite similar for all the cases, which means that the conversion rate for coal and char, or the velocities of reaction and pyrolysis fronts are same.

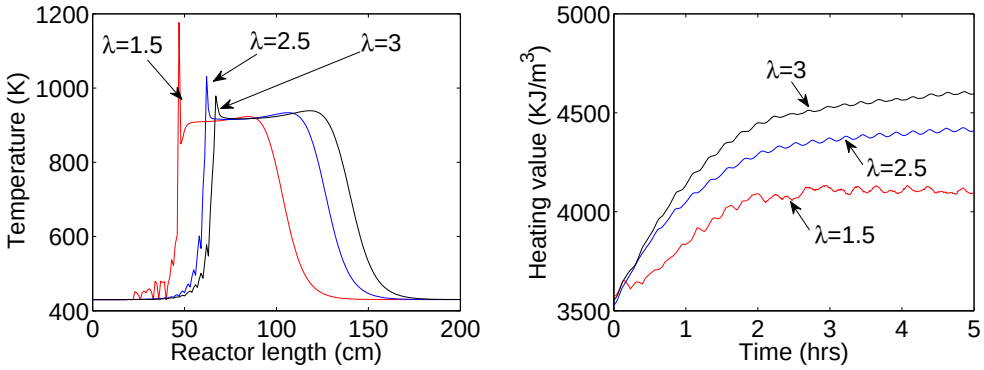

(a) $T_s(x)$ at $t = 5$ hrs

(b) y with time in gasification phase

Figure 3.11: Solid temperature and the heating value of product gas for three different values of λ

The dry heating value (without H_2O (g)) for different values of λ is shown in Fig. 3.11(b). By increasing the value of λ the amount of reactant gases is also increased, thus increasing y. The decrease in the concentration of H_2O (g) at lower values of λ, increases the molar fraction of N_2 in the reactor, which causes the decrease in y.

3.4.3 Effect of change in flow rate of injected gases

Here the effect of the variation in the flow rate of inlet gases is studied for three different cases: $u_1 = 10^{-4}$ moles/cm^2/s, $u_2 = 1.5 \times 10^{-4}$ moles/cm^2/s and $u_3 = 2 \times 10^{-4}$ moles/cm^2/s (base case). The inlet gas is air and $\lambda = 2.5$.

In Fig. 3.12(a), as the flow rate is increased from $u_1 \rightarrow u_3$, the overall magnitude of T_s distribution and the width of the reaction zone are also increased. Which indicates that the increase in the reactant gases raise the magnitudes of the chemical reaction rates within the UCG reactor. Thus, the rates of conversion of coal and char are also greatest for u_3.

The results in Fig. 3.12(b) show that for higher flow rates y decreases and vice versa. This scenario can be explained by investigating Eq. (3.27). The increase in the value of flow rate increases the reactant gases and N_2. The increased value of H_2O (g) increases m_{CO} and m_{H_2}, while the higher concentration of N_2 increases $\tilde{C_T}$. Due to its initial higher value, the increase in N_2 concentration dominates the reactant gases, hence reducing y.

The flow rate of the injected gases is always bounded: $u_l \leq u \leq u_u$, where u_l and u_u are lower and upper bounds on u respectively. For $u > u_u$, the increased amount of H_2O (g) may start eating up the temperature of the reactor and finally extinguishing the process. The temperature of the reaction zone can also drop below the critical value for $u < u_l$, which results from the deficiency of O_2 in the reactor.

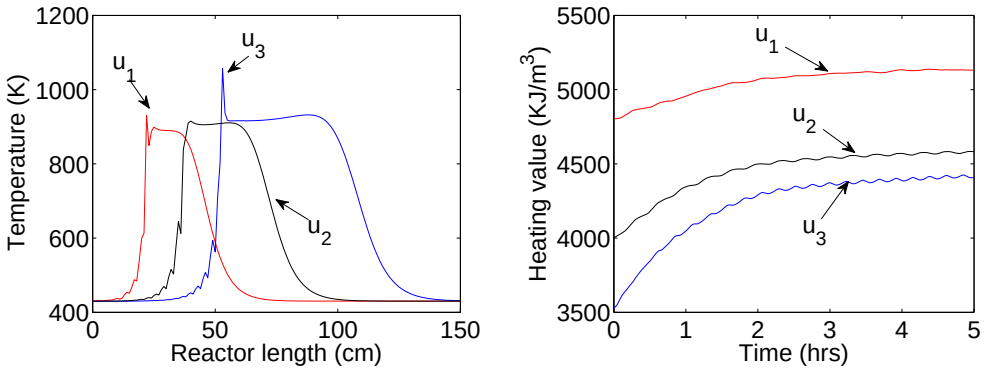

(a) $T_s(x)$ at $t = 4.5$ hrs

(b) y with time in gasification phase

Figure 3.12: Solid temperature and the heating value for three different flow rates of the injected gases: $u_1 = 10^{-4}$ moles/cm^2/s, $u_2 = 1.5 \times 10^{-4}$ moles/cm^2/s and $u_3 = 2 \times 10^{-4}$ moles/cm^2/s.

3.5 Conclusion

The computer model of the UCG process is developed and then solved by using the parametrization of the Thar UCG setup. The solved model is capable of providing estimates for some important parameters of the process, such as solid and gas phase compositions and temperatures profiles with a moving reaction zone. A comprehensive parametric study is also conducted for the solved model, which shows that the rates of conversion of coal and char and the composition of the product gas are sensitive to a range of operating conditions, such as amount of O_2 in the inlet gas, H_2O (g) to O_2 ratio at the inlet and molar flow rate of the injected gas. These results can be used to find such a set of operating conditions which can increase the performance of a UCG process.

The computer model of the UCG process is validated in the next chapter by comparing the results of the solved model with the experimental results of the gasification of Block V of the Thar coal field.

CHAPTER 4

Optimization and Model Validation

The computer model of UCG developed in the previous chapter is validated by comparing the results of the solved model with the UCG field test. Prior to the model validation, some uncertain parameters are optimized. The optimization is performed to compensate for the uncertainty in coal and char ultimate analysis, which is generally caused by the repeated measurements of different samples, and in H_2O (g) to O_2 ratio at the reaction front. Two different constrained nonlinear optimization problems are formulated, which differ in the number of optimization variables and constraint equations [122, 125].

The main components for the experimental set up of UCG field test are discussed in Section 4.1, the optimization of the UCG model is presented in Section 4.2 and the results of model validation are shown in Section 4.3. The chapter is concluded in Section 4.4.

4.1 Experimental setup

The working of experimental setup is shown in Fig. 4.1, which is composed of following important components:

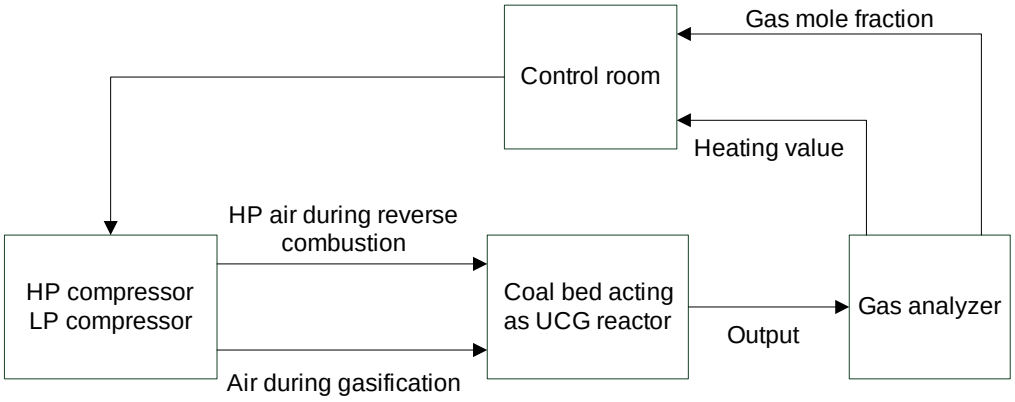

Figure 4.1: Block diagram of the UCG setup

4.1.1 Control room

The control room holds programmable logic controllers (PLCs) and the control valve. The percentage opening of the control valve sets the air flow rate sent to the coal seam during reverse or forward combustion of underground coal seam.

The opening of the valve is controlled by the PLCs. The data logging for the product gas mole fraction is also carried out in the control room.

4.1.2 Compressors

Due to the low permeability of virgin coal seam, it does not allow gases to flow through it. Therefore, prior to the process of gasification a permeable link is established between the inlet and outlet wells. The establishment of a permeable link between the wells can be accomplished by a number of known well linking techniques [126]. The technology used for this experiment is called reverse combustion linkage (RCL). During the process of RCL, the high pressure compressors in Fig 4.2 are used to supply air to the coal seam. Unlike gasification, which is also known as forward combustion, RCL involves injection of the oxidants in one well and ignition of coal seam from the other. The idea is to make the combustion front propagate towards the source of oxidant, which results in the establishment of low hydraulic resistance path between the wells [127]. During gasification of coal seam, the low pressure compressor in Fig. 4.3 is used to supply air to the already ignited coal seam.

Figure 4.2: SIAD TEMPO^2 1500 high pressure compressors

Figure 4.3: Atlas Copco GA 250 low pressure compressor

4.1.3 UCG field

A part of Block V of the Thar coal fields is shown in Fig. 4.4, which consists of a network of pipes and wells. The blue pipes take air at a specific pressure and flow rate to the injection well, while the red pipes carry product gas to the gas analyzer from the outlet well. In a commercial UCG process, several coal seams are gasified simultaneously and the product gas is recovered by multiple production wells. However, this experiment was performed on a single coal seam having thickness of 5 m and located at the depth of 144 m from the surface.

4.1.4 Gas analyzer

The gas analyzer (Fig. 4.5) is integrated on line, the steam is removed from the gas mixture and the molar fraction of remaining gases is measured.

The technologies used to measure molar fractions of different gases are listed below [124].

- CO, CO_2, CH4 and higher hydrocarbons: C_nH_m are measured by dual beam non dispersive infra red (NDIR) detectors.

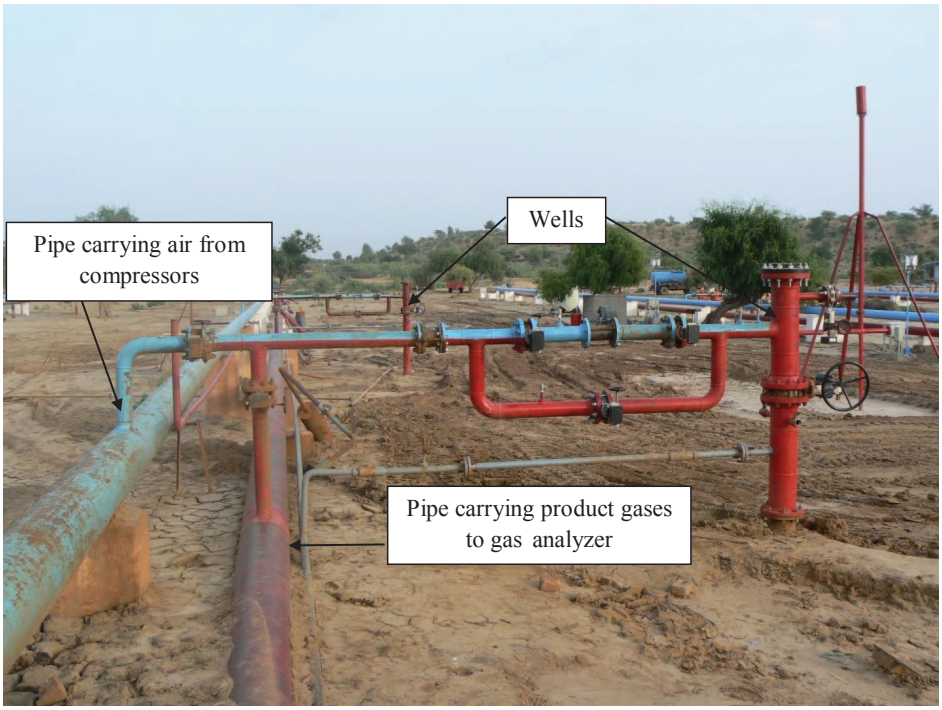

Figure 4.4: UCG field

- H_2 is measured by Thermal conductivity (TCD) detector.
- A galvanic fuel cell is used to determine the percentage volume content of O_2 in the sample gas.

The heating value of gases is calculated by using following relationship:

$$y_{exp} = m_{CO_{exp}} H_{CO} + m_{C_nH_{m_{exp}}} H_{C_nH_m} + m_{CH_{4_{exp}}} H_{CH_4} + m_{H_{2_{exp}}} H_{H_2} \tag{4.1}$$

where y_{exp} is the experimental heating value of the product gas (KJ/m^3), and $m_{i_{exp}}$ and H_i are the experimental percentage molar fraction and heat of combustion (KJ/m^3) of gas component i respectively. The measurements show that there are only traces of C_nH_m in the product gas.

4.2 Optimization

According to Antoniou and Lu [128], "The process of optimization is the process of obtaining the *best*, if it is possible to measure and change what is *good*

Figure 4.5: GAS 3100 R coal gas/syngas analyzer

or *bad*." The theory of optimization involves the quantitative study and methods for finding the optima (maxima or minima) of a function. On the other hand, optimization practice is comprised of all the methods, algorithms, procedures and techniques used for finding the optima. Optimization has application in almost every branch of science, such as, engineering, physics, social sciences and economics, etc.

The most general approach to solve optimization problems is through the use of numerical methods, which is also known as *mathematical programming*. This approach can solve real world optimization problems with a large number of optimization variables. In mathematical programing, optimization variables are initialized and iterative numerical techniques are used to generate a series of progressively improved solutions. The numerical routine is only terminated when some convergence criterion is met. This normally happens, when the changes in the cost function and the independent variables in two successive iterations become insignificant.

4.2.1 A general optimization problem

Before solving an optimization problem, it needs to be transformed in to a general frame work:

$$min_x f(x) \quad for \quad x \in \mathfrak{F} \tag{4.2}$$

$$\alpha_i(x) = 0 \quad for \quad i = 1,2,\ldots,m \tag{4.3}$$

$$\beta_j(x) \geq 0 \quad for \quad j = 1,2,\ldots,z \tag{4.4}$$

$$\mathfrak{F} = \left\{x : \alpha_i(x) = 0 \quad \& \quad \beta_j(x) \geq 0\right\} \tag{4.5}$$

where $x^T = [x_1, x_2, \ldots, x_n]$ is the vector of optimization variables, $f(x)$ is the objective or cost function to be minimized, $\alpha_i(x)$ and $\beta_j(x)$ are m equality and z inequality constraints respectively, and $\mathfrak{F} \subset \Re^n$ is the feasibility domain of $f(x)$.

There are three main components of an optimization problem:

4.2.1.1 Optimization variables

The optimization variables in x can be independent variables or some control parameters that can be manipulated. The identification of x is very critical in the formulation of an optimization problem.

4.2.1.2 Objective function

The objective function $f(x)$ is scalar and it can have various forms. It can represent the cost of a product in a manufacturing environment or it can be the difference between the desired and actual performance in a system. The elements of x can influence the cost of the product in the former case or the actual performance in the latter case.

Unlike (4.2), sometimes it is desired to maximize $f(x)$. But, still in this case the generality of (4.2) holds, because:

$$max[f(x)] = -min[-f(x)]$$

In some applications, it is desired to optimize a set of distinct functions of x, simultaneously. This situation can arise during the solution of r simultaneous algebraic equations:

$$f_i(x) = 0 \quad for \quad i = 1, 2, \ldots, r$$

In this way a vector of r objective functions can be obtained:

$$f^T(x) = \begin{bmatrix} f_1(x) & f_2(x) & \ldots & f_r(x) \end{bmatrix} \tag{4.6}$$

Now the problem is to find x^* (solution of the optimization problem, representing an optimum value of x) which yields $f(x^*) = 0$. Most of the times it is not possible to find such an x^* which reduces all $f_i(x)$ to zero simultaneously. But it is possible to find $f(x^*) \approx 0$, which meets the desired level of accuracy.

A similar situation arises in engineering applications, where $f(x)$ is also a continuous function of other independent variables, such as time. In this case $f(x,t)$ represents a vector of distinct functions, evaluated at different time instances:

$$f^T(x,t) = \begin{bmatrix} f(x,t_1) & f(x,t_2) & \ldots & f(x,t_q) \end{bmatrix} \tag{4.7}$$

where $t_1, t_2, \ldots, t_q$ indicate the instances of interest, where $f(x,t)$ is sampled.

If $f(x,t_i)$ is replaced by $f_i(x)$ then Eq. (4.7) becomes Eq. (4.6). The solution for this problem will also be an approximation, because the details of the function between the consecutive samples is ignored. However, the accuracy of the solution may be increased by increasing the number of samples, which on the other hand will increase the computational cost of the software.

As it has been said previously that $f(x)$ is scalar, therefore, the problem of minimizing a vector of objective functions in Eqs. (4.6) and (4.7) is generally

transformed in to the *norm* minimization problem. The L_p norm of vector $f(x)$ is:

$$\left\| f(x) \right\|_p \equiv L_p = \left(\sum_{i=1}^{r} \left| f_i(x) \right|^p \right)^{1/p} \tag{4.8}$$

The three most common types of L_p norms used for $f(x)$ are given as:

$$\left\| f(x) \right\|_1 \equiv L_1 = \sum_{i=1}^{r} \left| f_i(x) \right| \tag{4.9}$$

$$\left\| f(x) \right\|_2 \equiv L_2 = \left(\sum_{i=1}^{r} \left| f_i(x) \right|^2 \right)^{1/2} \tag{4.10}$$

$$\left\| f(x) \right\|_\infty \equiv L_\infty = \max_{1 \le i \le r} \left| f_i(x) \right| \tag{4.11}$$

Eqs. (4.9), (4.10) and (4.11) are obtained by substituting $p = 1$, $p = 2$ and $p = \infty$ in Eq. (4.8) respectively. In optimization problems involving $\left\| f(x) \right\|_1$, the sum of the magnitudes of individual elements of $f(x)$ is minimized. For $\left\| f(x) \right\|_2$, the *Euclidean norm* is minimized, and if the square root is omitted, then the sum of the squares $\left\| f(x) \right\|_2^2$ is minimized and the problem is formally known as a *least squares problem*. Eventually for $\left\| f(x) \right\|_\infty$, the maximum value of the magnitudes of individual functions is minimized, which is called a *mini-max problem* [128].

So far, the choice of objective functions give same weightage to the individual functions in $f(x)$, which results in the same residual error ε for the functions. But in some applications, it is required to give more emphasis to the critical elements, which results in the following objective function:

$$\left\| f(x) \right\|_p \equiv L_p = \left(\sum_{i=1}^{r} w_i \left| f_i(x) \right|^p \right)^{1/p} \tag{4.12}$$

where the design variable $w_i > 0$ is the weight of $f_i(x)$.

Now if the error in one element is:

$$error\left\{w_i\left|f_i(x)\right|\right\} \approx \varepsilon$$

then for the individual function:

$$error\left\{\left|f_i(x)\right|\right\} \approx \frac{\varepsilon}{w_i}$$

which shows that the element with higher value of w_i has a smaller residual error and vice versa. In this way a distinct function or a function at a critical instant can be given more emphasis.

4.2.1.3 Constraints

There are two types of constraints in a constrained optimization problem: equality (Eq. (4.3)) and inequality (Eq. (4.4)). The equality constraints confirm that the solution of the optimization problem does not violate any physical law, while the inequality constraints are imposed to ensure physical realizability of the problem. These constraints define the domain of feasibility $\mathfrak{F}$ for the computation of $f(x)$. All the points belonging to $\mathfrak{F}$ are called feasible points. For the solution of the optimization problem to be valid: $x^* \in \mathfrak{F}$.

If all the constraints are equalities then the feasible points are located on the intersection of m hypersurfaces corresponding to $\alpha_i(x) = 0$ (Eq. (4.3)). On the other hand, if all the constraints are inequalities, then they divide $\Re^n$ into three types of points. If $\beta_j(x) > 0, \forall j$ then the point is called an *interior point*, where as, $\beta_j(x) = 0$ represents a *boundary point* and $\beta_j(x) < 0$ is an *exterior point*.

4.2.2 Types of mathematical programing

Based on the structure of the optimization problem in section 4.2.1, the mathematical programing is classified into the following types [128].

4.2.2.1 Linear programing

In this type of mathematical programing, the objective and constraint functions are linear. A general structure of such problem is given below:

$$min_x f(x) = \sum_{i=1}^{n} \gamma_i x_i \quad for \quad x \in \Re^+$$
$$\alpha_j(x) = \sum_{i=1}^{n} \delta_{ij} x_i - \mu_j = 0 \quad for \quad j = 1,2,\ldots,m$$
$$\beta_k(x) = \sum_{i=1}^{n} \eta_{ij} x_i - \nu_j \geq 0 \quad for \quad j = 1,2,\ldots,z$$

where $\gamma_i, \delta_{ij}, \eta_{i,j}, \mu_j, \nu_j \in \Re^+$.

The simplex method and interior point algorithms are used to solve the linear programing (LP) problems. However, the interior point algorithms are much more efficient for LP problems with sufficiently large number of optimization variables.

4.2.2.2 Integer programing

It is a special case of linear programing (LP) in which at least some of the variables are assumed to be integers only.

4.2.2.3 Quadratic programing

A quadratic programing (QP) problem is usually represented as:

$$min_x f(x) = \alpha_0 + \alpha^T x + x^T Q x$$
$$\beta^T x \geq \gamma$$

where $f(x)$ is the quadratic objective function in x, $\alpha \in \Re^{n\times 1}$, Q is the positive definite or semi positive definite, symmetric and square matrix, $\beta \in \Re^{q\times 1}$, q is the number of linear constraints and $\alpha_0 \in \Re^+$.

The QP problems are efficiently solved using convex programing (CP) algorithms, such as, QR decomposition based methods, cutting plane and ellipsoid algorithms.

4.2.2.4 Nonlinear programing

In nonlinear programing (NLP) the objective and constraint functions are nonlinear functions of the optimization variables. It is the most general type of mathematical programing, and LP and QP problems are considered as special cases of these types of optimization problems.

The NLP problems can be solved by using various methods, which include but not limited to penalty and barrier function methods, gradient projection methods and sequential programing (SQP) algorithms. The SQP methods are highly efficient for NLP problems with smooth objective and constraint functions [129–131].

4.2.2.4.1 Sequential quadratic programing

The SQP method is based on the divide and conquer rule. A NLP problem is divided in to a sequence of QP subproblems. The objective function of a QP subproblem is a quadratic approximation to the Lagrangian function, whereas its constraints are the linearizations of the original constraints. The QP subproblems are iteratively solved to reach the solution [132].

In order to demonstrate the SQP method, it is convenient to reconsider the NLP problem defined by Eqs. (4.2), (4.3), (4.4) and (4.5).

$$
\begin{aligned}
&min_x f(x) \quad for \quad x \in \Re^n \\
&\alpha_i(x) = 0 \quad for \quad i = 1,2,\ldots,m \\
&\beta_j(x) \geq 0 \quad for \quad j = 1,2,\ldots,z \\
&\mathfrak{F} = \left\{ x : \alpha_i(x) = 0 \quad \& \quad \beta_j(x) \geq 0 \right\}
\end{aligned}
$$

where $f(x)$, $\alpha(x)$ and $\beta(x)$ are continuous functions and their second partial derivatives exist.

The Lagrangian functional associated with the problem is given by:

$$\mathscr{L}(x,\rho,\mu) = f(x) + \rho^T \alpha(x) + \mu^T \beta(x)$$

where vectors $\rho \in \Re^m$ and $\mu \in \Re^z$ are referred to as Lagrangian multipliers.

A simplified SQP method for solving the above NLP problem is given by the following Algorithm [131, 133]:

1: Set $x = x^0$ (x^0 need not to be feasible), $k = 0$ and initialize the tolerance ε
2: Evaluate the search direction d^0 by solving QP^0 subproblem.
3: Determine the step length c^0 by a 1D minimization of a merit function: $\mathscr{M}\left(x^0 + c^0 d^0\right)$
4: Compute $x^1 = x^0 + c^0 d^0$
5: **while** $\left\|c^k d^k\right\| > \varepsilon$
6: Set $k = k+1$
7: Evaluate d^k by solving QP^k subproblem
8: Determine c^k which minimizes: $\mathscr{M}\left(x^k + c^k d^k\right)$
9: Compute $x^{k+1} = x^k + c^k d^k$
10: **end while**
11: Output: $x^* = x^{k+1}$

where the function $\mathscr{M}$ guarantees a sufficient decrease in $f(x)$ and it also ensures the fulfillment of constraints along d^k with an appropriate c^k.

The search direction d^k is the solution of the following QP^k subproblem.

$$\begin{aligned}
\min_d \quad & \left\{\frac{1}{2} d^T \mathscr{H}_k d + \Delta f(x_k)^T d\right\} \\
s.t. \quad & \Delta\alpha_i(x_k)^T d + \alpha_i(x_k) = 0,\ i = 1,2,\ldots,m \\
& \Delta\beta_j(x_k)^T d + \beta_j(x_k) \le 0,\ j \in \mathscr{A}(x^k) \\
& \mathscr{A}(x^k) = \left\{ j \in \{1,2,\ldots,z\} \,|\, \beta_j(x_k) = 0 \right\}
\end{aligned}$$

where $\mathscr{H}_k$ is the Hessian of the Lagrangian: $\Delta_x^2 \mathscr{L}(x^k, \rho^k, \mu^k)$ and $\mathscr{A}(x^k)$ refers to the set of active constraints at x^k

4.2.2.5 Dynamic programing

In this approach a complex problem is divided into a sequence of simpler problems, which are solved as an LP, QP or nonlinear programing problems. Most of the times, the sub problems are solved sequentially as the subsequent problems are influenced by earlier ones. The dynamic programing basically provides a general frame work for analyzing various types of optimization problems.

4.2.3 Optimization of UCG reactor model

4.2.3.1 Problem statement

The mathematical model of UCG reactor is optimized in order to compensate for the uncertainties in coal and char composition parameters, which include a, b, $\bar{a}$ and $\bar{b}$, and in the H_2O (g) to O_2 ratio at the reaction front λ. In case of coal and char composition parameters, the uncertainty is introduced by conducting ultimate analysis for different coal and char samples. While the uncertainty in λ is quite obvious, as its measurement is not available.

Two different constrained nonlinear programing problems are formulated and solved to yield the optimized values of the variables.

4.2.3.2 Optimization problem I

The optimized values of the model parameters are obtained by solving the following least squares problem:

$$\begin{aligned} minimize \quad & f(x,t) = \left\| e(t) \right\|_2^2 \\ & e(t) = \frac{y(t) - y_{exp}(t)}{y_{exp}(t)} \end{aligned} \tag{4.13}$$

$$subject\,to: \quad \alpha x - \beta \leq 0 \tag{4.14}$$

where $x \in \Re^{3\times 1}$ is the vector of three optimization variables, the objective function $f(x,t)$ is square of the L_2 norm of the relative error between the solved

(y) and experimental (y_{exp}) heating values of the product gas at different time instances and the only linear inequality constraint is represented by the vector $\alpha \in \Re^{1\times 3}$ and scalar $\beta \in \Re^{+}$.

The solution of the mathematical model in section 3.2 does not yield $m_{C_nH_m}$ separately, but it contributes in m_{tar}. Therefore, Eq. (3.27) can be re written as given by Eq. (4.15).

$$y = m_{CO}(L)\,H_{CO} + m_{H_2}(L)\,H_{H_2} + m_{CH_4}(L)\,H_{CH_4} + m_{C_nH_m}(L)\,H_{C_nH_m} \quad (4.15)$$

where $m_{C_nH_m} \approx \sigma m_{tar}$, and $\sigma < 1$.

As it has been previously explained in section 4.1.4 that the amount of C_nH_m is almost negligible in the measurements, therefore its contribution in the heating value is not significant. The heating value y is a highly nonlinear function of the solutions of the solid and gas systems given in section 3.1.1. However, its implicit dependance on the input parameters for balancing the chemical reactions (Table 3.2) is very significant. Because, these parameters determine the moles of the gases produced as a result of all the chemical reactions, which greatly influence m_{C_i}, and hence y. It can be inferred from the description in Table 3.2 that the parameters $a_{s_{2,1}}$, $a_{3,1}$, $a_{5,1}$, s and r are dependent on a, b, $\bar{a}$ and $\bar{b}$. Therefore, any uncertainty in the coal and char composition parameters also affects there values.

This optimization problem does not consider the uncertainty in λ. Moreover, it is also assumed that the uncertainty in ultimate analysis of coal and char can be addressed by optimizing only the values of $a_{s_{2,1}}$, $a_{3,1}$ and $a_{5,1}$. Of course, this optimization problem does not completely address the uncertainty in coal and char ultimate analysis, but, still it can affect a part of coal pyrolysis reaction contributing in y and also serves as a foundation for the more accurate problem in section 4.2.3.3.

This problem was initially solved as an unconstrained optimization problem,

but it was observed that during the solution, moles of CO were staying at a negative value in the coal pyrolysis reaction, which is not true as CO is produced in the reaction. Therefore, the only constraint in Eq. (4.16) makes sure that the moles of CO stays greater than zero in the coal pryolysis reaction.

$$x_1 + 4x_2 + \left(2 - \bar{b} + \frac{\bar{a}}{2}\right) x_3 - 2 + b + \frac{a}{2} - 2s - \frac{rs}{2} \leq 0 \tag{4.16}$$

4.2.3.3 Optimization problem II

In this optimization problem all the parameters in Table 3.2 and λ are optimized, by minimizing the objective function in Eq. (4.13). The optimization problem is given by Eqs. (4.17), (4.18) and (4.19).

$$\begin{aligned}
&\textit{minimize} \quad f(x) \quad \textit{over} \quad x \in \Re^n && (4.17)\\
&\qquad x^T = \begin{bmatrix} a & b & \bar{a} & \bar{b} & \lambda & r & s & a_{3,1} & a_{5,1} & a_{s_{2,1}} \end{bmatrix} \\
&\textit{subject to}: \quad Ax - B \leq 0 && (4.18)\\
&\qquad c(x) \leq 0 && (4.19)\\
&\qquad \mathfrak{F} = \{x : Ax - B \leq 0 \quad \& \quad c(x) \leq 0\}
\end{aligned}$$

where $x \in \Re^{10}$ is the vector of optimization variables, $f : \Re^{10} \rightarrow \Re$ is the objective function to be minimized, $c : \Re^{10} \rightarrow \Re^3$ is a function which returns the vector of 3 nonlinear inequality constraints, $A \in \Re^{7\times 10}$ and $B \in \Re^7$ represent 7 linear inequality constraints and $\mathfrak{F}$ is the region of feasibility.

The purpose of the constraints is to make the system physically realizable, such that, all the chemical reactions are properly balanced and the magnitudes of the stoichiometric coefficients stay positive throughout the solution of the optimization problem. The values of λ_{lb} and λ_{ub} ($\lambda_{lb} \leq \lambda \leq \lambda_{ub}$) are very critical as they save UCG reactor cavity from starvation of H_2O (g) and flooding from the water influx respectively.

The linear constraints are given in the following set of equations. The first four constraints satisfy the relationship between coal and char composition parameters ($0.02a \leq \bar{a} \leq 0.2a$ and $0.02b \leq \bar{b} \leq 0.2b$), and the last three ensure that the magnitudes of all stoichiometric coefficients in reactions $2-5$ in Table. 3.1 are positive. The last three constraints are derived form Eq. (3.11).

$$\begin{aligned}
-0.5x_3 + x_4 - 1 &\leq 0 \\
x_4 - 1 &\leq 0 \\
0.25x_3 + x_4 - 1 &\leq 0 \\
-0.2x_1 + x_3 &\leq 0 \\
0.02x_1 - x_3 &\leq 0 \\
-0.2x_2 + x_4 &\leq 0 \\
0.02x_2 - x_4 &\leq 0
\end{aligned} \tag{4.20}$$

The matrix A and vector B in Eq. (4.18) can be written from Eq. (4.20):

$$A = \begin{bmatrix}
0 & 0 & -0.5 & 1 & 0 & 0 & 0 & 0 & 0 & 0 \\
0 & 0 & 0 & 1 & 0 & 0 & 0 & 0 & 0 & 0 \\
0 & 0 & 0.25 & 1 & 0 & 0 & 0 & 0 & 0 & 0 \\
-0.2 & 0 & 1 & 0 & 0 & 0 & 0 & 0 & 0 & 0 \\
0.02 & 0 & -1 & 0 & 0 & 0 & 0 & 0 & 0 & 0 \\
0 & -0.2 & 0 & 1 & 0 & 0 & 0 & 0 & 0 & 0 \\
0 & 0.02 & 0 & -1 & 0 & 0 & 0 & 0 & 0 & 0
\end{bmatrix} \tag{4.21}$$

$$B^T = \begin{bmatrix} 1 & 1 & 1 & 0 & 0 & 0 & 0 \end{bmatrix} \tag{4.22}$$

The nonlinear constraints in Eq. (4.23) ensure the magnitudes of the stoichiometric coefficients of coal pyrolysis reaction stay positive.

$$\frac{1}{2}x_1 - x_2 - x_8 - 3x_9 - \frac{1}{2}x_7(x_6+2) + \frac{1}{2}x_{10}(2x_4 - x_3 - 2) + 1 \quad < 0$$

$$-\frac{1}{2}x_1 + x_2 + x_8 + 4x_9 + \frac{1}{2}x_7(x_6+4) + \frac{1}{2}x_{10}(4-2x_4+x_3) - 2 \quad < 0$$

$$-x_1 + x_3x_{10} + 2x_8 + 4x_9 + x_6x_7 \quad < 0 \qquad (4.23)$$

4.2.3.4 Solution of the optimization problems

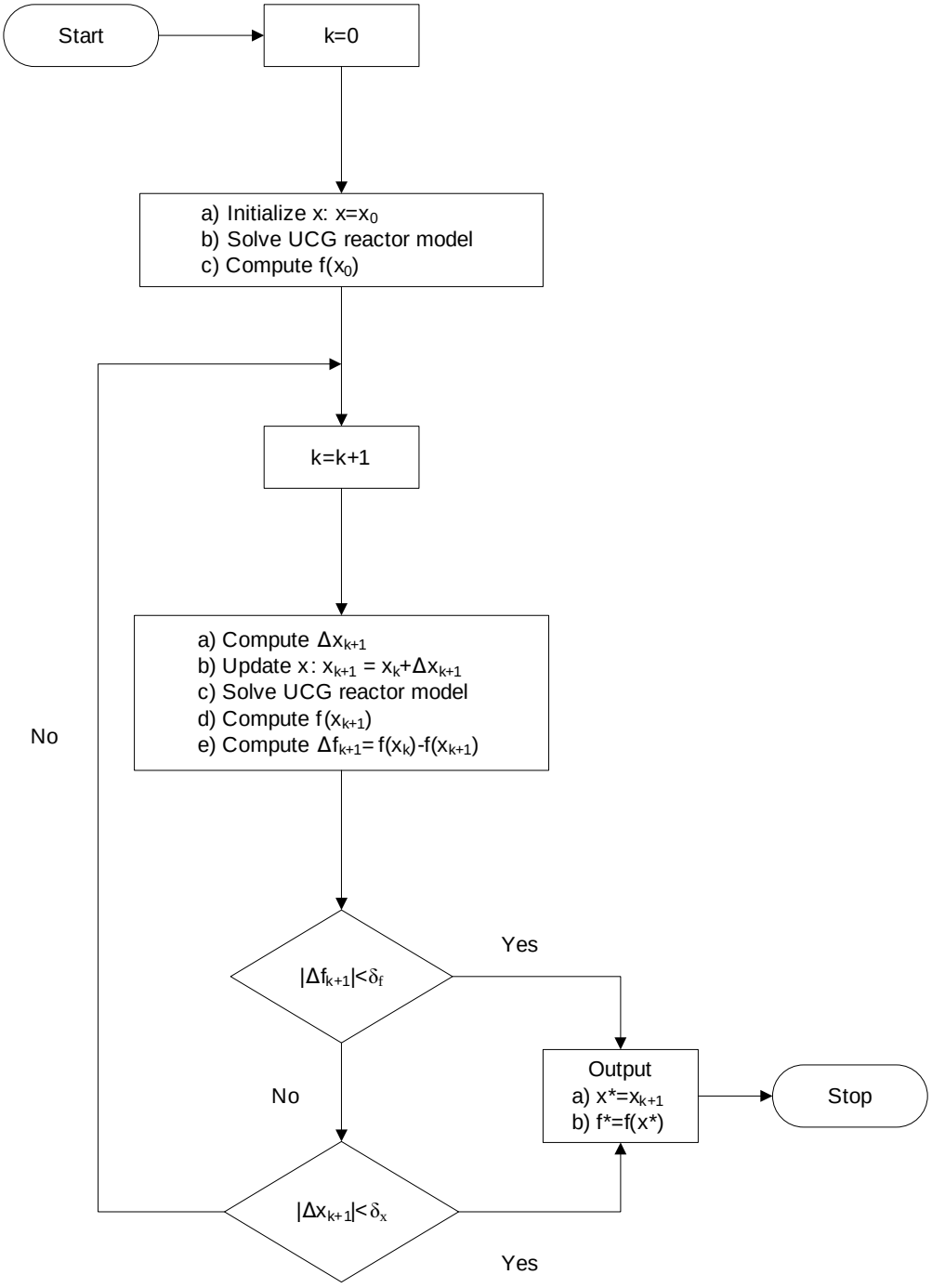

Figure 4.6: A general solution strategy for solving the nonlinear programing problems of the UCG reactor model

The aforementioned nonlinear programing problems are solved by Matlab function *fmincon*, using the sequential quadratic programing (SQP) algorithm. The *fmincon* function solves the optimization problems as shown in Fig. 4.6. The solution starts by providing initial guess x_0 for the optimization variables, which is followed by the solution of the UCG reactor model using the procedure given in Fig. 3.4 and the subsequent evaluation of $f(x_0)$ using Eq. (4.13). In the iterative loop for the variable k, the step length for optimization variables Δx_{k+1} is calculated using SQP algorithm and the updated vector of optimization variables x_{k+1} is obtained, then the UCG reactor model is solved for the updated set of optimization variables x_{k+1} and the objective function is evaluated at x_{k+1}. The iterative loop is terminated if any of the following occurs:

- $\left|\Delta f_{k+1}\right| < \delta_f$: where $\Delta f_{k+1} = f(x_k) - f(x_{k+1})$ and δ_f is the optimization tolerance for f.
- $\left|\Delta x_{k+1}\right| < \delta_x$: where δ_x is the optimization tolerance for the optimization variables in x

Eventually the solution of the optimization problem is $x^* = x_{k+1}$ and $f^* = f(x^*)$.

The values of δ_f and δ_x are provided by the user. The selection of the optimization tolerances is a trade off between the accuracy of the solution and computational cost of the software. Apart from δ_f and δ_x the user also has the provision to terminate the program after the specific number of iterations k and/or setting the maximum number of function evaluations within a single iteration. The average time it took to solve the second optimization problem was 24 hrs, for a *dual core i7 processor*, which is due to the high computational complexity associated with the solution of the UCG reactor model.

4.2.3.4.1 Robustness of the estimates of the optimization variables

The confidence intervals of the optimization variables are also calculated in order to validate the robustness of there estimates. The optimization problems

are solved for eleven different data sets and then *95% confidence interval* for the estimates of the variables is calculated in Eq. (4.24) by using the method given in [134]. The error statistics of the optimization variables for both the optimization cases is given in Table 4.1

$$\theta = \hat{\theta} \pm t_{tab} \frac{s}{\sqrt{n}} \tag{4.24}$$

where θ is the true value (mean of large set of replicates), $\hat{\theta}$ is the mean of the sub samples, $n = 11$ is the number of sub samples, $t_{tab} = 2.228$ (taken from the two sided *t-table* [134] against $df = n - 1 = 10$) is the statistical value for 95% confidence and s is the standard deviation of the mean of the sub samples.

Table 4.1: Error bounds at *95%* confidence interval for the optimized variables of both the cases. Case a refers to the optimization problem II, while Case b is for the optimization problem I

		Case a		**Case b**	
Sr	**Variable**	$\hat{\boldsymbol{\theta}}$	**Error bounds**	$\hat{\boldsymbol{\theta}}$	**Error bounds**
1.	a_{31}	0.0824	$\pm$ 0.0002	0.0488	$\pm$ 0.0016
2.	a_{51}	0.0304	$\pm$ 0.0044	0.0431	$\pm$ 0.0005
3.	$a_{s_{21}}$	0.7739	$\pm$ 0.0181	0.7746	$\pm$ 0.0030
4.	a	0.8543	$\pm$ 0.0266		
5.	b	0.1985	$\pm$ 0.0062		
6.	$\bar{a}$	0.0825	$\pm$ 0.0014		
7.	$\bar{b}$	0.0152	$\pm$ 0.0008		
8.	λ	2.0597	$\pm$ 0.0646		
9.	r	2.7514	$\pm$ 0.0378		
10.	s	0.1299	$\pm$ 0.0099		

4.3 Model validation

After solving the optimization problems, the simulated and experimental results for three different data sets are compared for the heating value and molar fractions of CO, H_2 and CH_4 as depicted in Figs. 4.7, 4.8 and 4.9.

Table 4.2 shows the L_2 norm relative errors (Eq (4.25)) of experimental and simulated results for both cases.

$$\left\|e\right\|_2 = \frac{\left\|\hat{y} - y\right\|_2}{\left\|y\right\|_2} \tag{4.25}$$

where e is the relative error of experimental (y) and simulated ($\hat{y}$) heating values.

Table 4.2: Relative error for experimental and simulated results of different parameters for three different data sets

	% Relative error (Case a)			**% Relative error (Case b)**		
Parameter	**Data 1**	**Data 2**	**Data 3**	**Data 1**	**Data 2**	**Data 3**
HV	4.81	7.93	5.96	15.92	7.55	18.07
m_{CO}	37.53	41.59	13.36	89.65	69.5	214.98
m_{H_2}	10.83	14.95	19.16	17.69	17.25	14.80
m_{CH_4}	23.40	11.35	10.95	48.44	15.71	16.17

It can be observed in the results of Figs. 4.7, 4.8 and 4.9 that, in general, there exists an inverse relationship between the flowrate and heating value. The reason for such relationship has already been discussed in Section 3.4.

Moreover, it can be seen that the results for *Case a* are better than those of *Case b*, which is due to the number of optimization variables in both the cases. The optimization problem in *Case b* covers the full range of variables that are affected by the uncertainty in coal and char ultimate analysis and in λ, while *Case a* considers only the optimization of three input parameters for balancing the coal pyrolysis reaction. It can also be seen that the relative error in case of

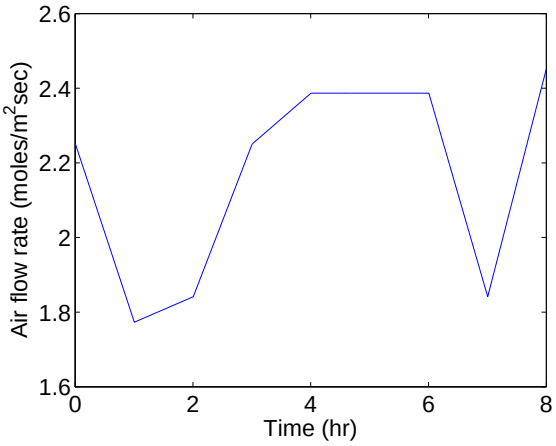

(a) Flow rate of injected air (u).

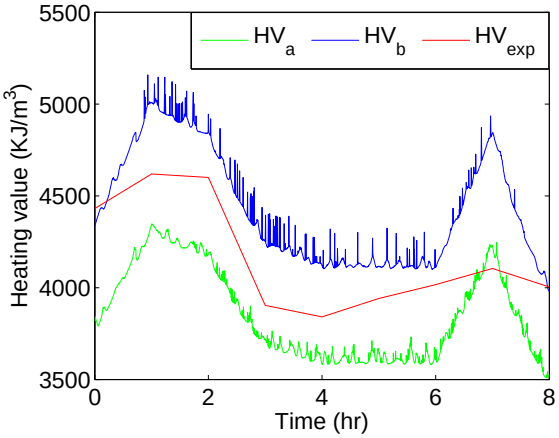

(b) Heating value of the product gas (y).

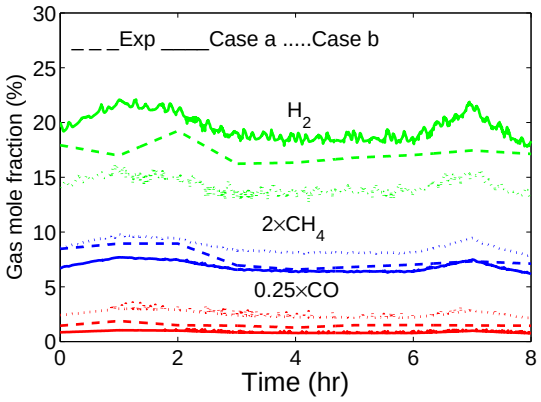

(c) Percentage molar fraction of gases.

Figure 4.7: Comparison between experimental and simulated results of Data 1 for both optimization cases (Case a: optimization using ten variables and Case b: optimization using three variables)

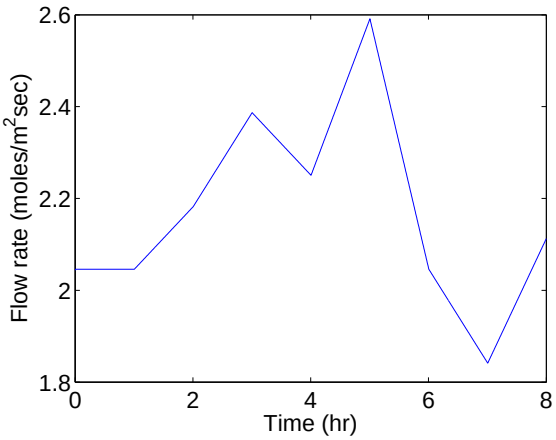

(a) Flow rate of injected air (u).

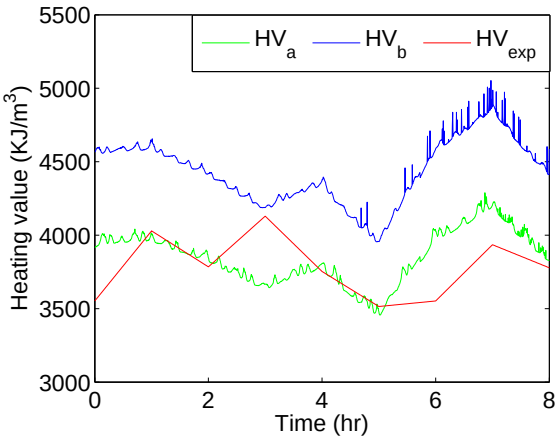

(b) Heating value of the product gas (y).

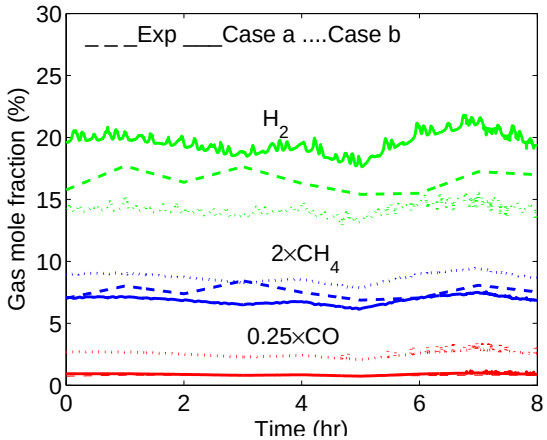

(c) Percentage molar fraction of gases.

Figure 4.8: Comparison between experimental and simulated results of Data 2 for both optimization cases (Case a: optimization using ten variables and Case b: optimization using three variables)

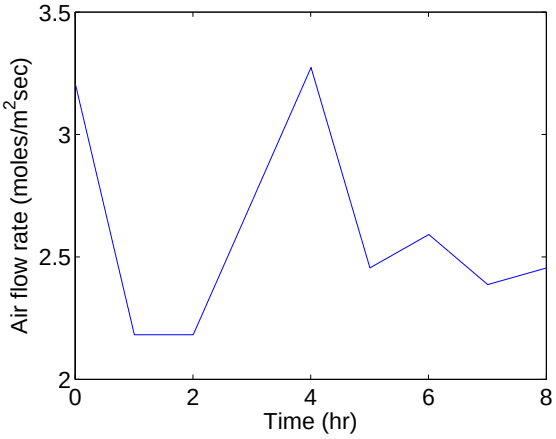

(a) Flow rate of injected air (u).

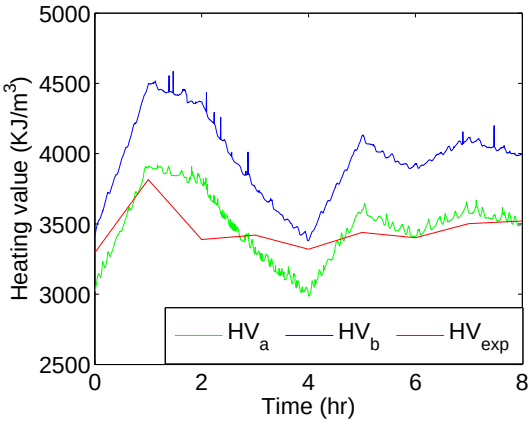

(b) Heating value of the product gas (y).

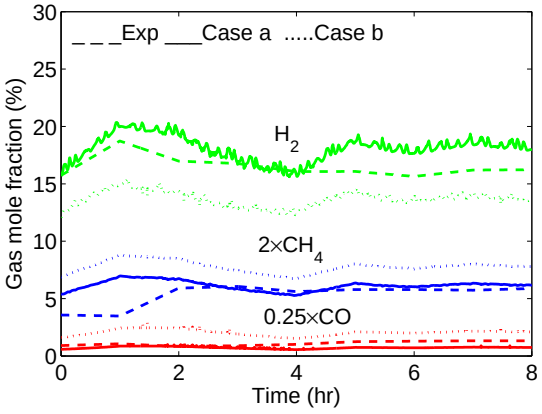

(c) Percentage molar fraction of gases.

Figure 4.9: Comparison between experimental and simulated results of Data 3 for both optimization cases (Case a: optimization using ten variables and Case b: optimization using three variables)

the gas molar fractions is higher than that of the heating value in both the cases. This is because the objective of both the nonlinear programing problems is to minimize the square of the L_2 norm of the relative error between y and y_{exp}.

4.4 Conclusion

In this chapter the computer model of UCG developed in Chapter 3 is successfully validated against the UCG field tests conducted in the Block V of Thar coal field. Before attempting the model validation, the uncertainties in coal and char ultimate analysis, and steam to oxygen ratio at the reaction front are catered by formulating two different nonlinear programing problems. Despite the differences in the structure of the optimization problems, they both aim to minimize the error between the measured and simulated heating values. The optimization problems are solved using SQP algorithm and the results of the solved model are compared with the UCG field test for both the optimization cases. The results show a good match between experimental and simulated heating value of the product gas, especially for the more complete nonlinear programing problem which considers all the parameters affected by the aforementioned uncertainties. However, the results for the molar fractions do not have a good similarity, which is due to the choice of objective function. These results can be improved by selecting an objective function, which considers the minimization of the simulated and experimental error for the molar fraction of the gases individually.

The control of UCG process in Chapter 5 requires the measurement of the heating value alone, therefore, the deviation in the molar fractions of the gases is not very critical for the UCG control system.

CHAPTER 5

Controller Design

The control of highly complex and nonlinear UCG process is a challenging job. As the process occurs under the surface of the earth, so it is either impossible or very expensive to measure all the important parameters of the process, which further complicates the control design. The input of the UCG process is the flow rate of the injected air and the heating value of the product gas is the output. In this chapter a SMC algorithm is designed for a simplified model of an actual UCG process in order to maintain a desired constant heating value. The relative degree of the sliding variable is zero, because the input is readily available in it. As the heating value is the only measurement available, the trivial control design is not possible because of the unavailability of the measurement of all the system's states and various parameters. Therefore, the time derivative of the control is selected as the system input, then the relative degree becomes one and the conventional SMC may be implemented. This approach allows to maintain the output at the desired level and provides insensitivity with respect to different types of uncertainties. The stability of the zero dynamics is proved, which ensures that the overall system is stable. The simulation results demonstrate the robustness of the SMC design against the input disturbance and the modeling inaccuracies.

The model simplifications and the control oriented model are presented in Section 5.1, the control problem is stated in Section 5.2, Section 5.3 details the outline of the SMC design procedure, the analytical design of SMC is discussed in Section 5.4, the solution of the closed system and simulation results are shown in Sections 5.5 and 5.6 respectively and the chapter is concluded in Section 5.7.

5.1 Control oriented model of the UCG process

In order to make model based control of UCG possible, following assumptions are considered in the UCG reactor model given in Section 3.1.

5.1.1 Assumptions for the simplification of the model

5.1.1.1 Constant gas pressure

It is assumed that the pressure of the gas is constant along the length of the reactor. If a well linked channel is established between the injection and production wells then the gas pressure does not drop significantly through the UCG channel [58, 125].

5.1.1.2 Simplification of reaction rate equations

Only three chemical reactions are considered in the simplified model, which include coal pyrolysis, char oxidation and steam gasification. This approximation is justified by the results shown in Fig. 3.6, where these three reactions dominate the reaction zone. Moreover, these three reactions include all the gases and solids considered in the model.

It is assumed that the total concentration of the gases near the reaction front is the sum of the concentrations of H_2O (g), N_2 and O_2: $C_T = \frac{u+\delta}{v_{g_0}}$, where δ is the flow rate of the H_2O (g) generated by water influx (mol/cm^2/s). This approximation simplifies Eqs. (3.13) and (3.14) for R_2 and R_3 respectively, because these reaction rates are only significant at the reaction front as shown in Fig. 3.6. The steam gasification reaction rate in Eq. (3.14) is further simplified by considering that R_3 occurs only in the forward direction as $y_4 > \frac{y_1 y_3}{KE_3}$. The modified reaction rates are given by Eqs. (5.1) and (5.2).

$$R_2 = \frac{v_{g_0} C_7}{u+\delta} CR_2 \tag{5.1}$$

$$CR_2 = \frac{9.55 \times 10^8 k_y \rho_2 P \exp\left(\frac{-22142}{T_s}\right)}{M_2 k_y \sqrt{T_s} + 9.55 \times 10^8 \rho_2 P \exp\left(\frac{-22142}{T_s}\right)}$$

$$R_3 = \frac{\delta}{u+\delta} \tag{5.2}$$

$$CR_3 = \frac{k_y P^2 \rho_2 \exp\left(5.052 - \frac{12908}{T_s}\right)}{P^2 \exp\left(5.052 - \frac{12908}{T_s}\right)\rho_2 + k_y M_2 \left\{P + \exp\left(-22.216 + \frac{24880}{T_s}\right)\right\}^2}$$

5.1.1.3 Simplification of the heating value

The heating value of the product gas y in Eq. (4.15) is rewritten in Eq. (5.3)

$$y = m_{CO}(L) H_{CO} + m_{H_2}(L) H_{H_2} + m_{CH_4}(L) H_{CH_4} + m_{C_nH_m}(L) H_{C_nH_m} \tag{5.3}$$

$$m_{C_i}(L) = 100 \times \frac{C_i}{\tilde{C_T}}\bigg|_{x=L}$$

$$\tilde{C_T} = \sum_{i=1, i\neq 4}^{8} C_i$$

Here it is desired to derive an explicit relationship between y and u. Therefore the mass balance of gas in Eq. (3.3) is analytically solved for all the gases except H_2O (g). This is done by assuming that the velocity of gas phase v_g does not change with the length of the reactor, and we have the simplified gas phase mass balance in Eq. (5.4).

$$\frac{dC_i}{dx} \approx \frac{1}{v_g} \sum_{j=1}^{3} a_{ij} R_j \tag{5.4}$$

The above equation can be easily solved to yield $C_1(L)$, $C_2(L)$, $C_3(L)$, $C_5(L)$ and $C_8(L)$ which represent the concentrations of CO, CO_2, H_2, CH_4 and C_nH_m respectively at $x = L$. All the three reaction rates in Eqs. (3.12), (5.1) and (5.2) do not depend on the concentrations of any of these gases, therefore, the particular solution for the concentration of these gases is given by Eq. (5.5).

$$\int_{C_i(0)}^{C_i(0)} dC_i(x) = \frac{1}{v_g}\sum_{j=1}^{3} a_{ij}\int_0^L R_j dx$$
$$C_i(L) = \frac{1}{v_g}\sum_{j=1}^{3} a_{ij}\int_0^L R_j dx \tag{5.5}$$

where $C_i(0) = 0$, for the product gases.

The solution for the concentration of O_2: C_7 is obtained by using separation of variables method [135], as R_2 in Eq. (5.1) depends on C_7

$$\frac{dC_7}{dx} = -\frac{|a_{7,2}|}{v_g}R_2$$
$$\int_{C_7(0)}^{C_7(L)} \frac{1}{C_7}dC_7 = -\frac{|a_{7,2}|}{u+\delta}\int_0^L CR_2 dx$$
$$C_7(L) = 0.21\frac{u}{v_g}\exp\left(-\frac{|a_{7,2}|}{u+\delta}\int_0^L CR_2\right)dx \tag{5.6}$$

where $C_7(0) = 0.21\dfrac{u}{v_g}$.

N_2 is an inert gas and does not participate in any reaction, hence $C_7(L) = C_7(0) = 0.79\dfrac{u}{v_g}$. After substituting the concentrations of all the gases in Eq. (5.3), an explicit relationship between the input and output of the UCG reactor model is obtained, which is given by Eq. (5.10).

5.1.1.4 Miscellaneous assumptions

The parameters like heat transfer coefficient h, mass transfer coefficient k_y, total gas phase heat capacity C_g and the thermal conductivity of the solids k given in Section 3.1.2 are considered constant to simplify control design.

5.1.2 Simplified model of UCG reactor

The single input (u) and single output (y) model is comprised of three state equations and an output equation (Eq. (5.10)). The state space of the UCG reactor model is comprised of two first order PDEs, one each for the density of

coal and char (Eqs. (5.7) and (5.8)) and one parabolic PDE for solid temperature (Eq. (5.9)).

$$\frac{\partial \rho_1}{\partial t} = -M_1 R_1 \tag{5.7}$$

$$\frac{\partial \rho_2}{\partial t} = M_2 \left(\left| a_{s_{2,1}} \right| R_1 - R_2 - R_3 \right) \tag{5.8}$$

$$\frac{\partial T_s}{\partial t} = \frac{B \frac{\partial^2 T_s}{\partial x^2} + h(T - T_s) - \Delta H_1 R_1 - \Delta H_2 R_2 - \Delta H_3 R_3}{(cp_1 \rho_1 + cp_2 \rho_2)} \tag{5.9}$$

$$y = \frac{100 \left(\alpha \int_0^L R_1 dx + \beta \int_0^L R_3 dx \right)}{\gamma \int_0^L R_1 dx + \eta \int_0^L R_3 dx + \zeta \int_0^L R_2 dx + 0.79 \frac{u}{v_g}} \tag{5.10}$$

$$\alpha = \frac{1}{v_g} (a_{11} H_1 + a_{31} H_3 + a_{51} H_5 + a_{81} H_8)$$

$$\beta = \frac{1}{v_g} (a_{13} H_1 + a_{33} H_3)$$

$$\gamma = \frac{1}{v_g} (a_{11} + a_{21} + a_{31} + a_{51} + a_{81})$$

$$\eta = \frac{1}{v_g} (a_{13} + a_{33})$$

$$\zeta = \frac{a_{2,2}}{v_g}$$

where $R_{i's}(\rho_1, \rho_2, T_s, u)$ with $i = 1,2,3$ are given by Eqs. (3.12), (5.1) and (5.2) respectively. Moreover, the parameter $B = (1 - \phi) k$ is a constant.

5.2 Problem statement

It is desired to design such a control system for the UCG process, which maintains the heating value at the desired level (y_r). The control problem should be solved in the presence of modeling inaccuracies and external disturbance. The flow rate of the steam δ acts as an input disturbance for the system, because, as u determines the initial concentration of O_2, the value of δ sets initial value of H_2O (g) at $x = 0$. Despite the optimization of λ in Section 4.2.3, there still exists the possibility that the value of δ may vary due to certain in-situ phenomena, such as thermomechanical failure of the over burden or bulk collapse of the

roof wall, etc. The value of δ is unknown but it needs to be in a certain range for the process to be operational [122, 123, 125]. Therefore, the control problem can be rephrased as to make $y = y_r$, in the presence of external disturbance δ and modeling inaccuracies. Due to the fact that y is the only measurement available [122, 125], the job of the control system design becomes even more challenging.

5.3 Outline of the design procedure

1. The sliding variable s is selected, such that sliding mode has desired properties. In arbitrary finite dimensional system with state $x \in \Re^n$, sliding mode appears if values $s(x)$ and $\dot{s}(x)$ have different signs. It means $\dot{s}(x)$ should depend on discontinuous control.

2. Discontinuous control is selected to enforce sliding mode based on the above condition: $s(x)$ and $\dot{s}(x)$ should have different signs.

3. Analysis of zero dynamics.

5.4 Control design

The schematic of the UCG control system is shown in Fig. 5.1. The controller computes u based on the values of y and y_r. The dynamics of actuator (control valve) is ignored. The gas analyzer which measures the molar fraction of the gases and computes the heating value y is replaced by Eq. (5.3). As the response time for the gas analyzer is only 15 s, which is quite smaller as compared to the characteristics time for solid and gases, therefore its dynamics are ignored.

5.4.1 Selection of sliding variable

The sliding variable is selected in order to keep the heating value at a desired constant level.

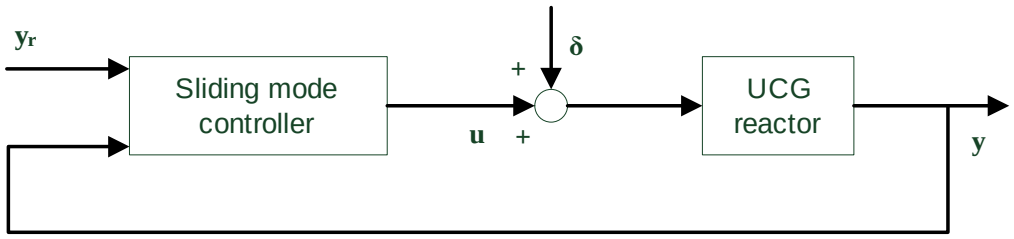

Figure 5.1: UCG reactor model with SMC

$$s = y_r - y \tag{5.11}$$

In order to meet the desired objective we need $s = 0 \implies y = y_r$, and then control can be designed by substituting Eq. (5.10) in Eq. (5.11)

$$\frac{100\left[\alpha\int_0^L R_1dx + \beta\int_0^L R_3dx\right]}{\gamma\int_0^L R_1dx + \eta\int_0^L R_3dx + \zeta\int_0^L R_2dx + 0.79\frac{u}{v_g}} = y_r \tag{5.12}$$

$$\sigma_1 + \sigma_2\frac{\delta}{u+\delta} - \sigma_3\frac{u}{u+\delta} - \sigma_4 u = 0$$

$$u^2\sigma_4 + u\left(-\sigma_1 + \sigma_3 + \delta\sigma_4\right) - \delta\left(\sigma_1 + \sigma_2\right) = 0$$

$$u_1 = \frac{-b + \sqrt{b^2 - 4ac}}{2a}$$

$$u_2 = \frac{-b - \sqrt{b^2 - 4ac}}{2a}$$

where,

$$a = \sigma_4$$

$$b = -\sigma_1 + \sigma_3 + \delta\sigma_4$$

$$c = -\delta\left(\sigma_1 + \sigma_2\right)$$

$$\sigma_1 = \left(100\alpha - \gamma y_r\right)\int_0^L R_1dx$$

$$\sigma_2 = \left(100\beta - \eta y_r\right)\int_0^L CR_3dx$$

$$\sigma_3 = 0.21\zeta y_r\int_0^L CR_2dx$$

$$\sigma_4 = 0.79\frac{y_r}{v_g}$$

where u_1 and u_2 are real as $\sqrt{b^2-4ac} > 0$, also $\sqrt{b^2-4ac} > b$ & $a > 0\ \forall t$, and only valid solution is u_1, because the molar flow rate of the air can not be negative.

However, the trivial control design is not realizable, because the right hand side of u_1 contains state variables and miscellaneous process parameters which are not measurable. So we try to overcome this problem by enforcing sliding mode and inserting integrator in the input, such that $\dot{u} = \nu$ and $\nu = -\kappa \operatorname{sign}(s)$, $\kappa \in R^+$. Therefore, $\dot{s}$ depends on discontinuous control ν. Now we need to find time derivative of the sliding variable in the form $\dot{s} = \nu\phi + \theta$, where ϕ and θ are state functions.

$$
\begin{aligned}
&\dot{s} = \dot{y_r} - \dot{y} \qquad (5.13)\\
&\dot{y} = \frac{100}{D^2}\left(D\dot{N} - N\dot{D}\right)\\
&\textit{where},\\
&N = \alpha\int_0^L R_1 dx + \beta\int_0^L R_3 dx\\
&D = \gamma\int_0^L R_1 dx + \eta\int_0^L R_3 dx + \zeta\int_0^L R_2 dx + \frac{0.79}{\nu_g}u\\
&\dot{N} = \alpha\int_0^L \dot{R}_1 dx + \beta\int_0^L \dot{R}_3 dx\\
&\dot{D} = \gamma\int_0^L \dot{R}_1 dx + \eta\int_0^L \dot{R}_3 dx + \zeta\int_0^L \dot{R}_2 dx + \frac{0.79}{\nu_g}\dot{u}\\
&\textit{where},\\
&\dot{R}_3 = \left(\frac{\delta}{u+\delta}\right)C\dot{R}_3 + CR_3\frac{d}{dt}\left(\frac{\delta}{u+\delta}\right)\\
&\quad = \left(\frac{\delta}{u+\delta}\right)C\dot{R}_3 + \frac{CR_3}{(u+\delta)^2}\left(u\dot{\delta} - \delta\dot{u}\right)\\
&\dot{R}_2 = 0.21\frac{d}{dt}\left(\frac{uCR_2E_u}{u+\delta}\right)\\
&\quad = \dot{u}\omega + \psi
\end{aligned}
$$

where,

$$E_u = \exp\left(-\frac{|a_{7,2}|}{u+\delta}\int_0^L CR_2 dx\right)$$

$$\omega = \frac{|a_{7,2}| u C R_2 E_u \int_0^L CR_2 dx}{4.762\,(u+\delta)^3} + \frac{\delta E_u \int_0^L CR_2 dx}{4.762\,(u+\delta)^2}$$

$$\psi = \frac{u E_u \dot{\delta} C R_2 \int_0^L CR_2 dx}{4.701\,(u+\delta)^3} - \frac{u E_u \dot{\delta} C R_2}{4.762\,(u+\delta)^2} + \frac{u E_u C \dot{R}_2}{4.762\,(u+\delta)}$$

By substituting $\dot{y_r} = 0$ (y_r is constant) and $\dot{y}$ in Eq. (5.13), the closed form expression for $\dot{s}$ takes the desired form

$$\dot{s} = \nu\phi + \theta,\ \dot{u} = \nu \tag{5.14}$$

where,

$$\phi = 100\frac{N\varphi}{D^2}$$

$$\theta = \frac{100}{D^2}\left[N\left(\vartheta_1 + \vartheta_2\right) - D\vartheta_3\right]$$

where,

$$\varphi = \frac{0.79}{v_g} + \frac{\int_0^L CR_3 dx}{(u+\delta)^2}(\beta - \delta) + \zeta\int_0^L \omega dx$$

$$\vartheta_1 = \int_0^L \dot{R}_1 dx\,(\gamma - \alpha) + \zeta\int_0^L \psi dx$$

$$\vartheta_2 = \frac{\eta}{(u+\delta)}\left[\frac{u\dot{\delta}\int_0^L CR_3 dx}{(u+\delta)} + \delta\int_0^L C\dot{R}_3 dx\right]$$

$$\vartheta_3 = \frac{\beta}{(u+\delta)}\left[\frac{u\dot{\delta}\int_0^L CR_3 dx}{(u+\delta)} + \delta\int_0^L C\dot{R}_3 dx\right]$$

The function $\phi = 100\frac{N\varphi}{D^2} > 0, \forall t \geq 0$, because N, D and φ in Eqs. (5.13) and (5.14) depend upon R_1, R_2, R_3, u, δ and v_g which are always positive. Moreover, the constants α, β, γ, η and ζ in Eq. (5.10) are also positive and $\beta >> \delta$ in φ. The function $\phi(t)$ is bounded by Φ_l and Φ_u such that: $0 < \Phi_l \leq \phi(t) \leq \Phi_u$, and $\theta(t)$ is upper bounded by Θ_u: $\left\|\theta(t)\right\| \leq \Theta_u$.

As $\phi(t) > 0, \forall t \geq 0$, therefore sliding mode can be enforced by selecting a suitable value of discontinuous controller gain κ

5.4.2 Enforcing sliding mode

In order to prove the existence of sliding mode a positive definite Lyapunov function is chosen, which is given by Eq. (5.15).

$$V = \frac{1}{2}s^2 > 0 \tag{5.15}$$

The time derivative of V is given by Eq. (5.16).

$$\begin{aligned} \dot{V} &= s\dot{s} \\ &= s(\nu\phi + \theta) \\ &= s(-\kappa \operatorname{sign}(s)\phi + \theta) \\ &\leq |s|(-\kappa\Phi_l + \Theta_u) \end{aligned} \tag{5.16}$$

If $\kappa = \dfrac{\tau + \Theta_u}{\Phi_l}$ with $\tau \in R^+$, then the time derivative of the Lyapunov function is negative definite (Eq. (5.17)), and sliding mode exists.

$$\dot{V} \leq -\tau|s| < 0 \tag{5.17}$$

Even more, sliding mode occurs after a finite time interval [115], and the main control problem is solvable.

5.4.3 Stability of the zero dynamics

The relative degree r of sliding variable s is zero, because u is readily available in s. Therefore, all the state equations in Section 5.1.2 constitute the zero dynamics of the system with $u = u_1$ (Eq. (5.12)), which makes $s = 0$ [116]. After the

establishment of sliding mode it is mandatory to check whether the motion of the system called zero dynamics is stable.

The zero dynamics are comprised of following set of equations, after $t \geq t_{ss}$ when $s = 0$. The Eqs. (5.18), (5.19) and (5.20) are obtained by replacing $R_i(\rho_1, \rho_2, T_s, u)$ by $\tilde{R}_i\left(\tilde{\rho_1}, \tilde{\rho_2}, \tilde{T_s}, u_1\right)$ in Eqs. (5.7), (5.8) and (5.9).

$$\frac{\partial \tilde{\rho_1}}{\partial \tilde{t}} = -M_1 \tilde{R_1} \tag{5.18}$$

$$\frac{\partial \tilde{\rho_2}}{\partial \tilde{t}} = M_2\left(\left|a_{s_{2,1}}\right|\tilde{R_1} - \tilde{R_2} - \tilde{R_3}\right) \tag{5.19}$$

$$\frac{\partial \tilde{T_s}}{\partial \tilde{t}} = \frac{1}{C_s}\left[B\frac{\partial^2 \tilde{T_s}}{\partial x^2} + h(T - \tilde{T_s}) - H_s\right] \tag{5.20}$$

where,

$C_s = cp_1\tilde{\rho_1} + cp_2\tilde{\rho_2}$

$H_s = -\left|q_1\right|\tilde{R_1} - \left|q_2\right|\tilde{R_2} + \left|q_3\right|\tilde{R_3}$

where $\tilde{t} = t - t_{ss}$ and H_s is the heat source generated from the chemical reactions. Since coal pyrolysis and char oxidation reactions are exothermic in nature, hence there heat of reaction is negative [122].

The boundedness of the zero dynamics is investigated in the subsequent paragraphs.

The solution of Eq. (5.18) is given as:

$$\tilde{\rho_1}(\tilde{t}, x) = C\exp(-5E_3\tilde{t}) \tag{5.21}$$

where,

$C(x) = \tilde{\rho_1}(0, x)$

$E_3(x) \leq \exp\left\{\frac{-6039}{\max\limits_{\tilde{t}\geq 0} \tilde{T_s}(\tilde{t}, x)}\right\}$

It is important to note that for $0 < \tilde{T}_{smin} \leq \tilde{T}_s(\tilde{t},x) \leq \infty$, the distribution $\tilde{\rho}_1(0,x)$ exponentially decays with time.

In order to evaluate the boundedness of $\tilde{\rho}_2$ and $\tilde{T}_s$, it is important to show that $\tilde{R}_1$, $\tilde{R}_2$, $\tilde{R}_3$ and u_1 are bounded. The Eqs. (3.12), (5.1) and (5.2) show that the reaction rates are dependent on $\tilde{\rho}_1$, $\tilde{\rho}_2$ and $\tilde{T}_s$. It has been proved in Eq. (5.21) that $\tilde{\rho}_1$ is stable, which also implies the stability of $\tilde{\rho}_2$, because $\tilde{\rho}_1$ is decomposed by coal pyrolysis reaction to yield $\tilde{\rho}_2$ and product gases, therefore, for law of conservation of mass to hold:

$$\max_{\substack{0\leq x\leq L\\ \tilde{t}\geq 0}} \tilde{\rho}_2(\tilde{t},x) < \max_{\substack{0\leq x\leq L\\ \tilde{t}\geq 0}} \tilde{\rho}_1(\tilde{t},x)$$

Now it can be inferred from Eqs. (3.12), (5.1) and (5.2) that for any $\tilde{T}_s$: $0 < \tilde{T}_{smin} \leq \tilde{T}_s(\tilde{t},x) \leq \infty$, the reaction rates are bounded. The input u_1 is also bounded as it is the function of the reaction rates (Eq. (5.12)).

Th complete solution of Eq. (5.19) is found by rewriting it in the following form, which is obtained by substituting Eqs. (5.1) and (5.2) in Eq. (5.19).

$$\frac{\partial \tilde{\rho}_2}{\partial \tilde{t}} + \tilde{\rho}_2 \xi = \chi \tag{5.22}$$

where,

$$\chi(x) \leq \left|a_{s_{2,1}}\right| M_2 \tilde{R}_1 \Big|_{\max\limits_{\tilde{t}\geq 0} T_s(\tilde{t},x)}$$

$$\xi(x) \leq \left(\frac{0.21 u_1 \tilde{E}_u \Pi_1}{\delta + u_1} + \frac{\delta \Pi_2}{\delta + u_1}\right)\Bigg|_{\max\limits_{\tilde{t}\geq 0} T_s(\tilde{t},x), U_1, \Delta}$$

$$\Pi_1 = \frac{9.55\times 10^8 P \exp\left(\dfrac{-22142}{\tilde{T}_s}\right) k_y}{M_2 k_y \sqrt{\tilde{T}_s} + 9.55\times 10^8 \rho_2 P \exp\left(\dfrac{-22142}{\tilde{T}_s}\right)}$$

$$\Pi_2 = \frac{k_y P^2 \tilde{E}_1}{P^2 \tilde{E}_1 \rho_2 + k_y M_2 \left(P + \tilde{E}_2\right)^2}$$

$$\tilde{E_u} = \exp\left(-\frac{|a_{7,2}|}{u_1+\delta}\int_0^x C\tilde{R}_2 dx\right)$$

where $0 < u_1 \leq U_1,\ 0 < \delta \leq \Delta,\ \tilde{E_1} = E_1(\tilde{T_s}),\ \tilde{E_2} = E_2(\tilde{T_s})$ and $C\tilde{R}_2 = CR_2(\tilde{T_s})$. The parameters CR_2, E_1 and E_2 are given in Eqs. (5.1) and (5.2).

Now (5.22) can be solved as a linear PDE.

$$\begin{aligned}
&Let,\ \varpi(\tilde{t}) = \exp\left(\int \xi \tilde{dt}\right)\\
&\frac{\partial\tilde{\rho}_2}{\partial\tilde{t}}\varpi(\tilde{t}) + \varpi(\tilde{t})\tilde{\rho}_2\xi = \chi\varpi(\tilde{t})\\
&\int \frac{d}{\tilde{dt}}\left[\tilde{\rho}_2 \exp(\xi\tilde{t})\right]\tilde{dt} = \chi\int \exp(\xi\tilde{t})\tilde{dt}\\
&\tilde{\rho}_2(\tilde{t},x) = \underbrace{\frac{\chi(\tilde{t},x)}{\xi(\tilde{t},x)}}_{S_1} + \underbrace{C\exp\left[-\xi(\tilde{t},x)\tilde{t}\right]}_{S_2} \qquad (5.23)\\
&where,\\
&C(x) = \left[\tilde{\rho}_2(0,x) - \frac{\chi(0,x)}{\xi(0,x)}\right]
\end{aligned}$$

Before investigating the solution of $\tilde{\rho}_2(\tilde{t},x)$ in (5.23), a brief description of the reaction zone [122] within the UCG reactor is mandatory. The reaction zone Ω is a region along the length of the reactor, where all the chemical reactions occur, when $\tilde{\rho}_1, \tilde{\rho}_2 > 0$ then: $x = 0 < x_r \leq \Omega \leq x_p < x = L$. The boundary of Ω towards $x = L$ is x_p which represents the *pyrolysis front*, whereas x_r towards $x = 0$ corresponds to the *reaction front*. The pyrolysis reaction occurs in the proximity of x_p with rate $\tilde{R_1}$, yielding char and product gases. The char produced by pyrolysis reaction spans whole Ω. The region beyond x_p contains unreacted coal, while the region before x_r contains ash produced from the burnt coal and char. The values of $\tilde{R_2}$ and $\tilde{R_3}$ are only significant near x_r, because $\tilde{T_s}$ has its maximum value here.

Now it can be inferred from (5.23) that $\tilde{\rho}_2$ is produced near x_p with rate

determined by S_1. The $\tilde{\rho_2}$ is consumed by $\tilde{R_2}$ and $\tilde{R_3}$ near x_r as suggested by S_2. The reaction zone Ω moves towards $x = L$ with time, as the coal and char are continuously consumed by the reactants: O_2 and H_2O (g). Therefore, when all the coal is consumed in the reactor then production of $\tilde{\rho_2}$ is ceased and it is only consumed around x_r:

$$\tilde{\rho_2}(\tilde{t},x) = \left[\rho_2(0,x) - \frac{\chi(0,x)}{\xi(0,x)}\right] \exp(-\xi\tilde{t})$$

The heat equation in (5.20) can be rewritten as:

$$\begin{aligned} & C_s\dot{\tilde{T}}_s = B\tilde{T_s}'' - h\tilde{T_s} + hT(x) + H_s \qquad (5.24)\\ & with,\\ & \tilde{T_s}(0,x) = \tilde{T_{s_0}}(x)\\ & \tilde{T_s}'(\tilde{t},0) = \tilde{T_s}'(\tilde{t},L) = 0 \end{aligned}$$

where $\dot{\tilde{T}}_s = \dfrac{\partial\tilde{T_s}}{\partial\tilde{t}}$, $\tilde{T_s}' = \dfrac{\partial\tilde{T_s}}{\partial x}$ and $\tilde{T_s}'' = \dfrac{\partial^2\tilde{T_s}}{\partial x^2}$.

The solution of Eq. (5.24) is acceptable if it is not unstable, strictly speaking we need to show that the solution is bounded. Formally speaking we have to deal with the analysis of a complex nonlinear system, since H_s depends on $\tilde{T_s}$. But as it has been shown previously that all the reaction rates are bounded for any value of $\tilde{T_s}$, hence H_s is also bounded. Therefore, our problem may be reformulated in the following way. It should be shown that solution to the linear PDE:

$$\begin{aligned} & \dot{\tilde{T}}_s = \frac{1}{C_s}\left[B\tilde{T_s}'' - h\tilde{T_s} + hT(x) + \mathscr{G}(\tilde{t},x)\right] \qquad (5.25)\\ & where,\\ & \left|\mathscr{G}(\tilde{t},x)\right| \leq \mathscr{G}_0,\ \mathscr{G}_0 \in \Re^+ \end{aligned}$$

can be represented in the following form:

$$\tilde{T}_s = \Delta\tilde{T}_s + \tilde{T}_{sx} + \tilde{T}_{sd} \tag{5.26}$$

where $\Delta\tilde{T}_s$ corresponds to the solution without the inputs $T(x)$ and $\mathscr{G}$, $\tilde{T}_{sx}$ is the forced component defined by $T(x)$ and $\tilde{T}_{sd}$ is the forced part which depends on the disturbance $\mathscr{G}(\tilde{t},x)$.

The boundedness of all the solution components in Eq. (5.26) is investigated independently.

Consider the homogeneous heat equation:

$$\begin{aligned} &C_s\Delta\dot{\tilde{T}}_s = B\Delta\tilde{T}_s'' - h\Delta T_s \\ &with, \\ &\Delta\tilde{T}_s(0,x) = \Delta\tilde{T}_{s_0}(x) \\ &\Delta\tilde{T}_s'(\tilde{t},0) = \Delta\tilde{T}_s'(\tilde{t},L) = 0 \end{aligned} \tag{5.27}$$

The stability of Eq. (5.27) is investigated by the positive definite Lyapunov functional:

$$V = \frac{1}{2}\int_0^L C_s\Delta\tilde{T}_s{}^2 dx > 0 \tag{5.28}$$

The time derivative of V is given as:

$$\dot{V} = \underbrace{\int_0^L \Delta\tilde{T}_s C_s \Delta\dot{\tilde{T}}_s dx}_{\dot{V}_1} + \underbrace{\frac{1}{2}\int_0^L \Delta\tilde{T}_s{}^2 \dot{C}_s dx}_{\dot{V}_2} \tag{5.29}$$

where,

$$\begin{aligned}
\dot{V}_1 &= B\int_0^L \Delta\tilde{T}_s\left(\Delta\tilde{T}_s'\right)' dx - h\int_0^L \Delta\tilde{T}_s{}^2 dx \\
&= -B\int_0^L \left(\Delta\tilde{T}_s'\right)^2 dx - h\int_0^L \Delta\tilde{T}_s{}^2 dx < 0 \\
\dot{V}_2 &= \frac{1}{2}\int_0^L \Delta\tilde{T}_s{}^2\left(cp_1\dot{\tilde{\rho}}_1 + cp_2\dot{\tilde{\rho}}_2\right) dx \\
&= -\frac{\left(M_1 cp_1 - \left|a_{s_{2,1}}\right| cp_2 M_2\right)}{2}\int_0^L \tilde{R}_1\Delta\tilde{T}_s{}^2 dx \\
&\quad - \frac{M_2 cp_2}{2}\int_0^L \Delta\tilde{T}_s{}^2\left(\tilde{R}_2 + \tilde{R}_3\right) dx < 0
\end{aligned}$$

where $M_1 cp_1 > \left|a_{s_{2,1}}\right| cp_2 M_2$.

As the time derivative of the Lyapunov functional in Eq. (5.29) is strictly negative, hence $\Delta\tilde{T}_s$ is asymptotically stable.

The following boundary value problem is solved to yield $\tilde{T}_{sx}$

$$\begin{aligned}
&B\tilde{T}_{sx}'' - h\tilde{T}_{sx} + hT(x) = 0 \\
&\tilde{T}_{sx}'(t,0) = \tilde{T}_{sx}'(t,L) = 0
\end{aligned} \tag{5.30}$$

The gas temperature $T(x)$ is obtained by solving the linear ODE in Eq. (3.4)

$$T(x) = T(0)\exp(-\lambda x) + \lambda\int_0^x \exp\{-\lambda(x-\mathscr{X})\}\tilde{T}_s(\mathscr{X})d\mathscr{X} \tag{5.31}$$

where $\lambda = \dfrac{h}{v_g C_g}$ is a constant

Eq. (5.30) can be rewritten in the following form by substituting $h(T-\tilde{T}_s) = -v_g C_g T'$ from Eq. (3.4)

$$B\tilde{T}_{sx}'' - v_g C_g T' = 0 \tag{5.32}$$

By differentiating Eq. (5.31) with respect to x and substituting T' in Eq. (5.32) yields the nonhomogeneous boundary value problem:

$$B\tilde{T}_{sx}'' - h\tilde{T}_{sx} = -\Lambda \exp(-\lambda x) \tag{5.33}$$

where $\Lambda = h\left[T(0) + \tilde{T}_s(0,0)\right]$ is a constant

The overall solution of Eq. (5.33) is: $\tilde{T}_{sx} = \tilde{T}_{sc} + \tilde{T}_{sp}$. The complementary solution $\tilde{T}_{sc}$ is obtained by solving the following equation:

$$B\tilde{T}_{sx}'' - h\tilde{T}_{sx} = 0 \tag{5.34}$$

The characteristic polynomial for the second order ODE is: $r^2 - \dfrac{h}{B} = 0$, which yields $r = \pm\sqrt{\dfrac{h}{B}}$. The general form of $\tilde{T}_{sc}$ is given as:

$$\tilde{T}_{sc} = C_1 \exp\left(\sqrt{\frac{h}{B}}\right) + C_2 \exp\left(-\sqrt{\frac{h}{B}}\right) \tag{5.35}$$

After incorporating the boundary conditions, $\tilde{T}_{sc} = 0$, as $C_1 = C_2 = 0$.

Let the particular solution be: $\tilde{T}_{sp} = \mathscr{A} \exp(-\lambda x)$. Now by substituting $\tilde{T}_{sp}$ in Eq.(5.33) the value of constant $\mathscr{A}$ is obtained

$$\begin{aligned} &B\mathscr{A}\lambda^2 \exp(-\lambda x) - h\mathscr{A} \exp(-\lambda x) = -\Lambda \exp(-\lambda x) \\ &\mathscr{A} = -\frac{\Lambda}{\lambda^2 B - h} \end{aligned} \tag{5.36}$$

The solution $\tilde{T}_{sx}$ is given as:

$$\tilde{T}_{sx} = -\frac{\Lambda}{\lambda^2 B - h} \exp(-\lambda x) \tag{5.37}$$

Therefore, the forced response $\tilde{T}_{sx}$ due to $T(x)$ is also bounded.

As the disturbance $\mathscr{G}$ in Eq. (5.24) is bounded, therefore, $\tilde{T}_{sd}$ is also bounded. The boundedness of $\tilde{T}_{sd}$ can be shown if it is represented in the modal form [136].

All the solution components of Eq. (5.26) are bounded, therefore, $\tilde{T}_s$ stays bounded throughout the process of gasification.

The results in (5.21), (5.23) and boundedness of $\tilde{T}_s$ show that the zero dynamics of the UCG process are bounded and SMC design is valid.

5.5 Numerical solution of the closed loop system

The process of UCG is solved in two modes: ignition for first t_0 s and then gasification for $t > t_0$. The purpose of the ignition is to heat up the coal seam so that it could become conducive to the gasification reactions. The detail description of the solution of the UCG reactor is given in Section 3.2, but, in order to keep the interest of the reader a brief description of the solution strategy is given in Table 5.1. However, the main objective of Table 5.1 is to show that how does the control input interacts with the system.

The UCG system is operated in open loop for $0 \leq t < t_{cl}$ with the input u_{ol}, and for $t \geq t_{cl}$ the operation is closed loop with the flow rate u. Actually the controller is brought in to the loop after the transients of the ignition phase are settled down.

The differential equation: $\dot{u} = -\kappa \operatorname{sign}(s)$ is numerically solved in Eq. (5.38) using the forward difference method [120] with $u(t_{cl}) = u_{ol}$.

$$u(t+dt) = -\kappa \operatorname{sign}\{s(t)\}dt + u(t) \tag{5.38}$$

where dt is the sampling time for the numerical solution.

The control input determines the concentration of the O_2 and N_2 at $x = 0$ required to obtain the desired heating value at $x = L$. One part of the input directly effects the output as the inert gas N_2 does not participate in any chemical reaction and the other part influences the heating value through the UCG process model.

Table 5.1: Solution of the closed loop system

1. Input all the model parameters
2. Initialize the solid subsystem (Eqs. (3.1) and (3.2)): $\rho_i(0,x) = \rho_{i_0}(x)$ and $T_s(0,x) = T_{s_0}(x)$
3. Solve gas equations: Eqs. (3.3), (3.4), (3.5) and (3.7) to yield the initial distributions with following inlet boundary conditions: $C_i(0) = \begin{bmatrix} 0 & 0 & 0 & 0 & 0 & \dfrac{0.79u_{ol}}{v_{g_0}} & \dfrac{0.21u_{ol}}{v_{g_0}} & 0 \end{bmatrix}$, $T(0) = T_0$, $v_g(0) = v_{g_0}$ and $P(0) = P_0$
4. Iterative loop for time
   - Solve the solid equations for new time.
   - Solve the gas equations to yield updated distributions of the solution variables with same values at $x = 0$ in step 3, except:

$$C_4(0) = \begin{cases} 0, & \text{if } 0 \le t \le t_0 \\ \dfrac{\delta}{v_{g_0}}, & \text{if } t > t_0 \end{cases}$$

$$\begin{bmatrix} C_6(0) & C_7(0) \end{bmatrix} = \begin{cases} \dfrac{u_{ol}}{v_{g_0}} \begin{bmatrix} 0.79 & 0.21 \end{bmatrix} & \text{if } 0 \le t < t_{cl} \\ \dfrac{u(t+dt)}{v_{g_0}} \begin{bmatrix} 0.79 & 0.21 \end{bmatrix} & \text{if } t \ge t_{cl} \end{cases}$$

5. Update time: $t^{n+1} = t^n + dt$
6. Stop if $t = t_{end}$, else go to step 4

5.6 Simulation results

This section presents some simulation results for the closed loop system. For simulations $t_{cl} = 1$ hr, $dt = 10$ s and the controller gain $\kappa = 2 \times 10^{-8}$. The simulations are performed on actual model of the UCG process given in Section 3.1.

The control effort in Fig. 5.2 drags y to y_r (Fig. 5.3). As discussed in Section 3.4 that a critical amount of steam is required for the process of UCG to exist, otherwise the starvation or flooding of the UCG cavity can occur. The

profile of δ used for evaluating the robustness of the SMC algorithm is shown in the Fig. 5.4. Despite the variation in δ the controller successfully keeps the output at its desired level. The increase in δ increases the production of syngas and hence y. The controller reacts to the situation by increasing u which provides more O_2 for char oxidation reaction, and results in higher concentration of CO_2, which decreases y by reducing the molar fractions of CO and H_2. Moreover, increasing u produces more moles of N_2 which directly decreases y. Similarly when δ decreases, the controller also reduces the moles of air entering the reactor to increase y.

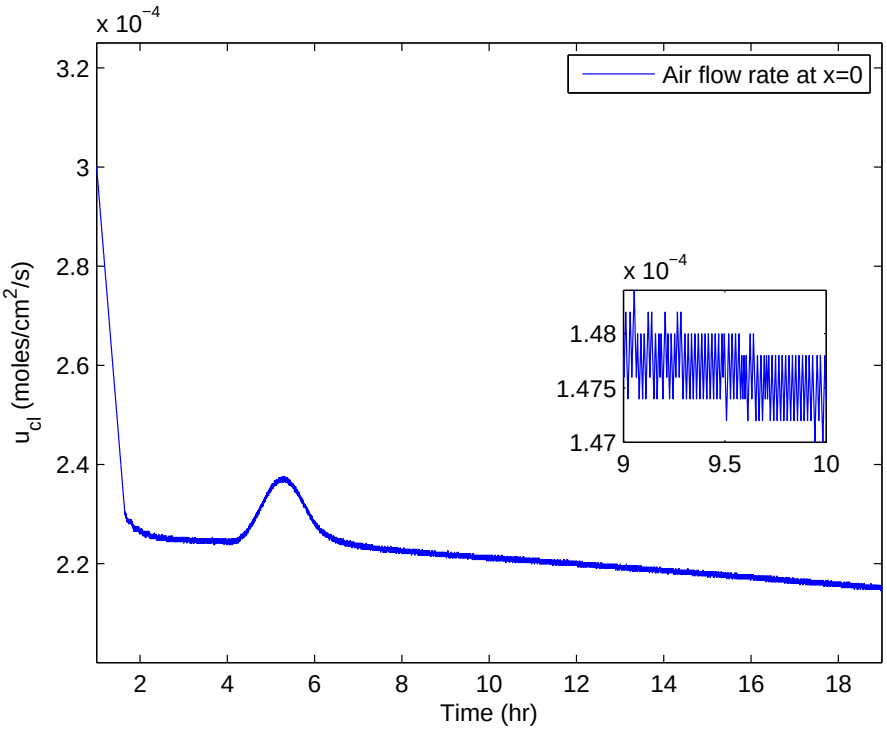

Figure 5.2: Control effort with time

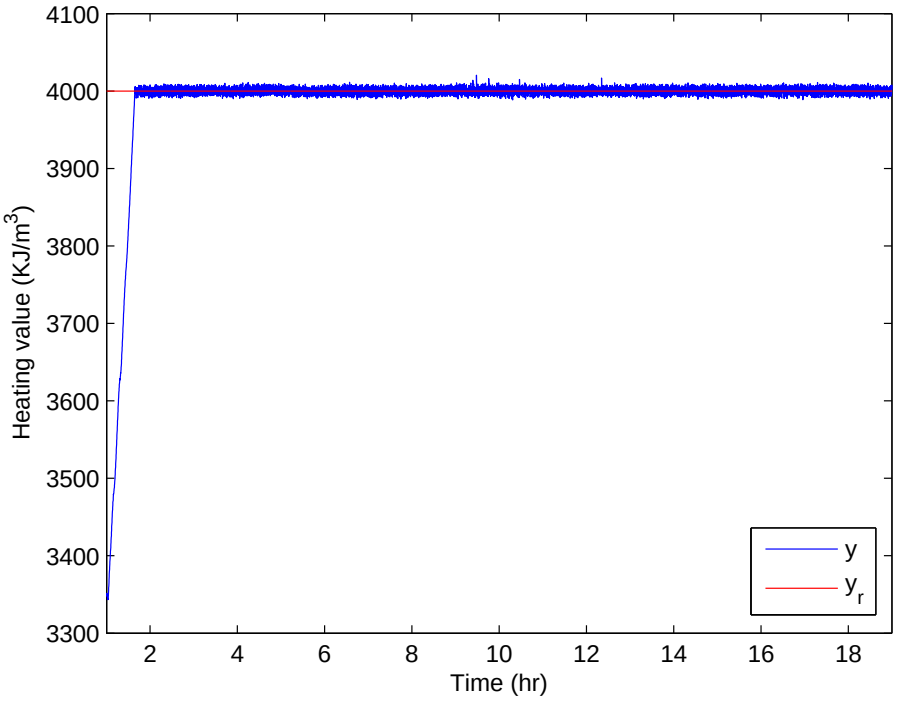

Figure 5.3: Output of the UCG process with time

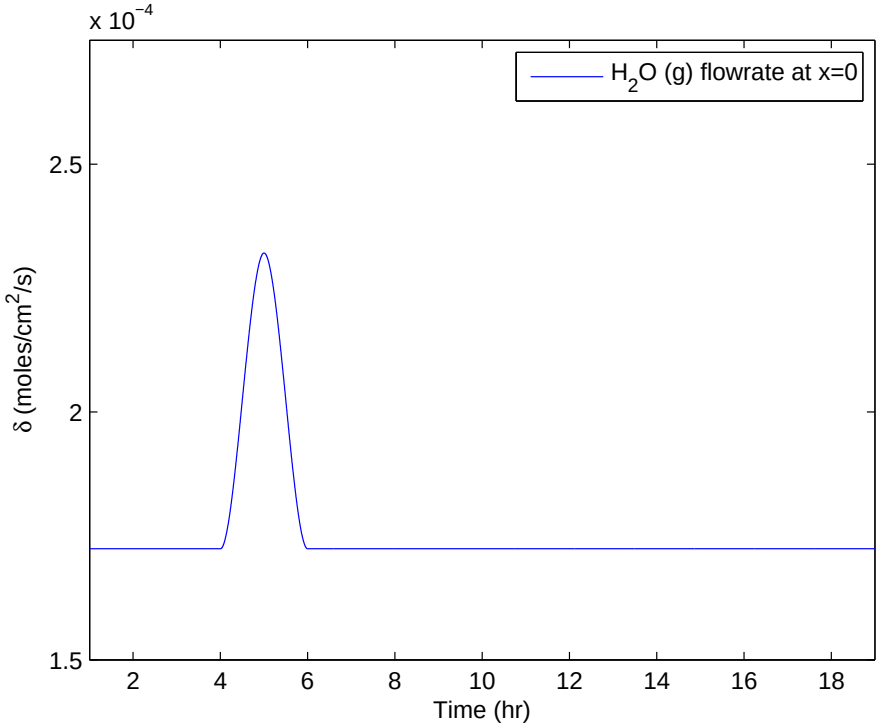

Figure 5.4: Disturbance with time

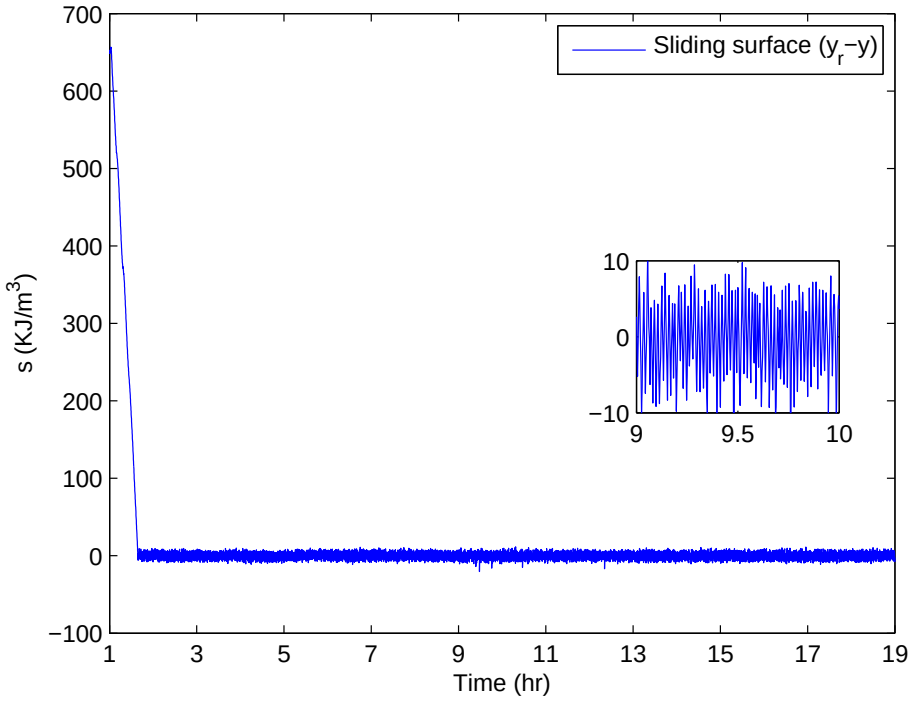

Figure 5.5: Sliding variable with time

The sliding variable s is shown in Fig. 5.5. In reaching phase: $s \neq 0$, the controller drags y to the sliding manifold in the presence of δ and modeling uncertainties. While the design of s keeps $y = y_r$ during the sliding motion: $s = 0$. The chattering phenomenon can also be seen in the zoomed view of Fig. 5.5, which is produced due to finite sampling frequency of discretization: $f_s = 1/dt = 0.1$ hz and modeling inaccuracies.

The solutions of the states of the UCG process are shown in Figs. 5.6, 5.7 and 5.8. The results are shown for 19 hrs and 400 cm, because during this time the coal bed is approximately consumed up to 350 cm.

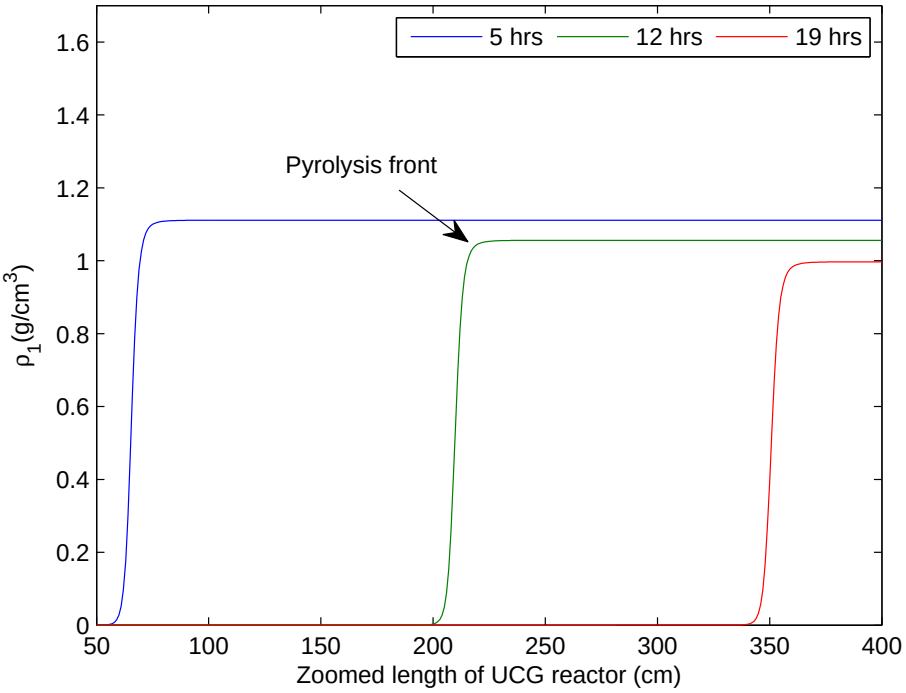

Figure 5.6: Coal density distributions with length at different simulation times

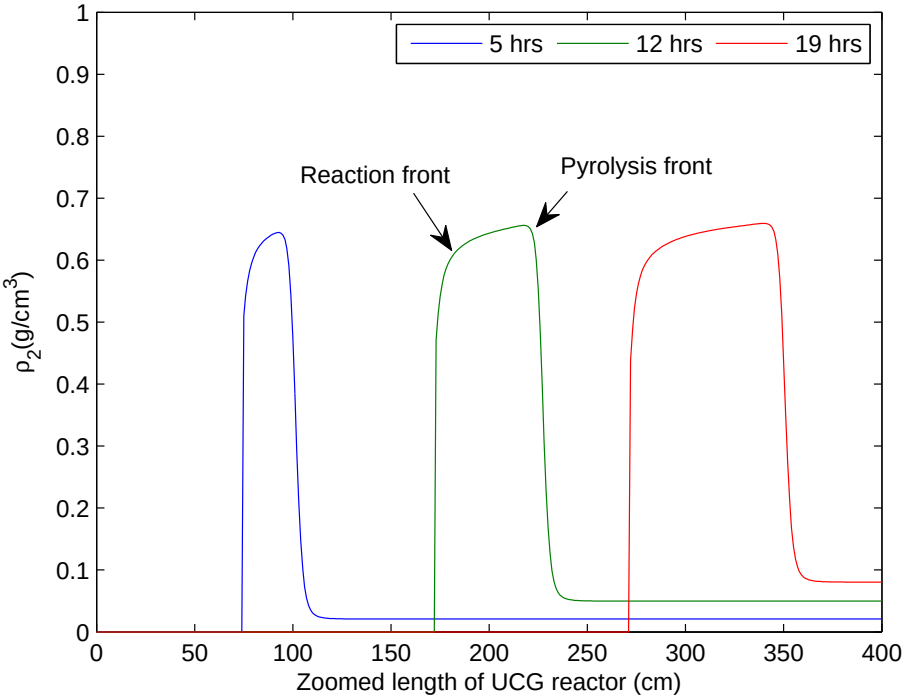

Figure 5.7: Char density distributions with length at different simulation times

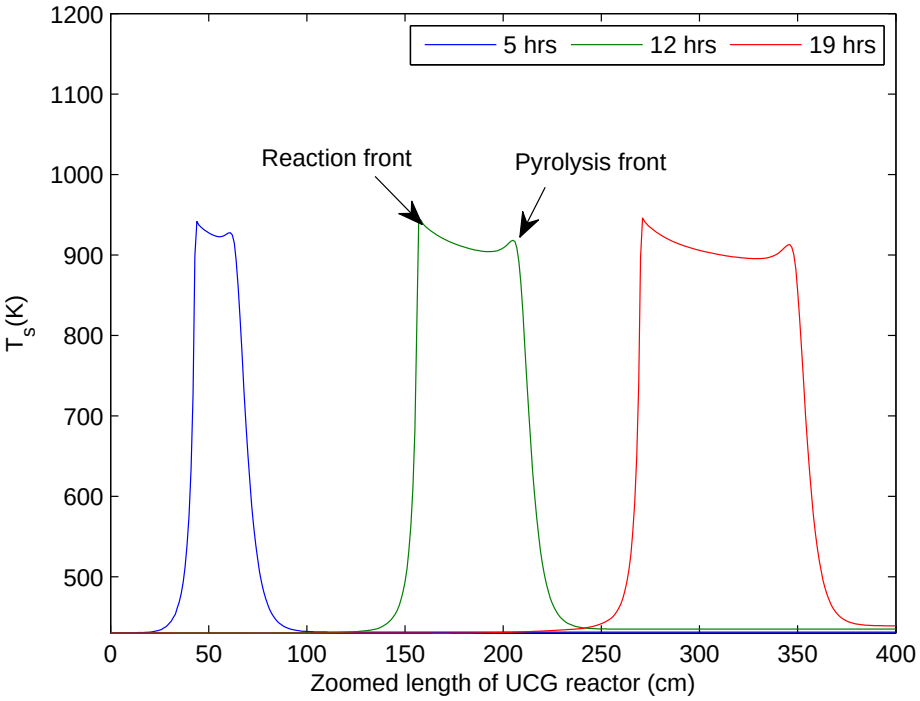

Figure 5.8: Solid temperature distributions with length at different simulation times

Fig. 5.6 shows that the magnitude of the coal density distribution is decreasing with time, which justifies the solution for the mass balance of coal in Eq. (5.21). It can also be noticed that the distribution of coal density is pushed towards $x = L$ with time.

The magnitude of the ρ_2 distribution is increasing with time (Fig. 5.7) due to the coal pyrolysis reaction, but this increase lessens as ρ_1 decreases. It can also be observed that the width of the reaction zone Ω is also widening with time. The char density is consumed by R_2 and R_3 near the reaction front.

Fig. 5.8 shows that the T_s distributions have higher values in Ω. All the chemical reactions occur within this region, beyond this region the temperature is not high enough to support any chemical reaction. A high value of temperature is maintained within the reaction zone by the exothermic nature of coal pyrolysis and char oxidation reactions. Therefore, when all of the coal and char is consumed then there is no more fuel to be burnt, and the temperature will at-

tain its lowest possible value determined by the respective boundary conditions.

The boundedness of the zero dynamics proved in Section. 5.4.3 can also be verified from the results in Figs. 5.6, 5.7 and 5.8.

5.7 Conclusion

SMC successfully maintains the desired heating value of the product gas mixture. The gain of the SMC is found by knowing the bounds of the auxiliary functions of the process variables. However, this methodology is applicable if in addition to tracking, the problem of stability is also solved. In our case it should be shown that so called zero dynamics are governed by a set of PDEs. For the mass balance equations, solutions were found analytically, whereas the boundedness of the heat equation was proved. The selected value of the controller gain also compensates for the input disturbance and the modeling approximations made for analytical control design. The simulation results show the success of the SMC algorithm.

The implementation of the designed SMC on the actual UCG site will hopefully further validate its effectiveness.

CHAPTER 6

Conclusion and Future Work

In this research work a computer model is developed for the underground gasification of Block V of the Thar coal field. The 1D packed bed model of the UCG process incorporates the mathematical equations of [39] with the properties of the Lignite B coal and the operating conditions for Thar UCG setup. The numerical solution of the model is carried out by incorporating a pseudo steady state approximation, which replaces gas phase PDEs with ODEs with respect to the length of the reactor. This approximation assumes that the concentration of the gases attain steady before any significant change occurs in the densities of coal and char. The large differences in the characteristics times for the burning of coal and the velocity of gases justify the pseudo steady state approximation. The PDEs for the densities of coal and char and solid temperature are solved by finite difference method, while the gas phase ODEs are simultaneously solved as a boundary value problem, marching from inlet to outlet. The solution of the model demonstrates its effectiveness. The simulation results show that the solution of the model is capable of providing space and time profiles for different physical quantities, such as, coal and char densities, concentration and molar fractions of different gases, rate of different chemical reactions and solid and gas temperatures. A detailed parametric study is also carried out for the model solution, which shows that the composition of the product gas is sensitive to various coal properties and operating conditions.

The parametrization of a complex process like UCG is a formidable job, which includes a large number of physical and chemical properties of coal, different operating conditions and various in-situ phenomena. In order to determine the composition of coal and char, the ultimate analysis of their samples is carried out. The results of the ultimate analysis are prone to uncertainty, because the measurements are obtained from different coal samples, which go through different handling procedures before they are analyzed. Therefore, to cater for the uncertainty in the results of the ultimate analysis two different nonlinear programing problem are formulated, which aim to minimize the square of the relative L_2 norm error between experimental and simulated heating val-

ues. The field trial of UCG is carried out by UCG project thar, which involves the gasification of a single coal seam. The heating value is calculated by the measurements of the molar fraction of different gases provided by the gas analyzer. After optimization, the results of the solved model are compared with the experimental data, which shows a good match for the heating value.

In order to increase the efficiency of the UCG process, a SMC is designed which maintains a desired constant heating value over a longer period of time. The model based control of UCG process is a very challenging job due to various factors, which include: highly nonlinear nature of various physical and chemical phenomena, strong coupling between the model equations, infinite dimensional nature of the system and unavailability of the measurement of system states. Apart from these issues, the process of UCG is very sensitive to the underground environment. In order to synthesize the controller analytically, a control oriented model of the process is developed which bears certain assumptions. The SMC is considered for the process as it offers robustness against parametric variations and external disturbances. As the relative degree of the sliding variable is zero, so the trivial solution is to derive an expression for the control input algebraically, but this strategy is not feasible as the right hand side of the control input equation depends upon the unmeasured states. Therefore, the conventional SMC is implemented by adding an exogenous input, which is the derivative of the actual control signal. By doing so the relative degree of the sliding variable becomes one with respect to the exogenous input and then SMC is enforced by selecting a suitable value of the discontinuous gain. The synthesized controller is then implemented on the actual model of the UCG process. The simulation results show that despite the modeling uncertainties and external disturbance the controller keeps the heating value at the desired level.

6.1 Future Work

There are three major contributions of the thesis: development of the computer model of the UCG process, estimation of the uncertain parameters and the SMC

design for the process. The following present some improvements which can further increase the effectiveness of these contributions.

6.1.1 Improved computer model of the UCG process

The computer model developed in Chapter 3 bears certain assumptions in order to simplify its solution. The accuracy of the model can be increased by incorporating following effects:

- The mass and energy balances of solids and gases can be extended from 1D to 2D or 3D.
- The effect of the cavity growth due to chemical reactions, thermomechanical failure and bulk collapse needs to be incorporated in the model.
- There is a need to include all the modes of intraphase and interphase heat transfer in the model.
- The interaction of the surrounding in-situ environment with the UCG reactor cavity needs to be included in the model. This can be achieved by incorporating submodels for water influx and heat and mass loss to the external environment.

However, the incorporation of the above mentioned improvements increases the complexity of model analysis, numerical solution, parameter estimation and control of the process. The complexity associated with the numerical solution is two fold, the discretization of 3D PDEs is not trivial and the computational cost of the software for solving these equations also increases. Therefore, the accuracy of the model needs to be compromised depending upon the application of the process model.

6.1.2 Improvement in parameter estimation

The parameter estimation is carried out by formulating the nonlinear programming problems in Chapter 4. These nonlinear programs can be improved by con-

sidering the following modifications:

- Apart from the coal and char composition parameters, a large number of other parameters also effect the heating value of the product gas. As the process occurs under the surface of the Earth, therefore, it is not possible to measure most of these parameters accurately. Hence, a large number of parameters can be optimized by solving the nonlinear programs.
- The sampling frequency of the experimental data needs to be increased, this can help in further minimization of the cost function.
- As the simulation results in Chapter 4 show that the difference between experimental and simulated molar fraction of the gases is large as compared to the heating value. Therefore, different weights can be assigned to the molar fractions of the gases which constitute the heating value. In this way more emphasis is given to the important gases.

The accuracy of the parameter estimation also increases the computational cost, as the objective function is computed after the UCG model is solved.

6.1.3 Implementation of SMC on the actual UCG site

The SMC designed for the UCG process in Chapter 5 is tested on the mathematical model. Therefore, the controller needs to implemented on the actual UCG process.

Bibliography

[1] BP, "Bp statistical review of world energy 2015," tech. rep., Whitehouse Associates, London Printing Pureprint Group Limited, UK, June 2015.

[2] A. W. Bhutto, A. A. Bazmi, and G. Zahedi, "Underground coal gasification: From fundamentals to applications," *Progress in Energy and Combustion Science*, vol. 39, no. 1, pp. 189 – 214, 2013.

[3] G. M. P. Perkins, *Mathematical Modelling of Underground Coal Gasification*. PhD thesis, The University of New South Wales, 2005.

[4] T. Brown, "Coal gasification combined cycles for electricity production," *Progress in Energy and Combustion Science*, vol. 8, no. 4, pp. 277 – 301, 1982.

[5] A. Khadse, M. Qayyumi, S. Mahajani, and P. Aghalayam, "Underground coal gasification: A new clean coal utilization technique for India," *Energy*, vol. 32, no. 11, pp. 2061 – 2071, 2007.

[6] C. Descamps, C. Bouallou, and M. Kanniche, "Efficiency of an integrated gasification combined cycle IGCC power plant including CO_2 removal," *Energy*, vol. 33, no. 6, pp. 874 – 881, 2008.

[7] K. R. Jillson, V. Chapalamadugu, and B. E. Ydstie, "Inventory and flow control of the {IGCC} process with {CO2} recycles," *Journal of Process Control*, vol. 19, no. 9, pp. 1470 – 1485, 2009.

[8] N. V. Gnanapragasam, B. V. Reddy, and M. A. Rosen, "Hydrogen production from coal gasification for effective downstream CO_2 capture," *International Journal of Hydrogen Energy*, vol. 35, no. 10, pp. 4933 – 4943, 2010.

[9] A. D. Pascale, F. Melino, and M. Morini, "Analysis of inlet air cooling for {IGCC} power augmentation," *Energy Procedia*, vol. 45, no. 0, pp. 1265

– 1274, 2014. {ATI} 2013 - 68th Conference of the Italian Thermal Machines Engineering Association.

[10] D. A. Bell, B. F. Towler, and M. Fan, "Chapter 7 - hydrogen production and integrated gasification combined cycle (igcc)," in *Coal Gasification and Its Applications* (D. A. Bell, B. F. Towler, and M. Fan, eds.), pp. 137 – 156, Boston: William Andrew Publishing, 2011.

[11] D. A. Bell, B. F. Towler, and M. Fan, "Chapter 3 - gasification fundamentals," in *Coal Gasification and Its Applications* (D. A. Bell, B. F. Towler, and M. Fan, eds.), pp. 35 – 71, Boston: William Andrew Publishing, 2011.

[12] R. W. Breault, "Gasification processes old and new: A basic review of the major technologies," *Energies*, vol. 3, no. 2, pp. 216 – 240, 2010.

[13] C. D., G. K., and H. S., "A review of the worldwide status of coalbed methane extraction and utilisation," Tech. Rep. ETSU-COAL-R–210, Department of Trade and Industry, London (United Kingdom). Cleaner Coal Technology Programme, Customer Services The British Library Customer Services Boston Spa, Wetherby LS23 7BQ, 2001.

[14] E. Shafirovich and A. Varma, "Underground coal gasification: A brief review of current status," *Industrial & Engineering Chemistry Research*, vol. 48, no. 17, pp. 7865–7875, 2009.

[15] M. Van der Riet, "Underground coal gasification," in *Proceedings of the SAIEE Generation Conference. Eskom College, Midrand*, Feb 2008.

[16] D. J. Schiffrin, "The feasibility of in situ geological sequestration of supercritical carbon dioxide coupled to underground coal gasification," *Energy Environ. Sci.*, vol. 8, pp. 2330–2340, 2015.

[17] D. W. Gregg and T. F. Edgar, "Underground coal gasification," *AIChE Journal*, vol. 24, no. 5, pp. 753–781, 1978.

[18] A. Y. Klimenko, "Early ideas in underground coal gasification and their evolution," *Energies*, vol. 2, no. 2, pp. 456 – 476, 2009.

[19] B. H. WEIL and J. C. LANE, *The technology of the Fischer-Tropsch process*. London, Constable & Co, 1949.

[20] J. Dossey, "Underground coal gasification technology in the USSR," Tech. Rep. SAND-76-0380, Sandia Labs., Albuquerque, N.Mex., USA, July 1976.

[21] D. Gregg, R. Hill, and D. Olness, "Overview of the Soviet effort in underground gasification of coal," Tech. Rep. UCRL-52004, California Univ., Livermore. Lawrence Livermore Lab., USA, January 1976.

[22] D. Olness and D. Gregg, "Historical development of underground coal gasification," Tech. Rep. UCRL-52283, California Univ., Livermore. Lawrence Livermore Lab., USA, June 1977.

[23] R. Hill and M. Shannon, "Controlled retracting injection point CRIP system: a modified-stream method for in situ coal gasification," in *7th underground coal conversion symposium*, (Fallen Leaf Lake, CA, USA), US department of energy, April 1981.

[24] R. Cena, J. Britten, and C. Thorsness, "Excavation of the Partial Seam CRIP underground coal gasification test site," in *13th annual underground coal gasification symposium*, (Laramie, WY, USA), US department of energy, August 1987.

[25] P. Ledent and C. Sonntag, "Controlled retracting gasifying agent injection point process for ucg sites," Nov. 10 1987. US Patent 4,705,109.

[26] J. Boysen, M. Canfield, J. Covell, and C. Schmit, "Detailed evaluation of process and environmental data from the Rocky Mountain i underground coal gasification field test," Tech. Rep. GRI-97/0331, Gas Research Institute, Chicago, IL, USA, February 1998.

[27] M. Seifi, Z. Chen, and J. Abedi, "Numerical simulation of underground coal gasification using the crip method," *The Canadian Journal of Chemical Engineering*, vol. 89, no. 6, pp. 1528–1535, 2011.

[28] A. Singleton, W. Noll, and J. Allen, "Summary report of the rawlins test 1 for gasification of steeply dipping coal beds," in *Proceedings of the Sixth Underground Coal Conversion Symposium, Shangri-La, Oklahoma*, pp. 1–30, 1980.

[29] B. Davis, "Underground coal gasification cavity definition study for Rawlins test 1," *In Situ*, vol. 7, Jan 1983.

[30] "Pakistan Energy Yearbook 2013," tech. rep., Hydrocarbon Development Institute of Pakistan, Ministry of Petroleum and Natural Resources, 2013.

[31] "Electricity production from coal sources (% of total)." `http://databank.worldbank.org/data/reports.aspx?source=2&country=&series=EG.ELC.COAL.ZS&period=#`.

[32] A. Mahmood, N. Javaid, A. Zafar, R. A. Riaz, S. Ahmed, and S. Razzaq, "Pakistan's overall energy potential assessment, comparison of lng, {TAPI} and {IPI} gas projects," *Renewable and Sustainable Energy Reviews*, vol. 31, pp. 182 – 193, 2014.

[33] A. W. Bhutto and S. Karim, "Coal gasification for sustainable development of the energy sector in pakistan," *Energy for Sustainable Development*, vol. 9, no. 4, pp. 60 – 67, 2005.

[34] "Thar CoalField." `http://sindhcoal.gos.pk/underground-coal-gasification-project-block-v/`.

[35] J. E. Fassett, N. A. Durrani, and B. Area, "Geology and coal resources of the thar coal field, sindh province, pakistan," *US Geol Surv open-file report*, pp. 94–167, 1994.

[36] ASTM, "D388-12," *Standard Classification of Coals by Rank. ASTM International, West Conshohocken, PA*, 2012.

[37] "Underground Coal Gasification Project Block V." `http://sindhcoal.gos.pk/thar-coalfield/`.

[38] M. Imran, D. Kumar, N. Kumar, A. Qayyum, A. Saeed, and M. S. Bhatti, "Environmental concerns of underground coal gasification," *Renewable and Sustainable Energy Reviews*, vol. 31, pp. 600 – 610, 2014.

[39] C. Thorsness, E. Grens, and A. Sherwood, "A one dimensional model for in-situ coal gasification," Tech. Rep. UCRL-52523, Lawrence Livermore National Laboratory, Livermore, CA, 1978.

[40] M. Seifi, *Simulation and Modeling of Underground Coal Gasification Using Porous Medium Approach*. PhD thesis, University of Calgary, Canada, 2014.

[41] M. M. Khan, J. P. Mmbaga, A. S. Shirazi, J. Trivedi, Q. Liu, and R. Gupta, "Modelling underground coal gasificationa review," *Energies*, vol. 8, no. 11, pp. 12603 – 12668, 2015.

[42] T. H. T. Tsang, *Modeling of heat and mass transfer during coal block gasification*. PhD thesis, University of Texas at Austin, USA, 1980.

[43] J. G. Speight, *Coal Analysis*, pp. 1–21. John Wiley & Sons, Inc., 2005.

[44] J. G. Massaquoi and J. B. Riggs, "Mathematical modeling of combustion and gasification of a wet coal slab-I: Model development and verification," *Chemical Engineering Science*, vol. 38, no. 10, pp. 1747 – 1756, 1983.

[45] J. G. Massaquoi and J. B. Riggs, "Mathematical modeling of combustion and gasification of a wet coal slab-II: Mode of combustion, steady state multiplicities and extinction," *Chemical Engineering Science*, vol. 38, no. 10, pp. 1757 – 1766, 1983.

[46] K. Y. Park and T. F. Edgar, "Modeling of early cavity growth for underground coal gasification," *Industrial & Engineering Chemistry Research*, vol. 26, no. 2, pp. 237–246, 1987.

[47] G. Perkins and V. Sahajwalla, "A mathematical model for the chemical reaction of a semi-infinite block of coal in underground coal gasification," *Energy & Fuels*, vol. 19, no. 4, pp. 1679–1692, 2005.

[48] G. Perkins and V. Sahajwalla, “A numerical study of the effects of operating conditions and coal properties on cavity growth in underground coal gasification,” *Energy & Fuels*, vol. 20, no. 2, pp. 596–608, 2006.

[49] R. D. Gunn and D. L. Whitman, “In situ coal gasification model (forward mode) for feasibility studies and design,” Tech. Rep. LERC/RI-76/2, Laramie Energy Research Center, Laramie, Wyoming, USA, February 1976.

[50] C. Thorsness and R. Rosza, “Lawrence livermore laboratory in-situ coal gasification program: model calculations and laboratory experiments,” Tech. Rep. UCRL-78302;, Lawrence Livermore Lab, California Univ, Livermore, USA, July 1976.

[51] C. B. Thorsness and R. B. Rozsa, “Insitu coal-gasification: Model calculations and laboratory experiments,” *Society of Petroleum Engineers Journal*, vol. 18, pp. 105–116, 1978.

[52] A. Winslow, “Numerical model of coal gasification in a packed bed,” *Symposium (International) on Combustion*, vol. 16, no. 1, pp. 503 – 513, 1977.

[53] C. B. Thorsness and S. W. Kang, “Method-of-line approach to solution of packed-bed flow problems related to undergound coal gasification processs.” 10th annual underground coal gasification symposium, Williamsburg, VA, USA, 1984.

[54] J. M. Hyman, “A method of lines approach to the numerical solution of conservation laws,” in *Advances in Computer Methods for Partial Differential Equations - III*, pp. 313–321, 1979.

[55] A. C. Hindmarsh, “Lsode and lsodi, two new initial value ordinary differnetial equation solvers,” *ACM SIGNUM Newsletter*, vol. 15, no. 4, pp. 10–11, 1980.

[56] C. W. Gear, “The automatic integration of ordinary differential equations,” *Communications of the ACM*, vol. 14, no. 3, pp. 176–179, 1971.

[57] E. A. A. Abdel-Hadi and T. R. Hsu, “Computer modeling of fixed bed underground coal gasification using the permeation method,” *Journal of Energy Resources Technology*, vol. 109, no. 1, pp. 11–20, 1987.

[58] A. Khadse, M. Qayyumi, and S. Mahajani, “Reactor model for the underground coal gasification UCG channel,” *International Journal of Chemical Reactor Engineering*, vol. 4, no. 1, 2006.

[59] L. F. Shampine and M. W. Reichelt, “The matlab ode suite,” *SIAM journal on scientific computing*, vol. 18, no. 1, pp. 1–22, 1997.

[60] C. Magnani and S. Farouq Ali, “Mathematical-modeling of stream method of underground coal gasification,” *Society of Petroleum Engineers Journal*, vol. 15, pp. 425 – 436, 1975.

[61] C. F. m, *Mathematical Foundations for the Process of Underground Gasification of Coal*. PhD thesis, The Pennsylvania State University, 1973.

[62] C. Magnani and S. Farouq Ali, “A two dimensional mathematical model of the underground coal gasification process,” *Society of Petroleum Engineers*, vol. SPE-5653, Jan 1975.

[63] M. Pasha *et al.*, “An advanced numerical model of underground coal gasification by the stream method using simultaneous solution,” in *SPE Annual Fall Technical Conference and Exhibition*, Society of Petroleum Engineers, 1978.

[64] B. Dinsmoor, J. Galland, and T. Edgar, “The modeling of cavity formation during underground coal gasification,” *Journal of Petroleum Technology*, vol. 30, no. 5, pp. 695–704, 1978.

[65] D. Batenburg, *Heat and mass transfer during Underground coal gasification*. PhD thesis, Dietz Laboratory, Delft University of Technology, The Netherlands, 1992.

[66] D. Batenburg, E. Beizen, and J. Bruining, “A new channel model for underground gasification of thin, deep coal seams,” *In Situ*, vol. 18, no. 4, pp. 419 – 451, 1994.

[67] R. Kuyper, *Transport Phenomena in Underground Coal Gasification Channels*. PhD thesis, Delft University of Technology, The Netherlands, 1994.

[68] R. Kuyper, T. V. D. Meer, and C. Hoogendoorn, "Turbulent natural convection flow due to combined buoyancy forces during underground gasification of thin coal layers," *Chemical Engineering Science*, vol. 49, no. 6, pp. 851 – 861, 1994.

[69] R. Kuyper, T. V. D. Meer, and J. Bruining, "Simulation of underground gasification of thin coal seams," *In Situ*, vol. 20, no. 3, pp. 311 – 346, 1996.

[70] G. Perkins and V. Sahajwalla, "Steady-state model for estimating gas production from underground coal gasification," *Energy & Fuels*, vol. 22, no. 6, pp. 3902–3914, 2008.

[71] M. Seifi, J. Abedi, and Z. Chen, "The analytical modeling of underground coal gasification through the application of a channel method," *Energy Sources, Part A: Recovery, Utilization, and Environmental Effects*, vol. 35, no. 18, pp. 1717–1727, 2013.

[72] J. A. Britten and C. Thorsness, "Cavism user manual," Tech. Rep. UCID-21667, Lawrence Livermore Lab, California Univ, Livermore, USA, 1976.

[73] C. Thorsness and E. Grens II, "Unconfined flow as a mechanism of water influx to a ucg system," in *13th annual underground coal gasification symposium*, (Morgantown, WV, USA), Lawrence Livermore National Lab., CA (USA), 1986.

[74] J. Britten and C. Thorsness, "Modeling thermal and material interactions between a reacting char bed and a gasifying/spalling coal proof," in *11th annual underground coal gasification symposium*, (Denver, CO, USA), Lawrence Livermore National Lab., CA (USA), August 1985.

[75] C. Thorsness and S. Kang, "General purpose, packed bed model for analysis of underground coal gasification processes," Tech. Rep. UCID-20731, Lawrence Livermore National Lab, CA, USA, 1986.

[76] J. A. Britten, "Recession of a coal face exposed to a high temperature," *International Journal of Heat and Mass Transfer*, vol. 29, no. 7, pp. 965 – 978, 1986.

[77] C. Thorsness and J. Britten, "A mechanistic model for axisymmetric cavity growth during underground coal gasification," *Preprints of Papers, American Chemical Society, Division of Fuel Chemistry*, vol. 33, no. 2, 1982.

[78] J. A. Britten, "Extinction phenomena in countercurrent packed-bed coal gasifiers: a simple model for gas production and char conversion rates," *Industrial & Engineering Chemistry Research*, vol. 27, no. 1, pp. 197–203, 1988.

[79] J. Britten and C. Thorsness, "A model for cavity growth and resource recovery during underground coal gasification," *In Situ*, vol. 13, no. 1, 1989.

[80] E. N. J. Biezen, J. Molenaar, and J. Bruining, "An integrated 3D model for underground coal gasification," *Society of Petroleum Engineers*, no. SPE 30790, 1995.

[81] E. N. J. Beizen, *Modeling Underground Coal Gasification*. PhD thesis, Delft University of Technology, Delft, Netherlands, 1996.

[82] J. Nitao, D. Camp, T. Buscheck, J. White, G. Burton, J. Wagoner, and M. Chen, "Progress on a new integrated 3-d ucg simulator and its initial application," in *International Pittsburgh Coal Conference*, (Pittsburgh, PA, USA), 2011.

[83] J. Nitao, T. Buscheck, S. Ezzedine, S. Friedman, and D. Camp, "An integrated 3D UCG model for predicting cavity growth, product gas and

interactions with the host environment," in *International Pittsburg Coal Conference*, (Istanbul, Turkey), 2010.

[84] D. Stephens, "Hoe creek experiments: LLNL's underground coal gasification project in wyoming," Tech. Rep. UCRL-53211, California Univ., Livermore. Lawrence Livermore National Lab., USA, October 1981.

[85] G. Samdani, P. Aghalayam, A. Ganesh, R. Sapru, B. Lohar, and S. Mahajani, "A process model for underground coal gasification- Part-I: Cavity growth," 2015.

[86] G. Samdani, P. Aghalayam, A. Ganesh, R. Sapru, B. Lohar, and S. Mahajani, "A process model for underground coal gasification: Part-II growth of outflow channel," 2015.

[87] L. Yang and S. Liu, "Numerical simulation on heat and mass transfer in the process of underground coal gasification," *Numerical Heat Transfer, Part A: Applications*, vol. 44, no. 5, pp. 537–557, 2003.

[88] L. Yang, "Thermophysical models of underground coal gasification and fem analysis," *Numerical Heat Transfer, Part B: Fundamentals*, vol. 52, no. 5, pp. 449–470, 2007.

[89] D. L. H. Yang, X. Zhang, and S. Liu, "Underground coal gasification using oxygen and steam," *Energy Sources, Part A: Recovery, Utilization, and Environmental Effects*, vol. 31, no. 20, pp. 1883–1892, 2009.

[90] L. H. Yang and Y. M. Ding, "Numerical study on convection diffusion for gasification agent in underground coal gasification. Part I: Establishment of mathematical models and solving method," *Energy Sources, Part A: Recovery, Utilization, and Environmental Effects*, vol. 31, no. 4, pp. 308–317, 2009.

[91] L. H. Yang and Y. M. Ding, "Numerical study on convection diffusion for gasification agent in underground coal gasification (ucg). Part II: Determination of model parameters and results analysis," *Energy Sources,*

Part A: Recovery, Utilization, and Environmental Effects, vol. 31, no. 4, pp. 318–324, 2009.

[92] L. H. Yang and S. Q. Liu, "Temperature-control blasting underground coal gasification in the inclined coal seams with a short wall," *Energy Sources, Part A: Recovery, Utilization, and Environmental Effects*, vol. 32, no. 6, pp. 532–541, 2010.

[93] K. Morris, "Control of systems governed by partial differential equations," in *Electrical Engineering Handbook*, ch. 67, pp. 1–37, CRC Press, 2010.

[94] V. Utkin, "Control of distributed-parameter plants," in *Sliding Modes in Control and Optimization*, Communications and Control Engineering Series, pp. 169–188, Springer Berlin Heidelberg, 1992.

[95] K. Kostúr and J. Kačúr, "The monitoring and control of underground coal gasification in laboratory conditions," *Acta Montanistica Slovaca*, vol. 13, no. 1, pp. 111–117, 2008.

[96] K. Kostur and J. Kacur, "Development of control and monitoring system of UCG by promotic," in *2011 12th International Carpathian Control Conference (ICCC)*, pp. 215 –219, may 2011.

[97] K. J. Aström and T. Hägglund, *PID Controllers: Theory, Design, and Tuning*. Instrument Society of America, Research Triangle Park, NC, 2 ed., 1995.

[98] I. U. Vadim, "Survey paper variable structure systems with sliding modes," *IEEE Transactions on Automatic control*, vol. 22, no. 2, pp. 212–222, 1977.

[99] J. Hung, W. Gao, and J. Hung, "Variable structure control: a survey," *Industrial Electronics, IEEE Transactions on*, vol. 40, pp. 2–22, Feb 1993.

[100] K. Young, V. Utkin, and U. Ozguner, "A control engineer's guide to sliding mode control," *Control Systems Technology, IEEE Transactions on*, vol. 7, pp. 328–342, May 1999.

[101] A. Arshad, A. Bhatti, R. Samar, Q. Ahmed, and E. Aamir, "Model development of ucg and calorific value maintenance via sliding mode control," in *2012 International Conference on Emerging Technologies (ICET)*, pp. 1–6, 2012.

[102] V. Utkin, "Mathematical description of motions on discontinuity boundaries," in *Sliding Modes in Control and Optimization*, Communications and Control Engineering Series, pp. 12–28, Springer Berlin Heidelberg, 1992.

[103] E. P. RYAN and M. CORLESS, "Ultimate boundedness and asymptotic stability of a class of uncertain dynamical systems via continuous and discontinuous feedback control," *IMA Journal of Mathematical Control and Information*, vol. 1, no. 3, pp. 223–242, 1984.

[104] J. A. BURTON and A. S. I. ZINOBER, "Continuous approximation of variable structure control," *International Journal of Systems Science*, vol. 17, no. 6, pp. 875–885, 1986.

[105] C. A. WOODHAM and A. S. I. ZINOBER, "Eigenvalue placement in a specified sector for variable structure control systems," *International Journal of Control*, vol. 57, no. 5, pp. 1021–1037, 1993.

[106] A. G. Bondarev, S. A. Bondarev, N. E. Kostyleva, and V. I. Utkin, "Sliding modes in systems with asymptotic state observers," *Automation and Remote Control*, vol. 46, pp. 679 – 684, 1985.

[107] B. Walcott and S. Zak, "Combined observer-controller synthesis for uncertain dynamical systems with applications," *Systems, Man and Cybernetics, IEEE Transactions on*, vol. 18, pp. 88–104, Jan 1988.

[108] C. Edwards and S. K. Spurgeon, "Robust output tracking using a sliding-mode controller/observer scheme," *International Journal of Control*, vol. 64, no. 5, pp. 967–983, 1996.

[109] S. Ramirez, "On the sliding mode control of nonlinear systems," *Systems & control letters*, vol. 19, pp. 303–312, 1992.

[110] A. Pisano and E. Usai, "Sliding mode control: A survey with applications in math," *Mathematics and Computers in Simulation*, vol. 81, no. 5, pp. 954 – 979, 2011. Important aspects on structural dynamical systems and their numerical computation.

[111] V. I. Utkin, *Sliding modes in control and optimization*, vol. 116. Springer-Verlag Berlin, 1992.

[112] V. I. Utkin, J. Guldner, and J. Shi, *Sliding Mode Control in Electromechanical Systems*. London: Taylor and Francis, 1999.

[113] W. Perruquetti, *Sliding Mode Control in Engineering*. New York, NY, USA: Marcel Dekker, Inc., 2002.

[114] V. Utkin, "Sliding mode control," in *Control systems, robotics, and automation*, UNESCO-EOLSS.

[115] A. Fossard and T. Floquet, "An overview of classical sliding mode control," in *Sliding Mode Control in Engineering* (J. P. Barbot and W. Perruquetti, eds.), Control Engineering, New York, NY, USA: Marcel Dekker, Inc., 2002.

[116] J. E. Slotine and W. Li, *Applied Nonlinear Control*. Englewood Cliffs, NJ: Prentice-Hall, 1991.

[117] M. Fliess, "Generalized controller canonical form for linear and nonlinear dynamics," *Automatic Control, IEEE Transactions on*, vol. 35, pp. 994–1001, Sep 1990.

[118] G. F. Froment and K. B. Bischoff, *Chemical reactor analysis and design*. Wiley New York, 1979.

[119] D. M. Himmelblau, *Basic principles and calculations in chemical engineering*. Prentice-Hall, Inc.,Englewood Cliffs, NJ, Jan 1982.

[120] G. W. Recktenwald, "Finite-difference approximations to the heat equation," 2001.

[121] M. Hosea and L. Shampine, "Analysis and implementation of TR-BDF2," *Applied Numerical Mathematics*, vol. 20, no. 12, pp. 21 – 37, 1996.

[122] A. A. Uppal, A. I. Bhatti, E. Aamir, R. Samar, and S. A. Khan, "Control oriented modeling and optimization of one dimensional packed bed model of underground coal gasification," *Journal of Process Control*, vol. 24, no. 1, pp. 269–277, 2014.

[123] D. U. Olness and L. L. N. Laboratory, *The Podmoskovnaya underground coal gasification station*. Livermore, Calif. : Lawrence Livermore Laboratory, University of California, 1981.

[124] G. E. I. T. EUROPE, *GAS 3100 R Coal gas/Syngas 19-3U Analyser*. Gas Engineering and Instrumentation Technologies Europe, B-3380 Bunsbeek, Belgium, 2011.

[125] A. A. Uppal, A. I. Bhatti, E. Aamer, R. Samar, and S. A. Khan, "Optimization and control of one dimensional packed bed model of underground coal gasification," *Journal of Process Control*, vol. 35, pp. 11 – 20, 2015.

[126] D. A. Bell, B. F. Towler, and M. Fan, "Chapter 5 - underground coal gasification," in *Coal Gasification and Its Applications*, pp. 101 – 111, Boston: William Andrew Publishing, 2011.

[127] M. Blinderman and A. Klimenko, "Theory of reverse combustion linking," *Combustion and Flame*, vol. 150, no. 3, pp. 232 – 245, 2007.

[128] A. Antoniou and W.-S. Lu, "THE OPTIMIZATION PROBLEM," in *Practical Optimization: Algorithms and Engineering Applications*, Springer Publishing Company, Incorporated, 2007.

[129] P. T. Boggs and J. W. Tolle, "Sequential quadratic programming," *Acta Numerica*, vol. 4, pp. 1–51, 1 1995.

[130] C. Lawrence and A. Tits, "A computationally efficient feasible sequential quadratic programming algorithm," *SIAM Journal on Optimization*, vol. 11, no. 4, pp. 1092–1118, 2001.

[131] A. Antoniou and W.-S. Lu, "GENERAL NONLINEAR OPTIMIZATION PROBLEMS," in *Practical Optimization: Algorithms and Engineering Applications*, Springer Publishing Company, Incorporated, 2007.

[132] P. E. Gill, W. Murray, and M. A. Saunders, "SNOPT: An SQP Algorithm for Large-Scale Constrained Optimization," *SIAM Journal on Optimization*, vol. 12, no. 4, pp. 979–1006, 2002.

[133] A. Geletu, "Quadratic programming problems - a review on algorithms and applications (Active-set and interior point methods)." `https://www.tu-ilmenau.de/fileadmin/media/simulation/Lehre/Vorlesungsskripte/Lecture_materials_Abebe/QPs_with_IPM_and_ASM.pdf`.

[134] L. van Reeuwijk, *Guidelines for quality management in soil and plant laboratories*. Food & Agriculture Org., 1998.

[135] P. Dawkins, "DIFFERENTIAL EQUATIONS," 2007. `http://tutorial.math.lamar.edu/terms.aspx`.

[136] V. Utkin, "Sliding mode control in discrete-time and difference systems," in *Variable Structure and Lyapunov Control* (A. Zinober, ed.), vol. 193 of *Lecture Notes in Control and Information Sciences*, pp. 87–107, Springer Berlin Heidelberg, 1994.

View publication stats